



POLITECNICO

MILANO 1863

School of Industrial and Information Engineering

Department of Chemistry, Materials and Chemical Engineering
“Giulio Natta”

Master’s Degree in Food Engineering

VALORIZATION OF FOOD WASTE TO CHEMICALS: RECOVERY OF VOLATILE FATTY ACIDS WITH FUNCTIONALIZED MAGNETIC NANOPARTICLES

Relatore: Prof. Maurizio Masi

Correlatore: Prof. Filippo Rossi

Correlatore: Ing. Elisa Lacroce

Tesi di laurea di:

Angela Di Marcantonio (Matr. 945739)

Lucia Placanica (Matr. 939943)

Academic year 2020/2021

Table of contents

List of figures	IV
List of tables.....	VI
List of abbreviations	VII
Abstract	VIII
Sommario	X
Chapter 1: Food waste.....	1
1.1. Food and urban waste: definitions, extent and impacts.....	1
1.2. Global and European food waste production	2
1.3. Waste production in Italy	3
1.3.1. Characterization of Italian household food waste	5
1.4. Lombardy cluster and the city of Milan.....	8
1.5. Treatments for the organic fraction.....	9
1.6. REVENUE project.....	11
Chapter 2: Introduction and state of the art.....	14
2.1. Magnetic iron oxides nanoparticles	14
2.1.1. MNPs synthesis	17
2.1.1.1. Biological methods.....	17
2.1.1.2. Physical methods.....	18
2.1.1.3. Chemical methods.....	18
2.1.2. MNPs functionalization	20
2.1.2.1. MNPs functionalization with APTES	20
2.1.3. MNPs applications	21
2.2. VFAs: characteristics and recovery from waste.....	21
2.2.1. Literature research method	24
2.2.2. Results classifications	25
2.2.3. Liquid-liquid extraction.....	26
2.2.3.1. Reactive extraction	29
2.2.4. Adsorption.....	29
2.2.5. Membrane processes	31
2.2.6. Pressure-driven membrane processes	32
2.2.7. Concentration gradient-driven membrane processes.....	33
2.2.8. Electric field-driven membrane processes	34
Chapter 3: Aim of the thesis	36
Chapter 4: Materials and methods	38
4.1. Analytical methods	38

4.1.1. Dynamic light scattering	38
4.1.2. Electrophoretic light scattering	38
4.1.3. X-Ray diffraction	38
4.1.4. Scanning electron microscopy	39
4.1.5. Fourier transform infrared spectroscopy	39
4.1.6. CHNS elemental analysis.....	39
4.1.7. Gas chromatography	39
4.2. Experimental synthesis and procedures	40
4.2.1. Materials	40
4.2.2. MNPs synthesis via chemical co-precipitation.....	40
S.1. MNPs synthesis with ammonium hydroxide	40
S.2. MNPs synthesis with sodium hydroxide	41
S.3. MNPs synthesis with excess of sodium hydroxide.....	41
4.2.3. APTES hydrolysis	42
4.2.4. MNPs functionalization	42
F.1. MNPs functionalization with hydrolysed APTES, 1:9 molar ratio, 5-hours procedure	43
F.2. MNPs functionalization with hydrolysed APTES, 1:18 molar ratio, 5-hours procedure	43
F.3. MNPs functionalization with hydrolysed APTES, 1:4 molar ratio, 5-hours procedure	44
F.4. MNPs functionalization with hydrolysed APTES, 1:4 molar ratio, 1-hour procedure.....	44
F.5. MNPs functionalization with APTES, 1:4 molar ratio, 1-hour procedure	45
F.6. MNPs functionalization with APTES, 1:4 molar ratio, 5-hours procedure.....	45
4.2.5. VFAs synthetic solution preparation.....	46
4.2.6. Adsorption experiments.....	46
4.2.7. Desorption experiments.....	47
4.2.8. Second-cycle adsorption experiments	47
Chapter 5: Results.....	49
5.1. MNPs synthesis by co-precipitation.....	49
5.1.1. X-ray Powder Diffraction phase identification	52
5.2. MNPs functionalization reaction with hydrolysed APTES.....	55
5.3. Characterization and comparison of MNPs and F-MNPs.....	57
5.3.1. Infrared spectroscopy	57
5.3.2. Zeta potential	58
5.3.3. CHNS elemental analysis.....	59
5.3.4. DLS analysis	60
5.4. Adsorption of VFAs with MNPs and F-MNPs	61
5.5. Desorption of VFAs from F-MNPs	69
5.6. Second-cycle adsorption of VFAs with F-MNPs	72
5.7. Functionalization reaction optimization.....	74
5.7.1. Scanning Electron Microscopy results	78
Chapter 6: Conclusions	80
Bibliography	82

List of figures

Figure 1: Per capita food losses and wastes at consumption and pre-consumption stages in different regions, from [10].....	3
Figure 2: Breakdown of Italian separate collection of the organic fraction, 2019 data from ISPRA.	4
Figure 3: Percentage breakdown of Italian organic waste treatment (2019), from ISPRA	11
Figure 4: Schematic representation of the REVENUE project scheme and main steps and products [34]	12
Figure 5: Schematic illustration of arrangements of magnetic dipoles for five different types of materials in absence ($H=0$) or presence (H) of an external magnetic field (via Jeong et al. 2007).	15
Figure 6: Schematic illustration of the dependence of magnetic coercivity on particle size; coercivity falls to zero for superparamagnetic colloidal particles (figure adapted from Jeong et al. 2007).	15
Figure 7: Magnetization characteristic of paramagnetic, ferromagnetic and superparamagnetic materials (via L. Mohammed et al. 2017)	16
Figure 8: (3-Aminopropyl)triethoxysilane (APTES).....	20
Figure 9: Publications' distribution over time, expressed as number of articles per year	25
Figure 10: Percentage of articles using a determined feedstock.....	25
Figure 11: Percentage of articles using a determined recovery technique.....	26
Figure 12: Classification of articles focused on membrane processes according to the driving force; data are expressed as percentage of the total number of retrieved articles focused on membranes.	31
Figure 13: Conventional ED working principle, example of concentration of sodium carboxylate (NaA) solution; where CEM stands for cation exchange membrane, and AEM for anion exchange membrane (image from [80])	34
Figure 14: APTES hydrolysis and condensation reaction.....	42
Figure 15: MNPs functionalization with hydrolysed APTES (image from [72]).....	43
Figure 16: MNPs functionalized with APTES (picture from Can et al., [17])	45
Figure 17: MNPs functionalized with APTES (picture from Can et al., [17])	45
Figure 18: Summary of desorption and second-cycle adsorption tests.	48
Figure 19: Magnetic decantation results in a dark nanoparticles' sediment at the bottom topped by a transparent and colourless supernatant.....	49
Figure 20: F.1 work-up. A) reaction liquid, B) first washing water, C) second washing water, D) third washing water.	50
Figure 21: Nanoparticles attracted by a small magnetic bar introduced in the vial. After introduction the liquid rapidly clears and the nanoparticles are collected at the bar's extremities.	52
Figure 22: X-Ray diffractogram of MNPs from S.3. Counts are indicated on the y-axis.	53
Figure 23: Peaks patterns of MNPs from S.3, Iron oxide, Calcium carbonate, and Akaganeite	53
Figure 24: The two co-existing phase-change pathways during magnetite nanoparticles coprecipitation reaction individuated by Ahn et. al., 2012 [145]	54
Figure 25: Magnetic decantation of functionalized magnetic nanoparticles. A) reaction flask during sedimentation, B) reaction liquid after 18 minutes, C) washing water after 18 minutes, D) washing ethanol after 23 minutes.....	56
Figure 26: FT-IR spectra for MNPs (top) and F-MNPs (bottom).....	58
Figure 27: ζ -potential measured at pH values equal to 2, 4, 6, 7, 8, 10 and 12 for MNPs (left) and F-MNPs (right). The red dot indicates iso-electric points.....	59
Figure 28: Percentages of adsorption of carboxylic acids using F-MNPs magnetically stirred for 5 (A.1), 30 (A.2), 60 (A.3), and 120 (A.4) minutes.	64
Figure 29: Percentages of adsorption of carboxylic acids using F-MNPs agitated with a shaker for 5 (A.5), 30 (A.6), 60 (A.7), and 120 (A.8) minutes.....	65
Figure 30: Percentages of adsorption of carboxylic acids using MNPs magnetically stirred for 5 (A.9), 30 (A.10), 60 (A.11), and 120 (A.12) minutes	65
Figure 31: Percentages of adsorption of carboxylic acids using MNPs agitated with a shaker for 5 (A.13), 30 (A.14), 60 (A.15), and 120 (A.16) minutes.....	66
Figure 32: Adsorption percentages for test A.1, A.1a, A.1b together with the mean values and standard deviations (red bars) for each analyte.	68
Figure 33: Adsorption percentages for test A.8, A.8a, A.8b together with the mean values and standard deviations (red bars) for each analyte.	68

Figure 34: Percentage of desorbed carboxylic acids compared to those adhering to the surface after absorption for sample D.1 (A.1a in methanol), D.2 (A.8b in methanol), D.3 (A.1b in water), D.4 (A.8a in water).....	71
Figure 35: Percentages of adsorption of carboxylic acids after second adsorption for sample R.1 (magnetically stirred for 5'), R.2 (agitated with shaker for 120'), R.3 (magnetically stirred for 5'), and R.4 (agitated with shaker for 120').	73
Figure 36: F.2 work-up supernatants. A) reaction liquid, B) washing water, C) washing ethanol.....	75
Figure 37: F.3 work-up supernatants. A) reaction liquid, B) washing water, C) washing ethanol	75
Figure 38: F.4 work-up supernatants. A) reaction liquid, B) washing water, C) washing ethanol	76
Figure 39: F.5 work-up supernatants. A) reaction liquid, B) washing water, C) washing ethanol	77
Figure 40: SEM micrograph of sample S3 (A) compare with literature image (B) from Indrayana (2019)	78
Figure 41: SEM micrograph of samples S3, F3 and F6	79

List of tables

<i>Table 1: Data of total and per capita urban waste (UW), total and per capita separate collection (SC), percentage of SC (ratio between SC and UW multiplied by 100) and quantity of organic fraction separately collected; Green values in % SC are above the 2012 target, while blue values in UW per capita are below the national average; 2019 data from [13].</i>	5
<i>Table 2: Main FW characteristics with a global validity, from [19]–[21], [23]; where TS stands for Total Solids, WW for wet weight, VS for volatile solids, BMP for Biochemical Methane Potential.</i>	6
<i>Table 3: Italian post-consumer waste composition expressed as percentages on wet weight of main food categories;</i>	7
<i>Table 4: Expected Outputs (E.O.) of the REVENUE project.</i>	13
<i>Table 5: VFAs chemical properties, market size and indicative prices. ^a Ramos-Suarez et al. (2021), ^b Zacharof (2013). European data about market size or prices weren't found, USA data are reported to give a general idea.</i>	22
<i>Table 6: Synthesis of MNPs.</i>	41
<i>Table 7: Synthesis of MNPs.</i>	41
<i>Table 8: Synthesis of MNPs.</i>	42
<i>Table 9: APTES hydrolysis.</i>	42
<i>Table 10: MNPs functionalization with hydrolysed APTES.</i>	43
<i>Table 11: MNPs functionalization with hydrolysed APTES.</i>	43
<i>Table 12: Functionalization with hydrolysed-APTES.</i>	44
<i>Table 13: Functionalization with hydrolysed-APTES.</i>	44
<i>Table 14: MNPs functionalization with APTES.</i>	45
<i>Table 15: MNPs functionalization with APTES.</i>	45
<i>Table 16: Ethanol and VFAs concentration [mg/L] via IRSA-CNR.</i>	46
<i>Table 17: Quantities used to prepare a synthetic solution of 500 mL.</i>	46
<i>Table 18: Different times and agitation methods used for adsorption experiments.</i>	47
<i>Table 19: Co-precipitation conditions of the three syntheses conducted (S.1, S.2, S.3) together with the resulting sedimentation and magnetic decantation; "n/a", not available indicates that sedimentation was not observed during the 1 hour of cooling.</i>	51
<i>Table 20: Percentages on a mass basis (% w/w) of nitrogen, carbon, and hydrogen obtained by CHNS elemental analysis of nanoparticles synthesised via S.1, S.2, and S.3.</i>	51
<i>Table 21: CHNS elemental analysis results for MNPs and F-MNPs.</i>	59
<i>Table 22: DLS results of three consecutive measures (1st, 2nd and 3rd) on MNPs and F-MNPs. The intensity distribution was used, for multiple peaks the intensity percentages are reported in parenthesis.</i>	61
<i>Table 23: Absorption experiments conducted along with the type of nanoparticles, agitation method, and contact time used for each.</i>	62
<i>Table 24: Gas chromatography results in mg/L for the starting VFAs solution (first row) and adsorption tests.</i>	63
<i>Table 25: Carboxylate concentration after adsorption using F-MNPs magnetically stirred for 5 minutes, three replicates A.1, A.1a, A.1b.</i>	67
<i>Table 26: Carboxylate concentration after adsorption using F-MNPs agitated with a shaker for 120 minutes, three replicates A.8, A.8a, A.8b.</i>	67
<i>Table 27: Gas chromatography results expressed as mg/L for desorption sample D.1, D.2, D.3, and D.4, together with starting adsorption sample and solvent used.</i>	70
<i>Table 30: Gas chromatography results expressed as mg/L for second adsorption samples R.1, R.2, R.3, and R.4, together with stirring methods and contact times used; values in red are higher than the concentration in the starting VFAs solution.</i>	72
<i>Table 29: Functionalization percentages of reactions with different MNPs to APTES molar ratio; for all the reactions hydrolysed-APTES was employed and the reaction time was of 5 hours.</i>	76
<i>Table 30: Functionalization reaction with different experimental conditions.</i>	77

List of abbreviations

FW	Food Waste
VFAs	Volatile Fatty Acids
MNPs	Magnetic Nanoparticles
F-MNPs	Functionalised Magnetic Nanoparticles
APTES	(3-Aminopropyl)triethoxysilane
FSC	Food Supply Chain
UW	Urban Wastes
SC	Separate Collection
AD	Anaerobic Digestion
DF	Dark Fermentation
AF	Acidogenic Fermentation
LCA	Life Cycle Analysis
CNR-IRSA	Consiglio Nazionale delle Ricerche – Istituto di Ricerca sulle Acque
UCBM	Università Campus Bio-medico di Roma
LE2C	Lombardy Energy Cleantech Cluster
MRI	Magnetic Resonance Image
LLE	Liquid-Liquid Extraction
DBU	1,8-diazabicyclo[5.4.0]-undec-7-ene
TMBG	N,N,N',N'-tetramethyl-N"-butylguani-dine
ILs	Ionic Liquids
DESs	Deep Eutectic Solvents
MF	Microfiltration
UF	Ultrafiltration
NF	Nanofiltration
RO	Reverse Osmosis
VPMC	Vapour Permeation Membrane Contactors
PTFE	Polytetrafluoroethylene
TDDA	Tridodecylamine
PDMS/PTFE	Composite silicon rubber/PTFE
FO	Forward Osmosis
SILM	Supported Ionic Liquid Membrane
ED	Electrodialysis
SEM	Scanning Electron Microscopy
DLS	Dynamic Light Scattering
ELS	Electrophoretic Light Scattering
XRD	X-Ray Diffraction
FT-IR	Fourier Transform Infrared Spectroscopy
GC	Gas Chromatography
ATR	Attenuated Total Reflection
VSM	Vibrating Sample Magnetometer
TEM	Transmission Electron Microscopy
TS	Total Solids
WW	Wet Weight
VS	Volatile Solids
BMP	Biochemical Methane Potential

Abstract

This thesis, one of the first for the master's degree program in Food Engineering at Politecnico di Milano, is focused on a hidden and less compelling trait of food supply chains: food waste. Food waste (FW) and losses are generated at each step of the food journey from farm to fork, ranking high on the list of global priorities. This major problem accounts for more than 1.3 billion tons of food wastage worldwide, corresponding to 1/3 of the overall food production. The socio-environmental and economic implications are vast, fuelling a context in which climate change and resource depletion are already at alarming levels, and coexisting with the silent scourge of hunger and malnutrition.

Prevention and remediation methods are available and implemented to some extent. Attention from virtuous companies, consumer awareness, and new technological solutions that extend the food products' life are some of the factors that prevent the transformation of food into waste; but when it is not possible to avoid food waste, nor to re-use it for human or animal consumption, the last valid option is to recover from it useful resources. The best treatment methods currently implemented are focused on the production of biofertilizers, energy, and fuels (biogas and biomethane primarily). These processes degrade a complex and rich substrate yielding low value-added products.

This thesis is part of the REVENUE project that proposes a 3-routes platform for REcovery of high Value products, ENergy, and bio-fertilizer from Urban biowaste fully exploiting the potential of food waste. The high-value products of interest are short-chain carboxylic acids, also referred to as volatile fatty acids (VFAs), important bulk chemicals largely employed in the pharmaceutical, chemical, and food industries. Currently, their production is done via chemical pathways, starting from non-renewable petrochemical sources. VFAs are intermediate products of microbial fermentation, therefore, is possible to exploit food waste as feedstock for their production, using microbial pathways.

To see this process implemented in the future it is necessary to overcome the main obstacle, represented by the separation of VFAs from the fermentation broth. To face the challenge a novel method is proposed in this thesis work: the use of iron oxide magnetic nanoparticles (MNPs) to selectively recover VFAs and release them for further purification. The aim will be the synthesis and appropriate functionalization of MNPs and their preliminary testing to verify capture, release, and re-use feasibility.

The first phase of the research was devoted to the synthesis via chemical co-precipitation of MNPs, and to its improvement in terms of work-up by changing the experimental conditions. The goal was to obtain MNPs that can be rapidly and effectively recovered by magnetic decantation. Successively, MNPs have been functionalized to limit oxidation and aggregation and tailor them for the designated use.

The properties of VFAs lead to selecting (3-Aminopropyl)triethoxysilane (i.e. APTES) for the coating. Carboxylic acids in the fermentation broth are present in dissociated form and hence can interact with the positive charge of the APTES's protonated amine groups. Thereafter a

synthetic VFAs solution was prepared, based on the average concentration of VFAs obtained at the end of the fermentation by the IRSA-CNR research group. This was used to assess the functionalized magnetic nanoparticles (F-MNPs) performance in adsorbing VFAs using different agitation methods and contact times. Subsequently, the desorption of VFAs in water and methanol and the possible reuse of the nanoparticles for the second adsorption were verified. In conclusion, an optimization of the functionalization reaction was conducted to maximise the number of amine groups on the surface of F-MNPs.

The results obtained confirm the great potential of this method and enable future studies on its implementation.

Sommario

Questa tesi, che è tra le prime del corso di laurea magistrale in Food Engineering al Politecnico di Milano, si concentra su un aspetto poco accattivante della filiera alimentare: lo scarto.

Ogni passaggio nel percorso dell'alimento dal campo alla tavola genera spreco e perdita di cibo, che figurano in cima alla lista delle priorità globali.

Questo annoso problema corrisponde a più di 1,3 miliardi di tonnellate di sprechi alimentari a livello mondiale, corrispondenti ad un terzo della produzione alimentare complessiva. Le implicazioni socio-ambientali ed economiche gravano in un contesto in cui il cambiamento climatico e l'esaurimento delle risorse sono a livelli allarmanti, e coesistono con la piaga della fame e della malnutrizione.

Metodi di prevenzione e rimedi sono disponibili e in parte già in atto. Alcuni dei fattori che contribuiscono a ridurre lo spreco alimentare sono: l'attenzione di aziende virtuose, la consapevolezza dei consumatori, le nuove soluzioni tecnologiche che prolungano la vita dei prodotti alimentari. Quando invece non è possibile evitare lo scarto, né riutilizzarlo per il consumo umano o animale, l'ultima opzione valida è ricavare da esso risorse utili. I migliori metodi di trattamento attualmente implementati si concentrano sulla produzione di biofertilizzanti, energia e combustibili, principalmente biogas e biometano. Questi processi degradano un substrato complesso e ricco, ottenendo prodotti a basso valore aggiunto.

Questa tesi si inserisce all'interno del progetto REVENUE, che propone una piattaforma a tre vie per il recupero dallo scarto organico urbano di prodotti ad alto valore aggiunto, energia e biofertilizzanti, sfruttando integralmente le potenzialità dei rifiuti alimentari.

I prodotti ad alto valore aggiunto sono acidi carbossilici a catena corta, chiamati anche acidi grassi volatili (VFAs). Si tratta di composti chimici ampiamente impiegati nell'industria farmaceutica, chimica ed alimentare che attualmente vengono prodotti per via chimica a partire da risorse petrolchimiche non rinnovabili. Sfruttando vie microbiche è possibile produrre i VFAs a partire da rifiuti alimentari, essendo essi intermedi del processo fermentativo.

L'implementazione di questo processo in futuro necessita il superamento del suo principale ostacolo tecnico: la separazione dei VFAs dal brodo di fermentazione. In questa tesi viene proposto e sperimentato un nuovo metodo che utilizza nanoparticelle magnetiche di ossido di ferro (MNPs) per il recupero selettivo dei VFAs e il loro successivo rilascio in solvente.

Gli obiettivi dello studio sono la sintesi e la funzionalizzazione appropriata delle MNPs e le prove preliminari per verificare la fattibilità della cattura, del rilascio e del riutilizzo.

La prima fase della ricerca è stata dedicata alla sintesi di MNPs tramite co-precipitazione chimica e al miglioramento della fase di separazione solido-liquido variando le condizioni sperimentali. L'obiettivo è stato ottenere nanoparticelle recuperabili velocemente ed efficacemente tramite decantazione magnetica. Successivamente le MNPs sono state funzionalizzate per limitarne l'ossidazione e l'aggregazione adattandole all'uso specifico. Sulla base delle proprietà dei VFAs è stato selezionato il (3-Aminopropyl)triethoxysilane (i.e. APTES)

per la funzionalizzazione. Gli acidi carbossilici nel brodo di fermentazione sono presenti in forma dissociata e possono interagire con la carica positiva dei gruppi amminici protonati dell'APTES.

A partire dalle concentrazioni medie di VFAs, ottenute a seguito della fermentazione studiata dal gruppo di ricerca IRSA-CNR, è stata preparata una soluzione sintetica. Quest'ultima è stata utilizzata per valutare le prestazioni delle nanoparticelle funzionalizzate (F-MNPs) nell'adsorbire i prodotti con diversi metodi di agitazione e tempi di contatto. Successivamente, è stato verificato il desorbimento dei VFAs in acqua e metanolo e il possibile riutilizzo delle nanoparticelle per un secondo adsorbimento. In conclusione, è stata condotta un'ottimizzazione della reazione di funzionalizzazione per massimizzare il numero di gruppi amminici sulla superficie delle MNPs.

I risultati ottenuti confermano le grandi potenzialità di questo metodo e pongono le basi studi futuri sulla sua applicazione.

Chapter 1: Food waste

1.1. Food and urban waste: definitions, extent and impacts

The number of publications on food waste is continuously growing, the literature investigates its causes, socio-economic drivers, extent, impacts, reduction and remediation measures. New awareness campaigns, seminars and guidelines on the subject are born along with documentaries, films, podcasts and blogs. Food waste is in the spotlight.

This pervasive problem represents a global priority and is explicitly addressed in the UN's 2030 Agenda. It is featured in the 12th Sustainable Development Goal which aims to "Ensure sustainable consumption and production patterns"; specifically within target 12.3 that calls for a reduction by half of the per capita global food waste at retail and consumer levels as well as a reduction of food losses along production and supply chains, including post-harvest losses [1].

However, the published studies dealing with food losses and food waste lack consensus on definitions of the terms "food loss" and "food waste", system boundaries, quantification and reporting methodologies [2], [3] thus producing non-comparable results.

For the scope of this thesis the definitions of "food", "food waste" and "food losses" are adopted from the 2021 Food Waste Index Report, released by the UNEP (United Nations Environment Programme). Therefore, the term "food" will refer to any substance intended for human consumption regardless of the extent of processing it has undergone; drinks and substances used during manufacturing, treatment or preparation are included. "Food waste" will identify food and the associated inedible parts removed from the human food supply chain at retail, food service or households. It comprises food destined to landfill, controlled combustion, sewer, litter, co- or anaerobic digestion, aerobic digestion and land application. While "food loss" will refer to losses for essential commodities throughout the supply chain, up to but not including retail [4]. Food losses and food waste will be collectively referred to as "food wastage". Finally, in this context "urban biowaste" or "municipal biowaste" will refer to the organic fraction of waste (the prefix bio- comes from biodegradable) generated by household and food service activities.

The vast impacts of this phenomenon on natural resources as water, land, climate and biodiversity and the worrying coexistence of it with the undernutrition silent pandemic and the overconsumption issue give momentum to research. Global food wastage only in 2007 accounted for 3.3 Gton of CO₂ equivalent (excluding greenhouse gases from land-use change), consumption of 250 km³ of surface and groundwater resources and occupation of 1.4 billion hectares of land; regarding biodiversity loss, the impacts are complex to assess, still it is evident that monoculture and agriculture expansion into wild areas endanger species and ecosystems [5]. The estimates for 2019 indicate that almost 690 million people were undernourished and 25.9 % of the global population suffered moderate or severe food insecurity; data regarding childhood overweight, chronic undernutrition and stunting are of significant concern too [6].

To face this emergency a whole supply chain multidisciplinary approach is needed. Edible food waste at retailers and markets is already prevented, to some extent, through redistribution systems, while for households it is still a paramount problem. This could be faced through sensibilization campaigns and the development of more conscious and sustainable food culture. To evaluate possible actions for each actor in the supply chain the Food Waste Hierarchy framework can be used. The concept from environmental literature, also present in European law [7], has been adapted to food waste. The hierarchy indicates prevention actions as the most preferable followed by re-use for human consumption, re-use for animal feed, recycling, and recovery actions, finally disposal actions are the least favourable option [8], [9]. In this framework, the REVENUE project is located among the recycling and recovery actions as it proposes an innovative 3-Routes Platform for urban biowaste treatment. The treatment is intended for food waste that cannot be prevented or re-used.

In the following subchapters an overview of food waste figures, findings and treatments will be presented. The section on the recent state of food waste in Italy and specifically in the Lombardy region constitutes the completion of the first work package of the REVENUE project.

1.2. Global and European food waste production

Roughly one-third of the food produced worldwide gets lost or wasted, accounting for about 1.3 billion ton yearly [10]. Agricultural production and post-harvest handling and storage represent 54 % of the total food supply chain (FSC) wastage volumes, while downstream operations including processing, distribution and consumption account for 46 % [5]. It emerges a difference between developing and industrialized countries. As illustrated in Figure 1, for the former more than 40 % of food losses occur at the post-harvest and processing stage due to larger technological inefficiencies, while for industrialized countries more than 40 % occur at retailer and consumer level [10].

The post-consumer losses are about 121 kg per capita. In particular, 74 kg at family level, 32 kg as restaurants wastes and 15 kg at retail shops. These losses are almost independent of the Gross Domestic Product per capita of the considered country [4].

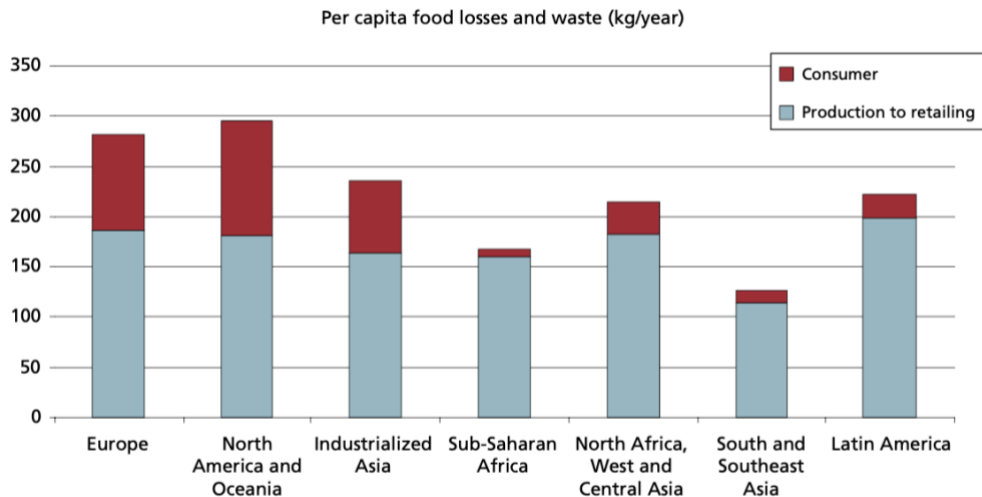


Figure 1: Per capita food losses and wastes at consumption and pre-consumption stages in different regions, from [10].

At the European level, approximately 129 million ton of food wastage are generated yearly. The largest share is produced at the consumption stage, accounting for 60 million ton (46 % of the total food wastage). Followed by primary production (25 %), processing and manufacturing (24 %), and distribution and retailing (5 %) [11].

Fruits and vegetables are the food groups with the highest amount of wastage, generated in similar amounts at the primary production stage and the consumption stage. This may be due to higher produced quantities, higher perishability and higher presence of inedible parts when compared to other food groups [11].

These European data should be seen as a red flag for the alarming level of food loss and waste. However, to address the issue is necessary to fragment the analysis on a national and regional basis to account for the nuances of the food and waste management systems of each country.

1.3. Waste production in Italy

In Italy, an estimated 20 million ton of food are wasted every year from the field to the point of sale. Going into details, it has been quantified that about 17.7 million ton of agricultural production remains in the fields, whereas 1.9 million ton are wasted by the food industry. Finally, the amount of “thrown away” food from wholesale markets appears to be about 0.3 million ton [12].

Concerning the post-costumer stage, in 2019 Italy has produced almost 30.1 million ton of urban wastes (UW), corresponding to 499.3 kilograms per capita. In the same year, separate waste collection stands at 18.5 million ton, resulting in a percentage of 61.3 % of total urban

wastes generated [13]. This figure is still below the 65 % target set for 31 December 2012 by the legislative decree 3 April 2006, n. 152, “Norme in materia ambientale” [14]. The organic fraction, mainly composed of food scraps, stands at almost 7.3 million ton, accounting for 39.5 % by weight of the total 2019 separate collection. As illustrated in Figure 2, the organic fraction is composed of biodegradable waste produced by kitchens and canteens (67.7 %), maintenance of gardens and parks (27.8 %), collection at markets (0.8 %) and comprise also the biodegradable waste destined for the practice of home composting (3.7 %, not collected). The waste from kitchen and canteens is composed of inedible food parts (peels, stones, bones etc.) and edible food. It was estimated that a person in Italy produces on average 530 g of edible food waste per week; this might be thrown away for different reasons, the main ones being: spoilage, taste preferences, excessive quantity cooked or served, excessive quantity bought, shopping mistake, leftovers, and accidents (e.g. burnt, felt on the floor) [15].

Organic fraction composition

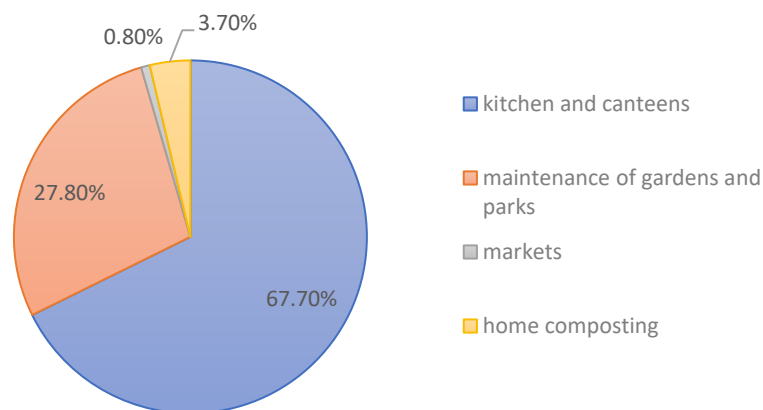


Figure 2: Breakdown of Italian separate collection of the organic fraction, 2019 data from ISPRA.

These figures are useful to grasp the extent of the food waste generated in Italy, however, this issue is characterized by a marked inhomogeneity [13], [16] highlighting the need for smaller aggregation units.

Regional Data summarized in Table 1, shows considerable differences both in UW per capita generation and percentage of separate collection (SC) which place Lombardia, Trentino-Alto Adige, Veneto, Friuli-Venezia Giulia, Emilia-Romagna, Umbria, Marche, and Sardegna over the 65 % goal for SC. However, Trentino-Alto Adige, Emilia-Romagna, Umbria and Marche show a pro capita UW production over the national average.

Table 1: Data of total and per capita urban waste (UW), total and per capita separate collection (SC), percentage of SC (ratio between SC and UW multiplied by 100) and quantity of organic fraction separately collected; Green values in % SC are above the 2012 target, while blue values in UW per capita are below the national average; 2019 data from [13].

Region	UW	SC	% SC	UW per capita	SC per capita	Organic fraction
	[t]	[t]	%	[kg/(inhab. year)]	[kg/(inhab. year)]	[t]
Piemonte	2.143.652	1.355.656	63,2	494	312	460.141
Valle d'Aosta	75.825	48.933	64,5	604	390	17.147
Lombardia	4.843.570	3.488.628	72,0	479	345	1.270.558
Trentino-Alto Adige	546.636	399.672	73,1	509	372	141.672
Veneto	2.403.335	1.795.251	74,7	490	366	767.966
Friuli-Venezia Giulia	603.107	405.089	67,2	498	334	167.759
Liguria	821.949	439.017	53,4	533	285	136.669
Emilia-Romagna	2.960.609	2.089.049	70,6	663	468	825.984
NORD	14.398.682	10.021.295	69,6	518	361	3.787.897
Toscana	2.277.254	1.370.962	60,2	612	368	550.489
Umbria	454.254	300.106	66,1	516	341	125.680
Marche	796.289	559.504	70,3	524	368	247.931
Lazio	3.038.263	1.586.262	52,2	518	270	561.608
CENTRO	6.566.059	3.816.833	58,1	548	318	1.485.708
Abruzzo	600.278	376.108	62,7	460	288	162.310
Molise	111.241	56.112	50,4	368	186	23.348
Campania	2.595.166	1.368.911	52,8	449	237	625.212
Puglia	1.871.828	946.823	50,6	467	236	382.606
Basilicata	197.214	97.370	49,4	354	175	35.384
Calabria	767.220	367.543	47,9	399	191	163.024
Sicilia	2.233.279	860.325	38,5	450	173	389.576
Sardegna	737.730	540.771	73,3	452	332	241.743
SUD	9.113.955	4.613.963	50,6	445	225	2.023.203
ITALY	30.078.697	18.452.091	61,3	499	306	7.296.808

1.3.1. Characterization of Italian household food waste

The composition of the food waste flow, both in terms of food groups and physical-chemical parameters, is significant in order to evaluate targeted measures and actions. Knowledge about the most wasted categories (milk and derivatives, bread, pasta and cereals, meat, fish etc.) is relevant to design targeted prevention and awareness campaigns. Together with chemical characterization of the waste, it allows assessment and recognition of the best-suited recovery and recycling actions. Moreover, the waste composition can provide useful information about the performance of a collection scheme in retrieving the materials it targets [17].

Food waste generation is thoroughly connected with dietary choices, eating habits, food culture and traditions [18], [19]. The result of these links is variable food waste characteristics depending on sources and world regions [19]–[21]. Whereas the analysis of food waste samples from 15 sites in four countries (UK, Finland, Portugal and Italy) conducted by Heaven et al. [17] concluded that seasonal or regional differences may be on a par with day-to-day variations, also that key analytical parameters values exhibited a significant degree of similarity. Other articles on the topic reported that certain FW features can be extrapolated worldwide [19]–[23], the main values are reported in Table 2.

Table 2: Main FW characteristics with a global validity, from [19]–[21], [23]; where TS stands for Total Solids, WW for wet weight, VS for volatile solids, BMP for Biochemical Methane Potential.

Characteristic	Value
Moisture content	74-90 %
pH	5.1 ± 0.7
TS (%WW)	20 %
VS (%TS)	90 %
Degradable carbohydrates	41-65 %
Proteins	15-25 %
Lipids	13-20 %
C/N ratio	13.2-24.5
BMP (mLCH ₄ /g VS)	460

Not many data have been found in the literature on the specific composition of Italian waste, and none were individuated regarding regional clusters. The available literature adopts several methodologies characterized by different accuracy. Some of the studies use questionnaires or interviews to investigate consumer behaviours [2], [3], [15], [24], [25]. These methods are easy, inexpensive and relatively quick however cannot be reliably used for quantitative information as biased and prone to underestimation [3], [4], [15]. A relevant qualitative common result is that bread, fruits, vegetables, milk and derivatives are the most wasted foods in Italy [7], [9], [10].

Other researchers performed calculations based on statistical data on the food supply chain or on municipal waste [16]. In these instances, there is no consumer involvement, but some uncertainties and limitations remain from assuming fixed waste or loss percentages taken from smaller studies [3]. According to the UNEP Food Waste Index Report [4], the preferable methods for quantitative estimation are diaries and waste compositional analysis. The first method uses digital or paper diaries that the consumer fill up with quantitative and qualitative information: weighted waste quantity, type of food, reasons for wasting etc. This requires active consumer involvement that may result in a consumers' behavioural shift, furthermore, it's expensive and heavy so generally a smaller sample size is used [3].

The second suggested method is waste composition analysis, which involves the analysis of the collected waste by a third party. The absence of customer involvement allows for great objectiveness and accuracy but doesn't allow knowledge of the motivations behind disposing of the item, if it was fresh or spoiled, and if it was cooked at home or purchased. Additional disadvantages are the lack of standardization and harmonization of collection systems in Italy and the inability to measure foods that are given to a pet or sewed [3].

In the literature concerning Italian waste composition, the diary method was implemented by Giordano et al. 2019 [15] while the composition analysis method was used by Heaven et al. 2010 [17], the resulting compositions are both reported in Table 3 together with the methodology used. Also in Table 3 is a third composition obtained by compositional analysis of the waste from the IRSA-CNR canteen in Rome (conducted as a preliminary study for the REVENUE project) [26] and the European composition obtained by calculations based on FSC statistical data [27]. The comparison of results is complicated by the slightly different categories used.

The percentages from IRSA-CNR, reported by Gianico et al. 2021 [26], shows similarities with those from Heaven et al. 2010 [17] except for the dairy fraction that results substantially smaller in the latter. The composition from Giordano et al. 2019 [15] is the one closer to the EU one, the largest difference being the cumulative percentage of "Pasta/rice/flour/cereals" and "Bread and bakery".

Table 3: Italian post-consumer waste composition expressed as percentages on wet weight of main food categories;

^a do not comprise fish as the quantity was not reported explicitly by Giordano et al.

^b comprise "Roots & Tubers", "Oilseeds & Pulses" and "Fruit & Veg"

^c comprises also eggs.

	Heaven et al. [17]	Giordano et al. [15]	Gianico et al. [26]	Gustavsson et al. [27]
Methodology used	municipal organic waste composition analysis (Italy)	diary on edible food waste (Italy)	IRSA-CNR canteen food waste sorting (Italy)	calculations based on FSC statistical data (Europe)
Fruit and vegetable waste	69	45.3	70	41 ^b
Pasta/rice/flour/cereals	12.4	8.2	15	33
Bread and bakery	2.8	12.4		
Meat and fish	6.2	7.0 ^a	0	9
Dairy	1.4	18.8	15	17 ^c
Drinks	0	4.3	0	-
Others	8.2	4.1	0	0

To have a comprehensive measurement and monitoring of the food waste flow a combination of the previously presented methods is best. However, to enrich the knowledge concerning primarily the composition of urban food, waste diaries and composition analysis are sufficient. While the composition analysis is able to give a detailed picture of the organic

waste that will reach the treatment site (including pollutants such as plastic, compostable polymers, metals), the diary will allow quantification of edible food waste. The ultimate goal is that of reducing and eliminating through prevention and re-use this type of waste to have a flow for treatment that's composed only of inedible parts like peels, cores and rinds. Recycling and recovery of edible food are not environmentally, nor ethically sustainable.

1.4. Lombardy cluster and the city of Milan

The document "Rapporto Rifiuti Urbani, Edizione 2020" (Urban Waste Report, 2020 Edition) [13] prepared by ISPRA (Istituto Superiore per la Protezione e la Ricerca Ambientale) presents detailed data regarding national and regional urban waste in Italy; the following paragraph summarizes and aggregates the main data regarding Lombardy as a useful brief inventory for the REVENUE project.

As presented in Table 1, in 2019 Lombardy produced over 4.8 million ton of urban waste and achieved a percentage of separate collection of 72 %, among the highest in Italy and with ten of the twelve provinces over the 65 % target set for 2012. In the same year, the organic fraction stands at 36.4 % of the total UW corresponding to 1.27 million ton. In addition to the quantities produced within the region, there are 385703 ton of organic waste received from outside, of which 262376 ton are biodegradable waste from kitchens and canteens. Lombardy represents the second largest receiver of organic waste among the regions and the biggest contributor to the treatment of this fraction in Italy. The region is home to 79 operative plants: 64 dedicated to composting, 7 to integrated aerobic/anaerobic treatment, and 8 to anaerobic digestion; resulting in a total treatment capacity of 2.5 million ton and over 1.6 million ton treated. This system produces around 0.5 million ton of compost to be used as a soil amendment, 157 million Nm³ of biogas, 36 million Nm³ of biomethane, and a total of 552 GWh/y of energy (electric, thermal and cogeneration).

A specific reality that has obtained interesting results in terms of food waste management is that of the city of Milan. In general, cities have been recognized by the EU as spaces in which is possible to efficiently implement a circular urban economy based on bioeconomy strategies, this is due to the combination of a large production of wastes and waste management systems concentrated in relatively small spaces. In particular, Milan is the first European city with a population of more than one million inhabitants for the quantity of urban waste that is sent to recycling. In 2019 the separate collection in Milan has reached 61.8 % accounting for 434 thousand ton, of which almost 154 thousand ton (35.5 %) are organic wastes (comprise wastes from commercial activities while do not comprise greenery trimmings) [28].

These results have been obtained through an excellent door-to-door collection system, Milan is the largest European city using this method of collection. Separate collection is performed also by all 94 outdoor local markets (2008 ton of organic waste).

Another interesting aspect of Milan's scenario is that the municipality owns more than 99 % of the shares of both SogeMi Spa and Milano Ristorazione. SogeMi is the company for the establishment and operation of wholesale Markets in Milan (fruit and vegetables, fish, flowers and meat market) which in 2018 produced 3260 Kg of biodegradable wastes. While Milano Ristorazione provides food services to schools, retirement homes, home food services for the elderly and many other municipal or private sectors accounting for a total of 85 thousand meals per day. The control over these services allows accessing food surpluses for redistribution and food wastes with a more homogeneous composition [28]. The collected waste is then shipped trying to optimize the volumes transported and the fleet. The organic fraction is first shipped to the Maserati Light transfer station, where is loaded on larger vehicles, and then transported to the Montello Spa plant near Bergamo where is converted to biogas, methane, liquid carbon dioxide and organic fertilizer through integrated aerobic/anaerobic treatment [28].

Milan has a collection system (done by AMSA) specifically devoted to collect organic wastes that are mainly constituted by food wastes. Households waste are collected typically two times a week, while the restaurant wastes are collected daily. Because most of the household wastes are packaged in biodegradable polymer bags a relevant amount of polymer fraction is present in the household bins that collectively merge the wastes of many families. That is a critical point to be considered as these materials are difficult to digest in conventional systems. On the contrary, restaurants usually have their own collection bin and often they do not use any plastic bags to contain wastes. Thus, in an experimental campaign to test the project feasibility at a higher scale, these are the wastes to be addressed primarily by the project.

The Lombardy region and on a smaller scale the city of Milan represents a fertile ground for the experimental implementation of the REVENUE project. This is thanks to the high percentage of collection and treatment of urban organic waste and the overall development of the treatment sector.

1.5. Treatments for the organic fraction

Food waste can have different destinations: landfill, controlled combustion, compost or aerobic digestion, co- or anaerobic digestion, sewer, litter and land application.

Disposal through the sewer, mostly performed for liquid foods and beverages poured into drains, is difficult to trace, measure and control; it may be relevant or negligible depending on culture, foods eaten and presence of waste disposal unit that discharges to the sewer [4]. These systems are not diffused in Italy. Also, the dispersion of food waste in the environment (or littering) is difficult to investigate and quantify.

Land application has been in use for a long time as a low-cost treatment for food industry waste-waters, these are applied to vegetated land using predominantly the slow rate system

based on sprinkler irrigation, drip irrigation or surface irrigation [29]. This destination is primarily for liquid effluents. While landfilling, controlled combustion, aerobic digestion, co- or anaerobic digestion are in-use destinations for separately collected solid or semi-solid food wastes.

Landfilling refers to the definitive storage of waste by burying it in a controlled way. This option is known to cause various environmental issues for instance leaching, greenhouse gas emission and odour production; furthermore, the cost is increasing due to European directives that eventually will limit its use [19]. This solution is a disposal action and so is the least favourable according to the food waste hierarchy.

Controlled combustion refers to oxidation and thermal degradation of waste; it allows to recover heat, reduce waste mass and volume and destroy hazardous organics and pathogens [30], but due to the high water content of food waste results inefficient, energy-demanding and air polluting [19].

Composting or aerobic digestion refers to the aerobic bacterial degradation of organic matter in controlled conditions of initial waste composition, humidity, temperature, oxygen and pH. This process produces a stable and rich soil referred to as compost, employed in agricultural activities as a fertilizer due to its high content in humic acids [31]. This option involves FW valorisation but produces low value-added products [19]. This method has a low prevalence in most countries; in Europe, it was estimated to be 8 % of total household food waste [4] while in Italy in 2019 it accounted for 3.7 % of the organic fraction [13].

Anaerobic treatment, also referred to as anaerobic digestion, produces biogas and digestate through biodegradation of organic waste in absence of oxygen. The gaseous product called biogas is a mixture mainly composed of methane and carbon dioxide which can be used as a fuel for energy and heat production. Instead, the digestate is a secondary solid product that can be employed as it is for soil amendment or it can undergo a further stabilization process by aerobic composting [31]. In case this second process is performed the treatment is referred to as co-digestion as both anaerobic and aerobic digestion are implied. The process is divided into four main steps: the first is hydrolysis which converts complex organic material to soluble monomer thanks to enzymatic activity; the second step is acidogenesis which involve the fermentative conversion of monomers to carbon dioxide, hydrogen and short-chain fatty acids; then acetogenesis takes place and the acidogenesis products are oxidized to produce acetate and hydrogen; finally in the fourth step the previously formed compounds are converted to methane by anaerobic archaea [19], [20]. If all four steps are completed the process is referred to as complete anaerobic digestion (AD). Whereas, if the process is stopped at acidogenesis (fermentation), the main resulting products can be hydrogen or VFAs. The former is referred to as Dark Fermentation (DF), the latter is named acidogenic fermentation (AF) [19]. Based on life cycle analysis (LCA), AD has been suggested as more environmentally friendly than other FW treatment methods [32], [33]; additionally, FW seems to be an exceptional substrate despite its regional and seasonal variations [19]. Nonetheless, some main operational challenges involve the accumulation of inhibitors, specifically VFAs and ammonia, that destabilize the process [19], [20].

Regarding the implementation of these methods in Italy, in 2019 a total of 345 plants were dedicated to the treatment of the organic fraction. Of these 281 were composting plants, 41 integrated aerobic/anaerobic treatment plants and 23 anaerobic digestion plants. As shown in Figure 3, overall 6.4 million of ton of urban organic waste were treated, of which 3.1 million ton by composting (49.2 %), 2.9 million ton by integrated aerobic/anaerobic treatment (45.7 %) and 328 thousand ton by anaerobic digestion (5.1 %) [13].

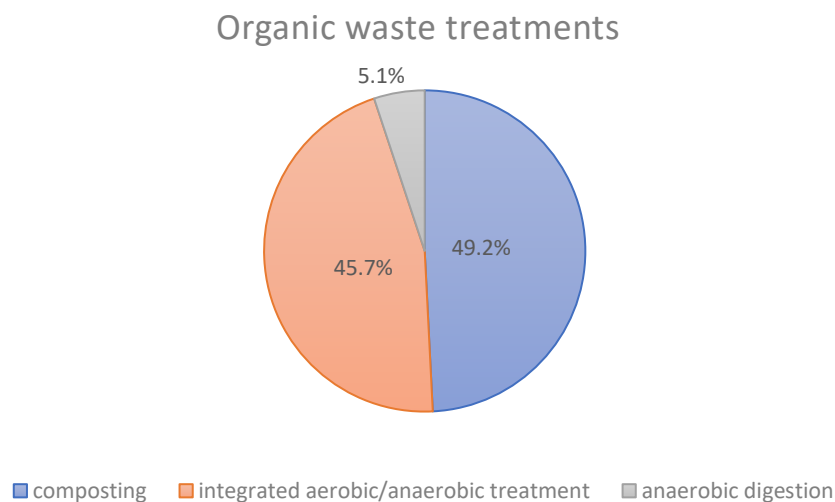


Figure 3: Percentage breakdown of Italian organic waste treatment (2019), from ISPRA

1.6. REVENUE project

The REVENUE project proposes an innovative 3-Routes Platform for REcovery of high Value products, ENergy and bio-fertilizer from Urban biowaste (REVENUE). This multidisciplinary research project aims at upgrading the AD process to a virtuous multi-step biorefinery process that, starting from waste, is able to produce valuable chemicals and materials as well as biomethane and hygienized digestate, to be used as biofertilizer. Thanks to the limited emissions, renewable energy production and minimum waste this biorefinery process could represent the best solution for food waste and urban biowaste treatment. The project is in line with the objectives of the Green Chemistry Specialization Area of Lombardy Region which focus on the development of supply chains based on the biorefinery concept able to extract decreasing value-added compounds in a waterfall logic [34].

The target products are short and medium-chain fatty acids, which have high value and wide application [35]–[37] therefore are considered a promising research topic [19]. Biomethane will be produced from the residual solid food-waste fraction; this product is considered as a “biobattery”, a source of dispatchable bio-energy to be used as fuel for mobility, electric energy generation or heat generation. And finally, the residues from methanogenesis will be

converted to an odour-free hygienized biofertilizer. The project scheme and the main steps and products are schematically represented in Figure 4.

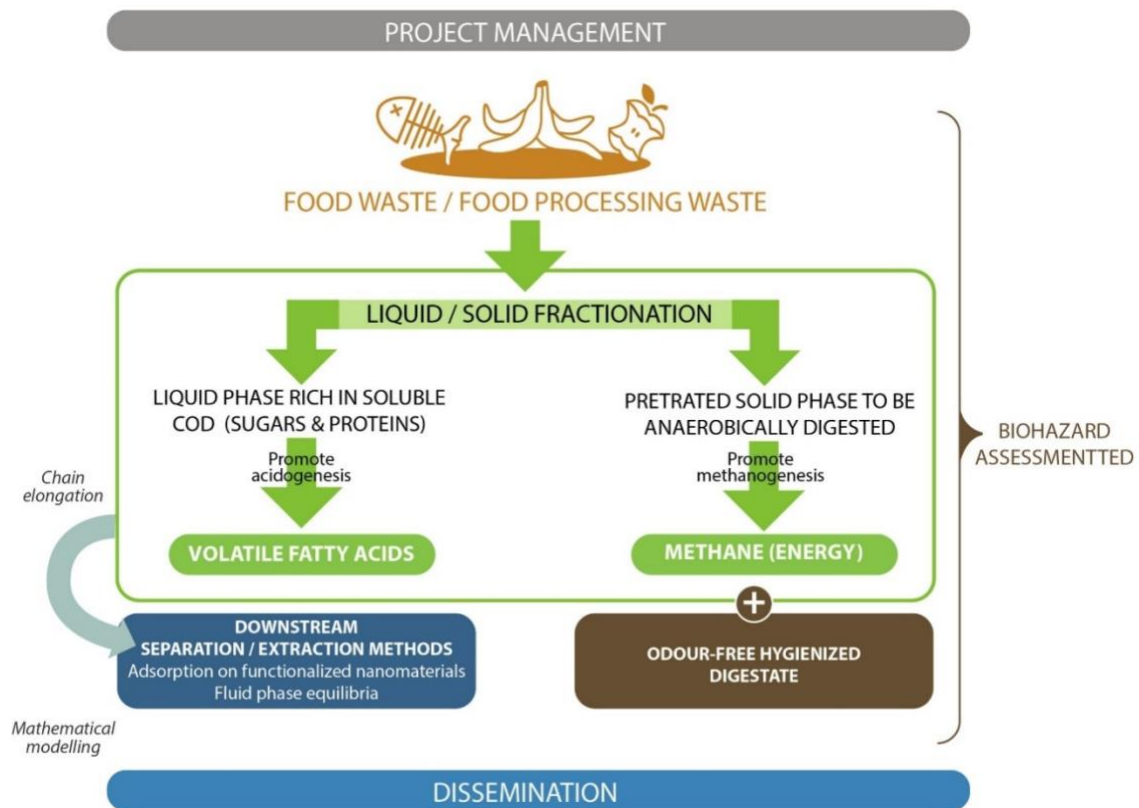


Figure 4: Schematic representation of the REVENUE project scheme and main steps and products [34]

The project, with the contribution of Fondazione Cariplo, started in February 2020 under the lead and coordination of Politecnico di Milano represented by professor Maurizio Masi as principal investigator. The research activities are conducted in collaboration with IRSA-CNR (Consiglio Nazionale delle Ricerche – Istituto di Ricerca sulle Acque) and UCMB (Università Campus Bio-medico di Roma) while the dissemination activities will be supported by the sub-contractor LE2C (Lombardy Energy Cleantech Cluster). The project duration is of 30 months.

The project will involve the development of:

1. a territorial inventory (with leader PoliMi) to collect and organize available data on the Lombardy food waste management system;
2. a process to convert biowaste into value-added products (with leader IRSA-CNR) that include thermal pre-treatment, acidogenic step optimization, the study of optimal condition for chain-elongation of ethanol up to caproic acid and production of methane and digestate;
3. a downstream separation and/or extraction method (with leader PoliMi) using functionalized nanomaterials and fluid-phase equilibria (with leader UCMB) together with the describing models;

4. an evaluation of the effects of the proposed biorefinery scheme on public health (with leader UCBM) in particular bio-hazard assessment and digestate quality assessment.

These will be complemented and supported by dissemination and project management activities. The REVENUE project expected outputs are resumed in Table 4. This thesis work chapter addresses E.O.1 (“Collection and data analysis on urban bio-waste production, their characteristics and present management systems in Lombardy territorial cluster”) while the experimental activities cover E.O.7 (“Methods for separation and purification of the value-added products”).

Table 4: Expected Outputs (E.O.) of the REVENUE project.

E.O. number	Short description
E.O.1	Collection and data analysis on urban bio-waste production, their characteristics and present management systems in Lombardy territorial cluster
E.O.2	Optimization of thermal pretreatment to maximize the transfer of sugars and proteins into the liquid phase
E.O.3	Fine control of acidogenic fermentation of liquid phase
E.O.4	Maximisation of VFAs yield from the pretreated fermented extract
E.O.5	Conversion of VFAs into caproic acid by minimizing ethanol addition
E.O.6	Correlation between short-medium chain fatty acids and microbial composition
E.O.7	Methods for separation and purification of the value-added products
E.O.8	Maximisation of biomethane yield from the residue after solid/liquid separation
E.O.9	Assessment of bio-hazard of the biorefinery integration in an urban context
E.O.10	Production of high quality digestate to be recycled in agriculture
E.O.11	Application of the communication plan activating the dual exchange between science and society
E.O.12	Young researcher expertise reinforcement

Chapter 2: Introduction and state of the art

2.1. Magnetic iron oxides nanoparticles

Nanotechnology is a paramount research and development frontier of modern science [38], it deals with materials ranging from 1 to 100 nm [39] and nanoparticles are at the forefront of the rapid development of this discipline [40]. They have unique electrical, magnetic and optical properties that are not found in their bulk counterparts [41], [42]. Recently, iron oxides nanoparticles are in the spotlight thanks to several applications in engineering, ecology and medicine [42], [43].

There are many pure phases of iron oxides in nature, the most widespread ones are magnetite (Fe_3O_4), maghemite ($\gamma\text{-Fe}_2\text{O}_3$) and hematite ($\alpha\text{-Fe}_2\text{O}_3$) [39]. Based on the iron oxidation state, they possess different physicochemical properties. Magnetite is the most studied and interesting one because of the presence of the Fe^{2+} state, which can potentially act as an electron donor [39]. Magnetite is a black colour iron oxide of both Fe(II) and Fe(III), the properties of magnetic nanoparticles (MNPs) made of this material are governed by the size, when sufficiently small they exhibit the peculiar superparamagnetic behaviour [44]. The attractive or repulsive forces between magnetic materials can be described in terms of magnetic dipoles, namely pairs of opposite magnetic poles separated by a very short distance [45]. This concept explains five basic magnetic behaviours, classified according to the response of the material sample to an external field [46], and schematised in Figure 5.

- I. Diamagnetism: no magnetic dipoles in absence of an external field and weak negative induced dipoles in presence of an external magnetic field.
- II. Paramagnetism: randomly oriented dipoles in absence of an external magnetic field, that become oriented when the external field is applied.
- III. Ferromagnetism: always exhibit magnetic dipoles, in the absence or presence of an external magnetic field, and macroscopically display a permanent magnetic moment.
- IV. Antiferromagnetism: antiparallel magnetic moments with opposite directions, lead to a zero net magnetization despite the magnetic ordering within the material.
- V. Ferrimagnetism: tendency to assume an ordered, but not antiparallel, arrangement so a spontaneous magnetization remains after removal of the magnetic field.

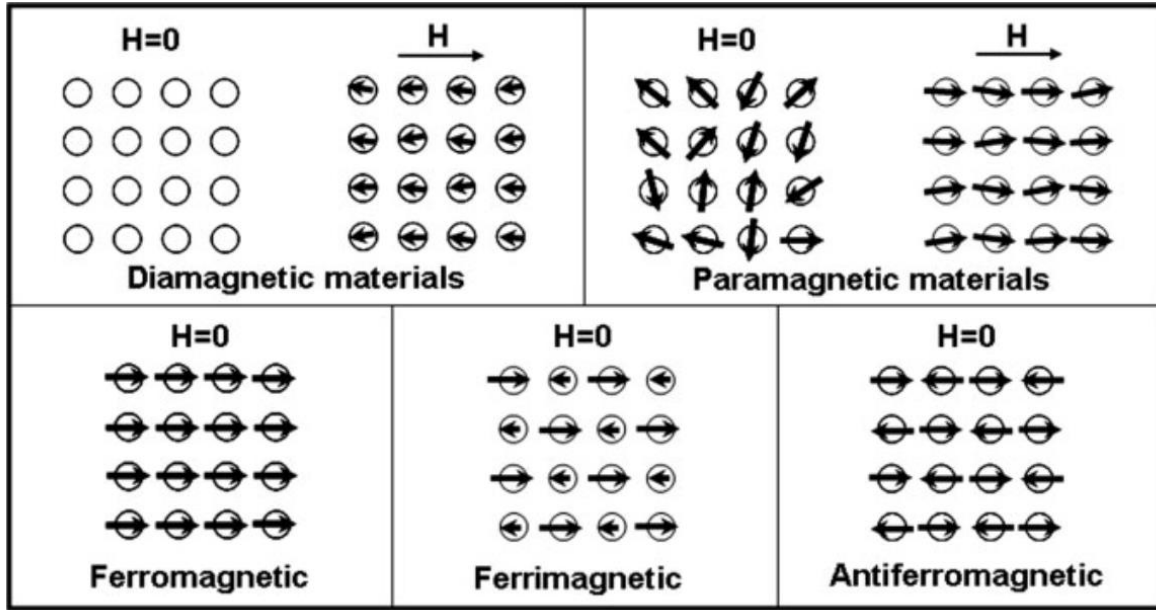


Figure 5: Schematic illustration of arrangements of magnetic dipoles for five different types of materials in absence ($H=0$) or presence (H) of an external magnetic field (via Jeong et al. 2007).

All these behaviours are determined by the domains, namely groups of spins collectively pointing in one direction. Domains' existence and formation are associated with a certain energy, the motion of domains walls is the mean for reverting magnetization. Coercivity, namely the reverse magnetic field needed to demagnetize a material, has been experimentally studied and results to be a function of the particle size. By reducing the size, magnetic materials go from the multi-domains regime to the single domain regime to the superparamagnetic regime [46], as shown in Figure 6.

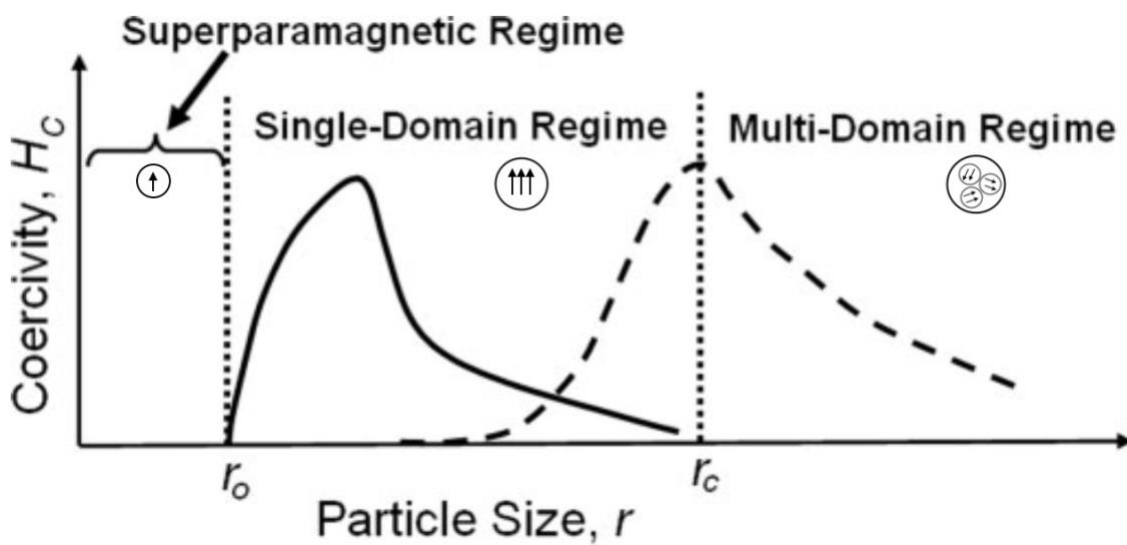


Figure 6: Schematic illustration of the dependence of magnetic coercivity on particle size; coercivity falls to zero for superparamagnetic colloidal particles (figure adapted from Jeong et al. 2007)

So, when sufficiently small, individual nanoparticles will express magnetic moment as a single domain if exposed to an external magnetic field. They manifest magnetisation behaving as a gigantic paramagnetic atom under an applied field, but when the external magnetic field is removed, the magnetisation of the individual particles becomes zero [40] (Figure 7).

Superparamagnetic materials are intrinsically nonmagnetic but can be easily magnetized in the presence of an external magnetic field [46]. Superparamagnetic materials reach a high saturation magnetism, like ferromagnetic ones, but they don't exhibit coercivity and remanence, like paramagnetic ones.

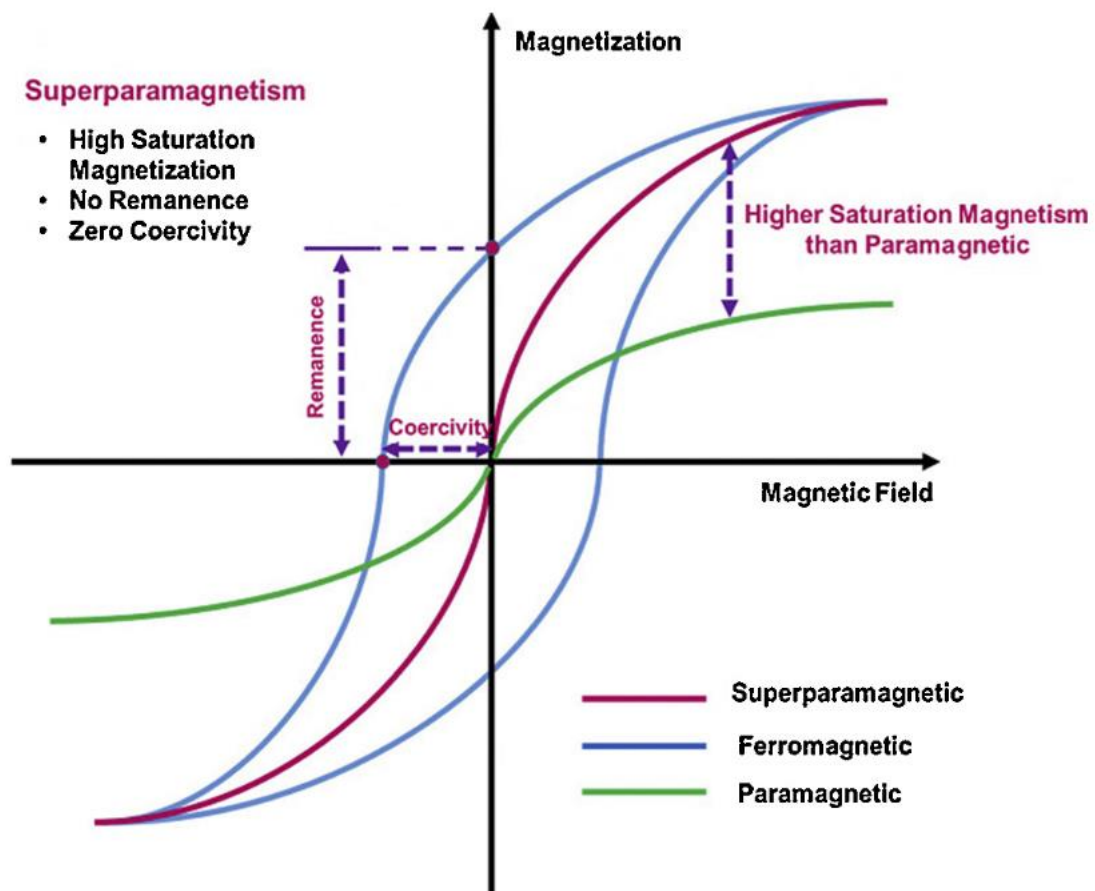


Figure 7: Magnetization characteristic of paramagnetic, ferromagnetic and superparamagnetic materials (via L. Mohammed et al. 2017)

The particle size to achieve superparamagnetic behaviours is in the order of magnitude of tens of nanometres [47], in literature is reported that MNPs to exhibit superparamagnetism should be smaller than 20 nm [48].

This behaviour is one of the reasons why MNPs are so intensely investigated lately: it allows to simply collect them employing an external magnet. Moreover, they are non-toxic and have a high surface area-to-volume ratio, which enables interaction with various types of chemicals [39], [49].

In the following subchapters the main synthetic pathways, functionalization techniques and application are briefly discussed.

2.1.1. MNPs synthesis

There are several methods for MNPs synthesis, starting from the less common to the most used, synthesis routes can be divided into the three following categories [39], [40], [50]:

- (i) biological methods: green approaches with a slow rate of synthesis [51];
- (ii) physical methods: elaborate procedures, unable to control the size of the particles [39];
- (iii) chemical methods: simple and cheap methods, through which size, composition and shape can be managed [39].

2.1.1.1. Biological methods

Currently, biological methods are the least used but are receiving a lot of attention as green alternatives to physical and chemical techniques.

They can be classified into four groups:

- Protein-mediated processes are the most used biological method, they exploit proteins of different origins as reducing and stabilizing agents for the green production of metal nanoparticles [14], [15]. To produce iron oxide nanoparticles horse spleen apoferritin is used, the reaction takes place in a buffer solution under an inert atmosphere and continuous stirring [54].
- Bacteria-mediated production uses inorganic materials often produced by microbes in nanoscale dimensions. Microbes survive toxic heavy metals through detoxification, achieved by reduction or precipitation of metal ions, these are retrieved to obtain metal nanoparticles. Detoxification can be achieved by intracellular bioaccumulation or extracellular biomineralization, biosorption, complexation or precipitation and so further step to retrieve metal nanoparticles are necessary [51].
- Fungi-mediated production exploits the same mechanisms as bacteria, but fungi present a set of advantages such as pressure and agitation resistance and easier management and handling of cultures and metabolites [51].
- Plant-mediate processes are also under investigation, they can use living plants (intracellular) or plant extracts (extracellular) to obtain metal nanoparticles. The produced nanoparticles are similar in shape and size to those produced via traditional physical and chemical methods [55].

Although these methods are more environment-friendly, the particles produced might be less stable, non-uniform and more agglomerated; for this reason, there are few reports on the biological agent-mediated synthesis of iron oxide nanoparticles [40].

2.1.1.2. Physical methods

Physical methods are also called top-down production processes since the production is from macroscale to nanoscale [56], the main ones are listed below.

- Vapour-phase deposition forms nanoparticles through the supersaturation of the precursor molecules present in the gaseous phase or by the consolidation by thermal treatment of composites onto a surface in an inert atmosphere. This method yields rough, non-uniform and poor adhesive nanoparticles but these are purer if compared to liquid-based techniques [57].
- Pulsed laser ablation, for iron oxides nanoparticles, consists of the ablation of the bulk material of an iron precursor in a container with a solvent through the use of a laser beam with known parameters such as intensity, wavelength, diameter etc [40].
- Laser-induced pyrolysis consists in heating an iron precursor gaseous mixture with a laser to produce dispersed iron oxide nanoparticles through combustion. Obtained particles are small but non-uniform and so have a broad size distribution [58].
- Power ball milling consists of the high-energy collision between powdered mixture and balls present in the mill. This method provides fine, uniform oxide nanoparticles with good dispersion. Final nanoparticles characteristics depend mostly on the rotational time and speed of the ball mill [40].
- Electron beam lithography exploits a beam of electrons emitted in a patterned manner upon a film or resin-coated substrate. This technique gives small-sized particles but has high production cost and is a time-consuming process [59].

Common drawbacks of physical pathways for the production of nanoparticles are the high process cost and the difficulty in controlling shape and size distribution [39].

2.1.1.3. Chemical methods

Chemical methods are the most used ones thanks to their simplicity, efficiency and reproducibility as well as better nanoparticles' chemical homogeneity [41]; these techniques are commonly called bottom-up processes since the production is from atom scale to nanoscale [56].

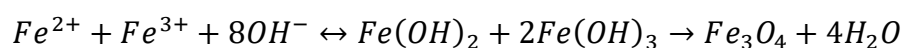
- The hydrothermal method is performed by dissolving the precursors in an aqueous solution with the surfactants agents and sealing in an autoclave [50]; in this method, iron oxide nanoparticles are formed through crystal growth under high temperature and pressure conditions [40].
- The microemulsion technique uses two immiscible phases (oil and water) to form nanoparticles in presence of a stabilising agent, which allows the formation of a monolayer at the interface. Varying the concentration of precursors, solvents and surfactants it is possible to control MNPs shape and size [50].
- Thermal decomposition consists of the high-temperature decomposition of organometallic precursors using organic solvents and surfactants. The main process

parameters to control size and morphology are the ratios of the starting compounds, solvents and surfactants [46].

- Sonochemical synthesis of nanoparticles exploits the cavitation bubbles produced by ultrasound, which can transform the reactants into products at ambient temperature. Managing irradiation time and power the shape and size of NPs can be modified [50].
- Co-precipitation is the most used technique [39] and the most promising one due to its ease of implementation and use of less hazardous chemicals and procedures [41]. This method employs an alkaline solution to precipitate metal ions in an aqueous medium under an inert atmosphere. There are two main co-precipitation methods: (i) partial oxidation of ferrous hydroxide suspension followed by co-precipitation [60]; (ii) stoichiometric mixtures of ferrous and ferric hydroxides in alkaline aqueous solution [61].

In choosing chemical methods, the trade-off is between common drawbacks such as the formation of intermediates, presence of impurities, and risk of colloidal agglomeration [41] and the typical advantages represented by low production cost, high yield, and the possibility to tune size and shape [39].

The chemical co-precipitation was selected for this work based on the advantages described above, therefore it will be expanded hereby. The general process for the preparation of MNPs via the co-precipitation method includes the use of $FeCl_2 \cdot 4H_2O$ and $FeCl_3 \cdot 6H_2O$ as raw materials and NaOH (or $NH_3 \cdot H_2O$) as precipitating agent [62]. The general reaction mechanism is the following one [41]:



The reaction was originally designed to mix Fe^{2+} and Fe^{3+} in the stoichiometric ratio 1:2. Anyway, it has been proved that the optimum molar ratio for the reaction is 1:1.75 [62].

To achieve complete precipitation a pH range between 8 and 14 is necessary [41], and the reaction should be performed under an inert atmosphere to prevent the oxidation of Fe^{2+} and so keep the fixed molar ratio [38].

Parameters that influence the shape and size of MNPs synthesised via co-precipitation are pH value, reaction temperature, stirring rate, and type of alkali solution [63]. Chin-Hua et al. (2008) demonstrate that increasing the temperature from 25° C to 100° C lead to higher crystallinity and larger grain size. They also proved that, on the contrary, an increase in stirring rate from 400 rpm to 1000 rpm causes a decrease in crystallite and particle size [38]. The influences of pH and the type of alkali used were investigated by some papers producing contrasting conclusions. Among the retrieved articles Mascolo et al., 2013 [64] report a decrease of mean dimension increasing the pH from 10.3 to 12.8. Contrarily, Mahdavi et al., 2013 [65] and J. Sun et al., 2007 [66] observe a decrease in dimension increasing the pH up to eleven, and a decrease in dimension further increasing the pH over eleven. Finally, Indrayana, 2019 [4] concludes that an increase in sodium hydroxide concentration results in larger particles. In the retrieved literature, a comprehensive study comparing different alkali at

different pH levels is missing, therefore the effect of this crucial parameter is still unclear especially in relation to other factors.

2.1.2. MNPs functionalization

Oxidation does not only affect Fe^{2+} but it is also one of the major issues mining the stability of MNPs. Under ambient conditions, rapid oxidation of the surface of MNPs takes place, leading to the formation of thin oxide layers that change MNPs properties [46]. The other big problem linked to the bare MNPs is the agglomeration [39]. Their surfaces tend to interact through hydrophobic interactions and van der Waals forces, causing aggregation and consequently the formation of bigger clusters [43]. This results in aggregates of increased size, thus the advantages linked to a high surface area-to-volume ratio are lost.

To avoid, or at least reduce, both oxidation and agglomeration the common practice is the coating, or functionalization, of the surface [67]. Functionalization can be performed using organic or inorganic compounds, polymers or small molecules. The choice is made based on the final application of the MNPs [39]. Usually, polymer or inorganic coatings are preferred when oxidation is the main concern, or when toxicity or pollution problems, arising from the core, must be prevented [68]. Despite this, surface functionalization can also have negative impacts on the activity and properties of MNPs [67], for example, can reduce saturation magnetization [69].

2.1.2.1. MNPs functionalization with APTES

A widely spread molecule for functionalization of MNPs is (3-Aminopropyl)triethoxysilane, commonly called APTES and represented in Figure 8.

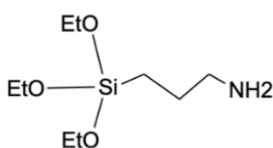


Figure 8: (3-Aminopropyl)triethoxysilane (APTES)

This molecule has been used for coating MNPs as it is [23], [24], or after hydrolyzation reaction [10][25], in both cases with excellent results.

Can et al. (2009) [71] show how the superparamagnetic behaviour is retained when MNPs are functionalized with APTES, and the same is demonstrated by Mahmad et al. (2020) [73] when using hydrolysed APTES.

Wu et al. (2008) [43] findings are also in line with this observation and show a slight dimensional increase in the average diameter when MNPs are functionalized, but the original saturation magnetization is almost completely retained. Authors conclude that APTES is

prone to maintain both morphology and properties of bare MNPs while contrasting oxidation and agglomeration [43].

2.1.3. MNPs applications

MNPs can be used in various ways and in different fields thanks to their peculiar properties. They have found a large application in the biomedical and health care sector, for example, they are used as drug delivery systems, magnetic resonance image (MRI) agents, nanocarriers for vaccination [39]. Feng et al. (2008) explain the use of MNPs for MRI [72], Karade et al. (2021) test the use of MNPs coated with APTES for anticancer drug delivery and controlled release in cancerous environments [74]. A comprehensive review about the use of MNPs for cancer-related application by Kandasamy et al. (2015) is available [50].

MNPs have been also successfully used as heterogeneous catalysts for Fenton-like reactions [75], [76].

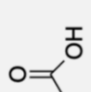
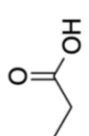
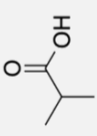
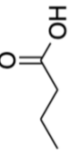
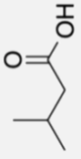
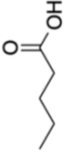

Environmental remediation is another discipline in which MNPs are largely applied, thanks to the high surface area-to-volume ratio they are optimal adsorption means [77]. Elmobarak et al. (2021) successfully use MNPs to recover oil from oil-in-water emulsion produced during oil and gas extraction [78]; Liu et al. (2008) and Shen et al (2009) both uses MNPs for treating wastewater, removing toxic heavy metals such as Cu(II), Pb(II), Ni(II), Cr(VI) [77] [79]; Mahmad Rozi et al. (2016) use them for extraction of polycyclic aromatic hydrocarbons in sewage sludges and landfill leachates [49].

Among the retrieved literature, no researches on the use of MNPs for the recovery of VFAs were present.

2.2. VFAs: characteristics and recovery from waste

Carboxylic acids are organic acids extensively used on large scale in the chemical and food industry [80]. The market share of organic acids was estimated to be ca. 6 billion US\$ in 2015 [81]. VFAs are linear saturated short-chain carboxylic acids [82]; some author considers VFAs only carboxylic acids with five or fewer carbon atoms [83], while others extend the definition up to eight carbon atoms [84]. In this work, the term VFAs will be used to address monocarboxylic acids with two to six carbon atoms, namely: acetic, propionic, iso-butyric, butyric, iso-valeric, valeric, and caproic acids. An overview of their main chemical properties along with some market information is shown in Table 5.

Table 5: VFAs chemical properties, market size and indicative prices. ^a Ramos-Suarez et al. (2021), ^b Zacharof (2013); European data about market size or prices weren't found, USA data are reported to give a general idea.

VFA	Chemical Structure	Molecular mass ^b [g/mol]	Density at 20°C ^a [g/mL]	Melting point ^b [°C]	Boiling point ^a [°C]	pKa ^a	Us production in 2016(Mt) ^a	Average price (usd, \$ kg ⁻¹) ^a
Acetic		60.05	1.05	16.6	117.9	4.79	1224-2449	0.89
Propionic		74.08	0.99	-21	141.1	4.87	11-17	2.20
Isobutyric		88.11	0.95	-47	154.4	4.84	–	2.75
Butyric		88.11	0.96	-7.9	163.7	4.82	1.13-2.27	2.55
Isovaleric		102.13	0.93	-29.2	176.5	4.77	–	–
Valeric		102.13	0.94	-20	186.1	4.82	0.45-0.91	4.63
Caproic		116.6	0.93	-3.4	205	4.88	–	2.5 ^b

Besides being important commodity chemicals themselves [85], VFAs are essential building blocks in the pharmaceutical, food, and chemical industries [80], [86] and for this reason are attractive platform chemicals.

Acetic acid is used in the chemical industry to manufacture paint, rubber, plastics, synthetic fibres, textile finishes, pesticides, polymer emulsions, paper coatings, and it is one of the major components of flavours, acidity regulators, and preservatives used in the food and beverage industries [86]. Still, the biggest acetic acid end users are the manufacturers of vinyl acetate, monochloroacetic acid, acetic anhydride, and acetate esters; these are produced by the acid-catalysed reaction of the acid with an alcohol (ethanol, methanol, propanol, and butanol), producing their respective acetate [81].

Propionic acid is used as a calcium and sodium salt in herbicides, flavours, fragrances, emulsions, environmentally friendly solvents for coating formulations, artificial fruit flavours, modified synthetic cellulose fibres, preservatives for food, and in animal feed [86].

Butyric acid is a valuable biodiesel source also used in the animal feed industry as a supplement and an antibiotic [86].

Caproic acid can be applied as an antimicrobial agent in the pharmaceutical industry, additive in animal feed for poultry and pigs, flavour additive in the food industry, feedstock for the chemical industry, and a possible precursor in the production of biofuels [87].

Nowadays, about 90 % of VFAs are produced via chemical routes that use petrochemical feedstock [88]. For example, acetic acid is produced by carboxylation of methanol even though there are bio-based production methods, but they have lower productivities [86]. Butyric acid is produced starting from the oxo synthesis of crude oil to have propylene, from which butyraldehyde is obtained and then oxidised to butyric acid [86].

These methods have a negative environmental impact. For example, the emissions of carbon dioxide from the petrochemical production of acetic acid have been reported to be 3.3 t CO₂ eq /t [86]. These current production processes face the major issue of resources depletion and lack of environmental sustainability [36], [85]. To face these issues the emerging circular economy approach can be useful [37], this disruptive new paradigm shifts the focus to recovery, reuse, and recycling, redesigning production systems so that they keep the materials and product in use and regenerate natural resources.

In this scenario, an alternative path for VFAs production is taking hold: the Carboxylate Platform. This term refers to the production of chemicals and fuels from biomass [85], [89], [90]. An extensive number of studies are in progress to discover or improve technologies that enable the production of chemicals, such as VFAs, from waste to reduce the carbon footprint [91]–[96]. Fermentation enables the production of chemicals from waste and renewable resources with high efficiency, and potentially at a low cost [96].

The use of food wastes to produce these important platform chemicals can improve waste management, limit the use of non-renewable resources, minimize the environmental issues associated with these wastes (paragraph 1.1) and create added value.

The Carboxylate Platform seems to be a prosperous field for two main reasons: VFAs commercial costs and value have increased due to the large increment in costs of key

petroleum-derived raw materials, energy and transportation costs [36], also non-fuel compounds are generally priced fifteen times higher per ton than fuels [89], so they represent an economically advantageous opportunity.

Nevertheless, the economics and sustainability of biochemical production are often weakened by the expensive pre-treatments and purification processes needed. Production and recovery of compounds from a complex substrate, such as fermented food waste, require a strategy that includes both the conversion of non-ideal substrates and the targeted separation of products from fractions with overlapping physicochemical characteristics.

In the specific case of VFAs, the total cost of integrated production and recovery systems is mainly dominated by the upstream production, and about 30–40 % of the total cost is contributed by the downstream VFAs recovery processes [85]. Recovery refers to the operations needed to extract VFAs from the original mixture [81], for example, a waste stream or a fermented sludge. Recovery and separation technology is recognized as a major challenge within the Carboxylate Platform [89]. The technology for the separation of organic acids from wastes or complex streams, to produce high-quality organic acids with a high degree of purity, has to be energy efficient [36].

These potentialities and hurdles fuelled research and numerous methods for the recovery of VFAs have been developed, investigated, and proposed during the last decades; these will be briefly described in this chapter, and the literature supporting them will be presented.

2.2.1. Literature research method

To frame the main trends and concepts linked to VFAs recovery from wastes, a preliminary snowball search was conducted. From it emerged that different keywords are used in literature to address the topic, mostly depending on the type of downstream process used: separation, recovery, extraction, and so on. To be the most comprehensive possible for the systematic review, we decided to use the most common keywords identified during the snowball search. All titles and abstracts of the results were investigated and only the pertinent documents were read entirely and classified. Anyway, the number of relevant scientific publications is very large and for this reason, only part of them will be cited.

The search was conducted on the Scopus database using the following query string:

TITLE-ABS ((extraction W/2 vfa) OR (separation W/2 vfa) OR (recovery W/2 vfa) OR (extraction W/2 "Volatile fatty acids") OR (separation W/2 "Volatile Fatty Acids") OR (recovery W/2 "Volatile Fatty Acids") OR (extraction W/2 "carboxylic acids") OR (separation W/2 "carboxylic acids") OR (recovery W/2 "carboxylic acids") AND waste).

It resulted in 89 documents of which 40 were selected as pertinent, among these 5 are literature reviews.

2.2.2. Results classifications

By looking at the distribution of documents by year it can be noticed that the topic is not completely new for researchers. Anyway, as shown in Figure 9, it has gained interest in the last decade resulting in a visible increasing trend. Probably the increasing concern for environmental issues is pushing the research in this direction.

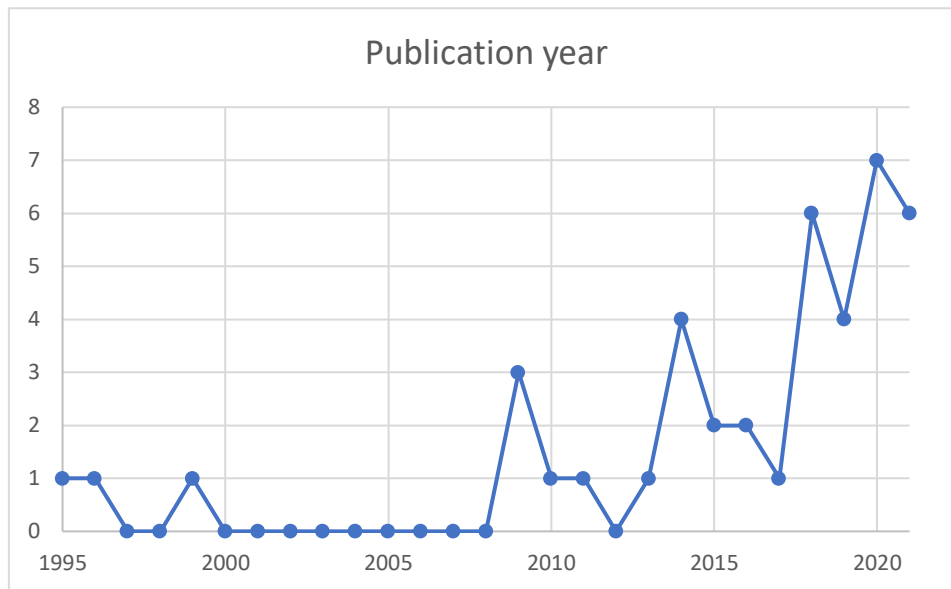


Figure 9: Publications' distribution over time, expressed as number of articles per year.

An interesting detail to be noticed is that almost half of the documents analysed work with synthetic aqueous VFAs solutions and the other half with fermented food waste (Figure 10). This could be interpreted as a tendency towards the implementation of real cases and processes in the near future. Currently, biochemical production of acetic acid is already at the industrial stage [97], the one for propionic [98] and butyric acids [99] it is at the design stage, namely an early phase of the process development.

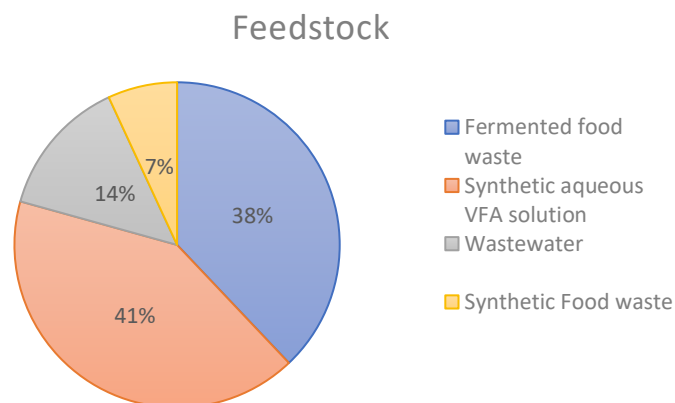


Figure 10: Percentage of articles using a determined feedstock.

For the VFAs recovery or separation process, three main techniques were identified: liquid-liquid extraction (LLE), adsorption, and membrane separation. The classification of each article into one of these groups is shown in Figure 11. These categories are in line with those individuated by the literature reviews [36], [80], [81], [86], [100].

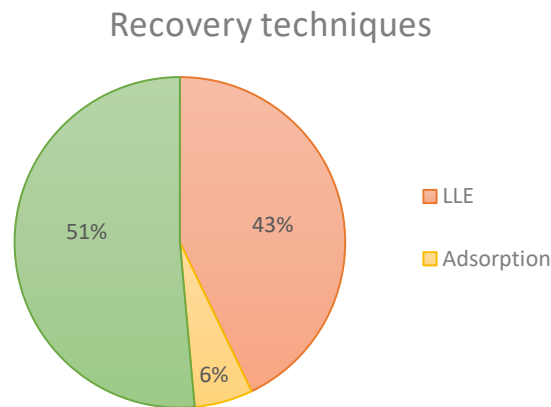


Figure 11: Percentage of articles using a determined recovery technique.

2.2.3. Liquid-liquid extraction

LLE is a purification method that uses two different and immiscible liquids to separate compounds based on their relative solubilities [86]; the target product is selectively transferred from one phase to the other [35].

LLE is popular for the recovery of VFAs from dilute aqueous solutions because it provides an effective separation [86]. It is one of the first methods proposed, present in literature since the 1990s, and it has been the most studied technology for the primary recovery of carboxylic acids [80]. Specifically, LLE results to be the most practical and feasible option to recover carboxylic acids from an aqueous solution where the acid content is below 50 wt. % [96]. Since this threshold is significantly higher than the acid content of waste streams and fermented broths, LLE is the most suited and used technique.

LLE is an affinity-based separation technique, this means that it exploits affinity agents that target the carboxylic acids to selectively separate them [96]. In the case of VFAs recovery, these agents are usually organic solvents that are immiscible in water and able to interact with VFAs [36]. The affinity agents offer a high distribution coefficient that enables the extraction of the desired substance. The distribution coefficient for a generic VFA (D_{VFA}) is defined as the ratio between the concentration of VFA in the extract and in the raffinate (1):

$$D_{VFA} = \frac{[VFA]_{extract}}{[VFA]_{raffinate}} \quad (1)$$

Since the extraction is usually performed on aqueous streams, it is also important to know the selectivity (S_{VFA}) of the solvent for the VFA in presence of a third species X (water), it is defined as the ratio between the distribution coefficient of the VFA and of the third species (D_X) in the solvent (2):

$$S_{VFA} = \frac{D_{VFA}}{D_X} \quad (2)$$

However, the efficiency of VFA recovery with LLE depends also on a set of operational parameters such as pH, targeted VFA or VFAs, extractant type, and composition of the VFAs-rich stream [86].

After the extraction of the organic acid, solvents are regenerated to be recycled in the extraction process. Therefore, two different cyclic phases can be identified in an LLE:

- 1 Separation of desired compounds from the feed stream;
- 2 Regeneration of the solvent to recycle it for further separations and to recover the separated compounds.

P. Saboe et al. (2018) demonstrate the complete recovery of acids from the extractant and recyclability of the organic phase through multiple extraction–distillation cycles while working with wastewater and beet-pulp from a processing factory [101].

Solvents used for LLE can be grouped in two categories according to the interaction they have with the target molecules:

- (i) Physical solvents have weak interactions and so do not form complexes with the molecules. In the specific case of VFAs, some examples of such solvents are ketones, alcohols, and esters [84], [96].
- (ii) Chemical solvents have strong interactions and so form complexes with the molecules. For VFAs extraction amines and organophosphorus compounds are commonly used as chemical solvents [82], [102].

These last usually achieve higher distribution coefficients and, as a result, more efficient extractions, but the regeneration step is more challenging [96].

Another classification adopted is the one based on the solvent boiling point in relation to that of the desired compound. A difference in boiling points allows to effectively separate the product from the solvent using distillation. This property is crucial and critical to the success of the process, it strongly influences it and is not linked to the chemical or physical nature of the solvent [80]. This parameter allows to distinguish:

- i. High-boiling solvents, with a boiling point higher than that of the desired compound. The advantage of this group is that, since the flow of the solvent is typically higher, this configuration has a lower energy request during the distillation [96]. Conventional high boiling point solvents are large amines or organophosphorus compounds, that interact strongly with VFAs causing a problematic regeneration step [103].

- ii. Low-boiling solvents, with a boiling point lower than that of the desired compound. These solvents result to be more energy-intensive [96]. Conventional low boiling solvents are ketones, alcohols, ethers, and they are used for high-boiling point carboxylic acids, e.g. lactic or succinic acids.

Special reference also needs to be made to the so-called switchable solvents; these solvents are able to switch their chemical identity (i.e. polar or non-polar) thanks to an external trigger, like CO₂. Two examples are piperylene sulfone or ionic liquids based upon 1,8-diazabicyclo[5.4.0]-undec-7-ene (DBU) and N,N,N',N'-tetramethyl-N''-butylguanidine (TMBG) and an alcohol [104][105].

Some of the traditional extractants mentioned until now are flammable, volatile, or toxic, which significantly limit their applicability; therefore it is necessary to develop a new generation of more environmentally friendly and safer solvents, that can be easily recovered [106]. Some innovative high-boiling solvents, objects of study in the last years, are ionic liquids (ILs) and deep eutectic solvents (DESs) [96].

ILs are defined as compounds completely composed of ions with a melting point below 100°C [63]. For undissociated acids, it seems that no clear advantage comes from the use of ILs. They do have a higher distribution coefficient than amine-based extractants, but the acid-back extraction is inefficient, requiring strong acids or alkali [80]. Moreover, the relatively complicated synthesis process and expensive raw chemicals make ILs difficult to apply to large-scale industrial applications [106].

Conversely, DESs are an emerging class of mixtures characterized by significant depressions in melting points compared to those of the constituent components, and for this reason, promising in tailored applications [83], [107]. DESs have been widely considered due to their biodegradability, easier preparation, lower cost, and more environmental benignity [106]. Among the articles reviewed, the work by D. Rodriguez-Llorente et al. (2019) come to the conclusion of the non-reusability of (C₈OOH+thymol) and (C₈OOH+menthol) DESs when performing cycles of extraction [108].

Finally, based on the solvent nature and the targeted VFA, or VFAs mixture, various sequences of operations can be designed to implement the extraction cycle. The main process configurations for LLE are:

- a. Extraction and distillation with a high boiling solvent. It is applicable only to volatile carboxylic acids and allows producing a highly concentrated acid stream at a relatively low cost. Solvents are obtained at the bottom of the distillation column, therefore the energy requirement is dictated by the quantity of VFAs to evaporate, resulting in a direct proportionality between cost and acid concentration [109].
- b. Extraction and distillation with a low boiling solvent. These solvents are mainly used and suitable for the purification of non-volatile carboxylic acids; in these cases, the solvent is the top product of the distillation column, but these applications are beyond the scope of this work.

- c. Extraction and back-extraction. The product obtained with this technique is a low-purity carboxylic acid stream that needs further purification (either by dehydration or crystallization). When water is used for back-extraction the addition of an alkali increases the carboxylate content of the resulting solution. This leads to the production of carboxylate salts and requires acidification to obtain the carboxylic acid but generates also salt by-products. This step represents an additional cost for the extraction.

In literature different techniques are reported to enhance the LLE of VFAs, E. Reyhanitash et al. (2018) have written a comprehensive review dedicated to them [96].

2.2.3.1. Reactive extraction

The term “reactive extraction” is used in the field to indicate LLE operations during which association complexes or chemical compounds are formed as a result of intermolecular or chemical interactions between the solute and the extractant [80].

Lately, the interest has shifted from single-component solvents to tailor-made multicomponent solvents in which the key characteristics are enhanced and optimised. For this reason, modern extraction solvents for carboxylic acids are generally formed by an extractant, a modifier, and a diluent. The extractant is the active component primarily responsible for the transfer of the target component to the solvent phase. It is usually viscous or solid so the diluents are used to improve the physical properties like surface tension and viscosity [110]. In some cases also a modifier, to improve the solvation of the complex can be added [80].

Some examples of applications of reactive extractions can be found in the works by A. Keshav et al. (2009) [110], S. Kumar et al. (2010) [111], V. Inyang et al. (2020) [112]. A. Keshav et al. report that the extraction is improved by the increase of the volume ratio of the organic phase and the use of mixed extractants [110]. S. Kumar et al. (2010) demonstrate that the extraction power of the amine/alcohol system is remarkably higher due to the simultaneous effect of the physical extraction and chemical interaction through hydrogen bonding [111]. V. Inyang et al. (2020) found optimal conditions for process variables, such as temperature and acid concentration, that result in an efficiency of 93.25 % [112].

LLE is defined as the most efficient and economic method from A. Gaeta-Bernardi et al. (2015) [113], experimental recoveries of 61-98 % [82] and 75-80 % [114] are reported in the literature. However, E. Reyhanitash et al. (2018) highlight how LLE energy demand is strictly connected to acids concentration and can easily become unprofitable when the feedstock is very diluted, as for VFAs derived by fermentation [96].

2.2.4. Adsorption

Adsorption is a common technique used for product recovery from bioprocesses [35]. It is a surface-based process that involves the adhesion of compounds, ions, or molecules from a

gas or liquid to a surface [86]. It exploits the formation of an interaction between the target compound and a selective adsorption resin, namely the surface [35].

Specifically for VFAs recovery, the adsorption process involves the passage of a VFAs-rich stream through a column of adsorbent, which is usually an ion exchange resin [86]. Adsorbents for VFAs recovery are classified according to their electric properties into [80]:

- 1 Weak anion exchangers, that become charged over a limited range of pH;
- 2 Strong anion exchangers, that become charged over a wide range of pH;
- 3 Non-ionic exchangers, that work through hydrophobic interactions.

Resins can entrap VFAs via ion exchange when the acids are in the dissociated form ($\text{pH} > \text{pK}_a$) or via hydrophobic interactions when they are in free acids forms ($\text{pH} < \text{pK}_a$) [35]. This possibility certainly increases the range of applicability of adsorption, since the resin can be specifically chosen according to the pH of the fermentation broth or the waste stream that is used as feedstock, or vice versa.

A lot of VFAs adsorption investigations focused on amine-based anion exchange resins [35], [115]. Rebecchi et al. (2016) concluded that tertiary amine-functionalized resins are the best due to their high ion exchange performances and low prices [116]. Instead, Reyhanitash et al. (2017) found out that the polystyrene-divinylbenzene non-functionalized resin to have the highest VFAs adsorbing capacities, relying on hydrophobic interactions. This higher capacity could also be explained by the fact that this resin, unlike functionalized ones, does not co-adsorb mineral acids, which are commonly present in fermented wastewaters. Also, E. Fufachev et al. (2020) adsorbed waste-derived VFAs on a non-functionalized polystyrene-divinylbenzene resin characterized by high selectivity, efficiency, and stability [88].

A disadvantage of this technique is that adsorbents are prone to fouling, and this phenomenon can limit the operational lifetime of the material and the whole process [80]. Key factors such as diffusivity, ion selectivity, exchange kinetics, and osmotic stress resistance depend on the morphology of the bed. The most used for this application are microporous (or gel-type polymer) and macroporous (or macro-reticular polymer) ion exchangers. Indeed, polymers are preferred as supporting materials because they don't suffer from availability problems or mechanical instability, as zeolite or silica [80], [117].

When using adsorption for VFAs recovery, also a desorption step is necessary. It is needed both to retrieve VFAs and to regenerate the adsorbent so that it can be further used. For this key step, various possibilities can be found in the literature. S. Rebecchi et al (2016) use ethanol and water for solvent-based desorption; ethanol proved to be a better solvent with respect to water, reaching a desorption rate of 67 % [116]. C. S. López-Garzón and A. J. J. Straathof (2014) report an alkaline solvent-based desorption process, where water action is improved by the addition of NaOH; this leads to the retrieval of VFAs as sodium salts, which requires an acidification step to have free VFAs [80]. S. M. Husson and C. J. King (1998) propose a solvent-based desorption step with trimethylamine in an organic solvent; this leads to the formation of a new acid-base complex prone to thermal decomposition. After the

thermal treatment, the acid remains in solution and the vaporized trimethylamine is reabsorbed in the corresponding solvent to be reused [118].

Regarding the desorption step, E. Reyhanitash et al. (2017) report the use of nitrogen stripping at elevated temperature as an effective technique [119]. A quite different example is that of Cabrera-Rodríguez (2017), this work develops a CO₂-expanded alcohol process able to directly convert VFAs to esters [120]. This is one of the very few examples in which end-product use was considered prior to VFAs recovery development [35].

At the end of solvent-based desorption, the column is full of solvent and so a third regeneration step is needed. With this step, the actual re-use of the resin is allowed. If the desorption step has been carried out with methanol or ethanol a thermal regeneration is possible, ethanol is also easy to be recovered through distillation and re-used [116]. In the other cases, a washing step at a high temperature is usually proposed. In general, high energy consumption is associated with the regeneration step, which makes the adsorption process very expensive [36].

2.2.5. Membrane processes

Membrane technology is based on a simple mechanical separation process through a semi-permeable medium, namely the membrane [81]. Membranes allow a selective separation of species and for this reason, represent a potentially effective treatment for the removal and recovery of VFAs [36]. Membrane processes can be driven by:

- 1 pressure;
- 2 concentration gradient;
- 3 electrical field.

Among the articles analysed, the most investigated technique results to be the electrical field-driven (Figure 12).

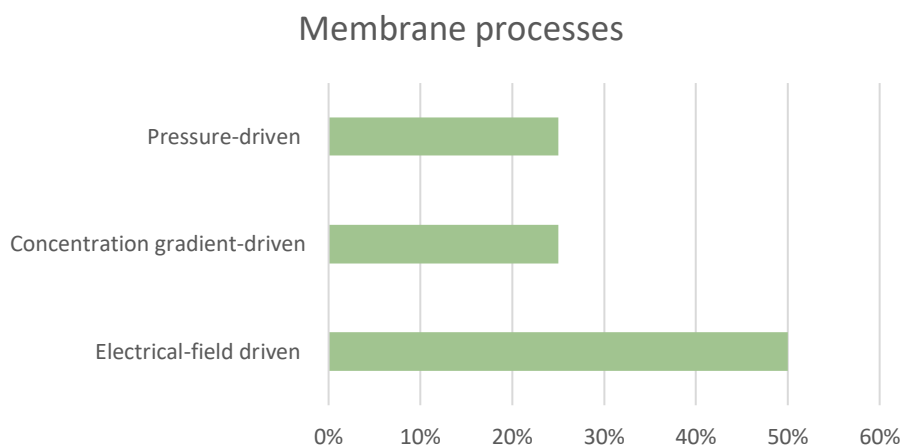


Figure 12: Classification of articles focused on membrane processes according to the driving force; data are expressed as percentage of the total number of retrieved articles focused on membranes.

2.2.6. Pressure-driven membrane processes

In pressure-driven membrane processes, a pressure exerted on the solution at one side of the membrane serves as a driving force to separate it into a permeate and a retentate.

They are classified into four main groups, with different operating conditions and applications, according to the retained particle size [81]:

- I. Microfiltration (MF): uses symmetric microporous membranes with a pore size in the range of 0.1-10 μm and a driving force of 1-5 bar;
- II. Ultrafiltration (UF): uses asymmetric microporous membranes with a pore size in the range of 1-10 nm and a driving force of 1-10 bar;
- III. Nanofiltration (NF): uses thin-film membranes with a pore size in the range of 1-5 nm and a driving force of 10-30 bar;
- IV. Reverse osmosis (RO): uses asymmetric skin-type membranes with a pore size in the range of 0.5-1.5 nm and a driving force up to 200 bar.

Each technology is used with a different purpose, for example, the clarification or the sterile filtration use microfiltration while the separation of salts and micro solutes require reverse osmosis. Interesting findings regarding these methods are available in literature and some are condensed below.

Zacharov and Lovitt (2014) focused on demonstrating the possibility to effectively use NF to separate and recover VFAs from complex streams, concluding that pre-treatment and microfiltration are essential for a good NF operation and that the use of alkali treatment in the digester effluent enhance NF retention [121]. Instead, Bona et al. (2020) compare the use of NF and RO as pressure-driven membrane processes; after a statistical examination, they conclude that RO has the highest average retention (84 % with 6 bar of transmembrane pressure) whereas NF provides a high selectivity between different VFAs along with the highest permeance [122]. R. van Reis and A. Zydney (2007) claim that, as a general rule, NF can be used for the recovery of valuable products while RO performs better in the recovery of high-quality water to be re-used in the process [123].

Pressure-driven membranes are investigated also as *in situ* solutions. Parchami et al. (2018) and (2020) assess the possibility to use an immersed membrane bioreactor for the stable production and in situ recovery of clarified VFAs [124], [125]. The membranes proposed in these two works are for UF and require frequent backwashing to avoid an excessive reduction of flow.

In general, pressure-driven membrane processes do not require heating, which makes them much more energy-efficient compared to traditional separation processes, on the other hand, fouling and cleaning cycles represent their main disadvantages [81].

2.2.7. Concentration gradient-driven membrane processes

Vapour permeation membrane contactors (VPMC) and pervaporation are processes driven by partial pressure difference or concentration gradient between the two sides of the membrane [126].

VPMC uses microporous hydrophobic membranes to separate the two phases, the system differs from the conventional MF because it is not pressurised, ions or liquids can't pass through the membrane, there is not a convective flow through the pores, and exclusively volatile species or dissolved gases can be transferred [126]. S. Aydin et al. (2017) assess the recovery of mixed VFAs using a VPMC system with air-filled polytetrafluoroethylene (PTFE) and two tertiary amine extractant filled PTFE membranes [126]. It turns out that the air-filled PTFE is not able to selectively separate VFAs from each other, while trioctylamine-filled PTFE increases the separation as the alkyl chain length grows. According to the authors, this system can be successfully applied to the recovery of VFAs. Also, Yesil et al. (2014) and (2021) investigated the use of VPMC with air-filled PTFE membranes and found that filtration of the fermented organic wastes is essential to prevent cake formation on the membrane and that the optimal condition for the recovery of VFAs is a temperature of 38°C and the use of 0.1 N NaOH solution as alkaline permeate [90], [127].

On the other hand, pervaporation processes are controlled by a sorption-diffusion mechanism, and only volatile species can pass through the selectively permeable membrane [128]. Mass transfer in pervaporation processes follows four consecutive steps: desorption from liquid at feed side, sorption into the membrane, diffusion through the membrane, and desorption into a vapour phase at permeate side [129], [130]. Although there are a lot of recent studies for material recovery through pervaporation [85], few references on VFAs recovery are available. Yesil et al. (2020) studied the pervaporation process for the recovery of VFAs mixture through PTFE, tridodecylamine (TDDA) filled PTFE, and composite silicon rubber/PTFE (PDMS/PTFE) membranes [85]. They observed a higher flux, permeance, and separation factor in TDDA filled PTFE compared to the PTFE. For the composite membranes, a decrease in flux and permeance was noted when membrane thickness was increased, this is probably because diffusion is the only transportation mechanism for this type of membrane [85]. Finally, Bona et al. (2020) studied two different concentration gradient-driven membrane processes, namely forward osmosis (FO) and supported ionic liquid membrane (SILM) [122], both resulted to be effective. The most influencing process parameter is the acid concentration while fouling mechanisms is the authors' major concern but was not investigated yet.

2.2.8. Electric field-driven membrane processes

Electrodialysis (ED) is an electrical field-driven membrane process therefore the solutes targeted for this extraction must be charged particles. Typically, a system consists of alternating cationic and anion membranes through which ions pass selectively [36].

In the conventional ED process, a feed solution of a carboxylate salt is introduced between cation and anion exchange membranes; the cations and anions diffuse in opposite directions driven by electrostatic potential, but they can pass only cation or anion exchange membrane respectively. This leads to a more concentrated solution and a more dilute solution of carboxylate salt [80]. The principle is better illustrated in Figure 13, in real applications the electrolysytic chamber can assume configurations different from the one shown. For example, Zhang and Angelidaki (2015) introduced also bipolar membranes to control pH fluctuations [131].

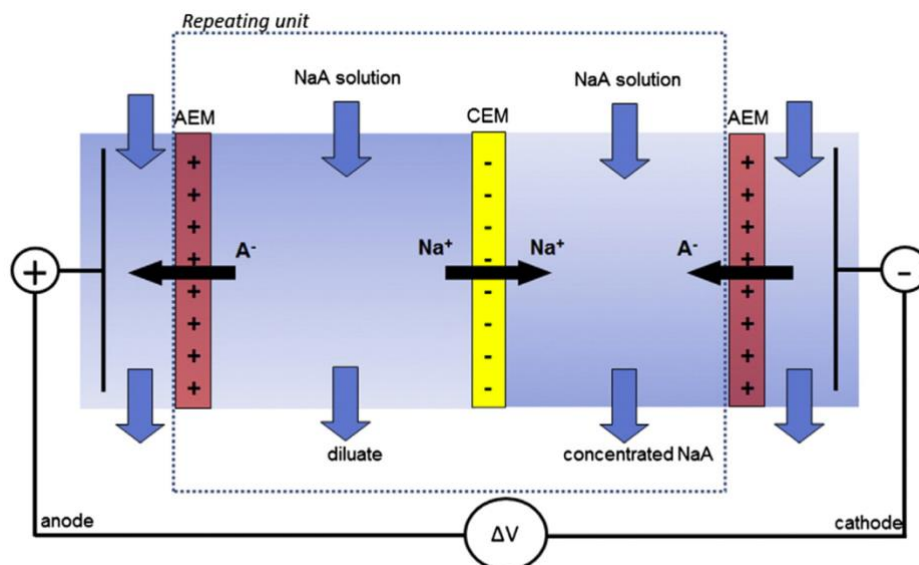


Figure 13: Conventional ED working principle, example of concentration of sodium carboxylate (NaA) solution; where CEM stands for cation exchange membrane, and AEM for anion exchange membrane (image from [80]).

ED technology is widely applied for VFAs separation and recovery [36], indeed in our review, it is the most numerous group among articles regarding membrane processes.

Vertova et al. (2009) demonstrate that ED can be successfully performed on a real wastewater stream, without pre- or post-treatments, to recovery organic compounds while purifying water. The system is said to be energetically and economically competitive, though long-life tests still need to be performed [132]. Wastewater is not the only stream on which ED has been successfully applied, Zhang and Angelidaki (2015) demonstrate, through the treatment of a digestate from a continuous stirred tank reactor, that this technique can manage a wide range of VFAs concentrations. Their experiments lead to simultaneous recovery and concentration of VFAs [131]. Regarding the process parameters, Henandez et al. (2021) observed that during a batch extraction test there is the need to increase the voltage to keep

a constant current and obtain a good recovery, probably because of the reduction in conductivity of the dilute chamber. In particular, it was observed that only caproic and butyric acids were mainly recovered in the oily phase [37].

Even though this technique has proved its validity for the extraction of carboxylates, there are still hurdles for its widespread use. In order to implement these processes industrially it is necessary to achieve improved antifouling characteristics, increased selectivity for co-ions [133], and reduced membrane costs [80].

Chapter 3: Aim of the thesis

This thesis work is framed within the REVENUE project, a multidisciplinary research initiative with the aim of generating valuable products, energy, and bio-fertilizer from urban food waste. The focus of this work will be on two project objectives: the collection and organization of relevant food waste data concerning Italy and specifically the Lombardy cluster, and the development of a method for the separation of value-added products. These last are represented by short-chain carboxylic acids, also referred to as Volatile Fatty Acids (VFAs).

Based on the current research interest in VFAs recovery and the wide applicability of nanoparticles, the aim of this thesis is to propose a novel method for VFAs recovery from fermented food waste through the use of iron oxide magnetic nanoparticles. The underlying idea is to synthesise F-MNPs able to selectively recover VFAs from fermented food waste and then release them for further purification. The strength of this method lays in the high surface-to-volume ratio of the MNPs, and the possibility to separate them using an external magnetic field. A recovery cycle consists of (i) addition of F-MNPs to pre-treated fermentation broth and consequent VFAs capture, (ii) collection of F-MNPs along with attached VFAs, (iii) release of attached VFAs and regeneration of F-MNPs for re-use in further cycles.

This is the first work investigating the innovative separation described above, no literature is yet available on the topic. For this reason, a crucial part of the work was the synthesis and functionalization of MNPs tailored for this application. This was followed by a preliminary study of each separation step, using a synthetic VFAs solution to test the feasibility and the effectiveness of the developed nanoparticles. The work can be divided into six parts:

1. Identification of the optimal synthesis for MNPs.

The synthesis method chosen is the chemical co-precipitation, it consists of the precipitation of MNPs in an alkaline aqueous solution under an inert atmosphere. The aim was to achieve fast magnetic decantation and a transparent supernatant, to this purpose different experimental conditions, such as temperature, stirring rate, and alkali type were tested.

2. Selection and execution of fit-for-purpose functionalization.

(3-Aminopropyl)triethoxysilane (APTES) was chosen because of its amine functional groups. These, bounded to the nanoparticle's surface, will interact with carboxylates and protect MNPs from oxidation and agglomeration, two of their main problems. Silanization reaction was used to bound APTES to hydroxyl groups on the MNP's surface.

3. Adsorption experiments.

A solution with pH = 7 was used to have both protonated amine groups and short-chain carboxylate anions and thus favour the interaction. Different contact times and agitation methods were tested to verify the suitability of the F-MNPs for VFAs

adsorption. The adsorption percentage was obtained from the measurement of VFAs remaining in the solution after contact with the nanoparticles.

4. Desorption experiments.

Methanol and water were selected to perform preliminary release tests by contacting these solvents with F-MNPs bearing VFAs adsorbed on the surface. The desorption percentage was obtained by measurement of the VFAs released into the solvent. These tests verified the suitability of the F-MNPs and provided insight into the strength of the interaction between carboxylates and nanoparticles.

5. Second-cycle adsorption experiments.

After desorption, the nanoparticles were contacted again with the VFAs solution to investigate their behaviour when re-used. The re-usability represents a crucial property to reduce process waste generation and resource consumption, for this reason, it was considered in this preliminary study phase.

6. Optimization of the MNPs functionalization with APTES.

Different experimental conditions, such as molar ratios, temperature, and reaction time, have been tested to study their effect and maximize the number of amine groups present on the surface of nanoparticles. For each test, the functionalization percentage was computed from elemental analysis results. The samples with the highest functionalization percentages and the MNPs were further characterized using scanning electron microscopy (SEM) imaging.

Chapter 4: Materials and methods

4.1. Analytical methods

This section briefly illustrates the methods and instruments used for products characterization. The MNPs and F-MNPs were characterised by dynamic light scattering (DLS), electrophoretic light scattering (ELS), X-ray diffraction (XRD), scanning electron microscopy (SEM), Fourier transform infrared spectroscopy (FT-IR), and CHNS analyses. The evaluation of the adsorption and desorption of VFAs was assessed through gas chromatography (GC).

4.1.1. Dynamic light scattering

DLS is a technique for measuring the size and size distribution of molecules and particles in the submicron region. The motion of particles in suspension causes the laser light to be scattered at different intensities. Through the analysis of intensity fluctuations, the translational diffusion coefficient is derived, and so is the particle size through the Stokes-Einstein relationship [134]. The analysis was performed with a Malvern Zetasizer Nano ZS at a scattering angle of 173° (backscatter) to identify the hydrodynamic diameters of F-MNPs and MNPs produced. The temperature was kept at 25°C and an equilibration time of 30 seconds was provided before each measurement, except for the first measurement for which the equilibration time was 120 seconds. Each sample was analysed three times.

4.1.2. Electrophoretic light scattering

ELS is a technique used to measure the electrophoretic mobility of dispersed particles. This mobility can be converted to Zeta potential to enable the comparison of materials under different experimental conditions. The fundamental physical principle is that of electrophoresis, a dispersion is introduced into a cell containing two electrodes. An electrical field is applied to the electrodes, and particles that have a net charge, or more strictly a net zeta potential, will migrate towards the oppositely charged electrode with a velocity, known as the mobility, that is related to their zeta potential [135]. For this work, the measurements were performed on the same instrument of the DLS, with solution pH ranging from 2 to 12. The temperature was kept at 25 °C and each sample was left equilibrating for 120 seconds before each measurement.

4.1.3. X-Ray diffraction

XRD analysis is a technique that can be used to study the material crystal structure [136]. This is done by irradiating a sample with incident X-rays and then measuring the intensities and scattering angles of the X-rays that leave the material [137]. In this work, the aim was to confirm that the synthesized MNPs were magnetite (Fe₃O₄). X-ray diffraction experiment was carried out by SAMM laboratory at Politecnico di Milano on Empyrean diffractometer by

Malvern Panalytical®, equipped with Cu radiation (K-Alpha1, wavelength = 1.54060 Å) and it was performed at 25°C.

4.1.4. Scanning electron microscopy

SEM is an analysis technique that reveals the sample surface topography thanks to its interaction with a beam of electrons [138]. The tests were performed by SAMM laboratory at Politecnico di Milano with Evo 50 EP Instrumentation (Zeiss, Jena, Germany), samples were sputtered with gold and the analysis was carried out at 15 kV or 20 kV with the probe from 10 pA to 100 pA.

4.1.5. Fourier transform infrared spectroscopy

FT-IR is based on the ability of most of the molecules to absorb light in the infrared region of the electromagnetic spectrum and convert it into molecular vibration. The absorption is characteristic of the nature of the chemical bonds present in a sample [139]. For the analyses, a Varian 640-IR spectrometer equipped with a single bounce ZnSe ATR accessory was used. The attenuated total reflection (ATR) technique was employed, and so the solid powdered samples were directly analysed without treating them with KBr.

4.1.6. CHNS elemental analysis

CHNS is an elemental analysis that provides the rapid determination of carbon, hydrogen, nitrogen, and sulphur in the sample. The basic principle is the combustion process, which converts carbon into carbon dioxide, hydrogen into water, nitrogen into nitrogen gas or oxides of nitrogen, and sulphur into sulphur dioxide. The detection of the gases allows quantifying the carbon, hydrogen, nitrogen, and sulphur initially present in the sample [140]. The analyses needed for this work were performed on a COSTECH ECS 4010.

4.1.7. Gas chromatography

Chromatography is a technique that separates components in a mixture, namely the mobile phase, according to the different interactions they have with the stationary phase [141]. GC analyses for this work have been performed by the IRSA-CNR laboratory in Rome on an Agilent 8860 equipped with a flame ionization detector (FID) and a capillary column DB-FFAP (Agilent J&W). The samples have been filtrated (0.2 µm) and diluted with 10% oxalic acid (0.33 M). The gas carrier used is nitrogen at 4 bar, the injector and detector temperature respectively 250°C and 320°C, while the oven temperature is kept at 60 °C for 1 minute, then increased of 10 °C/min up to 150 °C and finally of 20 °C/min to reach 175 °C.

4.2. Experimental synthesis and procedures

The synthesis of MNPs, the procedure for functionalization, the preparation of the synthetic VFAs mixture, the absorption and desorption tests are described in this section.

4.2.1. Materials

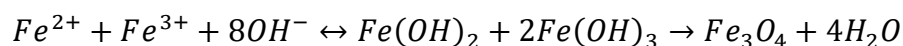
Ethanol (C₂H₆O, MW=46.07 g/mol, ≥99.8%), sodium acetate (C₂H₃NaO₂, MW=82.03 g/mol, ≥99.0 %), sodium propionate (C₃H₅NaO₂, MW=96.06 g/mol, ≥99.0 %), sodium butyrate (C₄H₇NaO₂, MW=110.09 g/mol, 98 %), isobutyric acid (C₄H₈O₂, MW=88.11 g/mol, 99 %), valeric acid (C₅H₁₀O₂, MW=102.13 g/mol, ≥99 %), isovaleric acid (C₅H₁₀O₂, MW=102.13 g/mol, 99 %), sodium hexanoate (C₆H₁₁NaO₂, MW=138.14 g/mol, 99-100 %) and (3-Aminopropyl)triethoxysilane (APTES, C₉H₂₃NO₃Si, MW=221.37 g/mol, 99 %) were purchased from Sigma-Aldrich®, Germany. Colour-fix pH indicator sticks (pH-Fix 0-14, No. 10642751), 25 mm syringe filter (nylon, 0.2 μm, No. 15121499) and heating plate equipped with a thermocouple were obtained by Fisherbrand®. Iron (II) chloride tetrahydrate (FeCl₂·4H₂O), Iron (III) chloride hexahydrate (FeCl₃·6H₂O), sodium hydroxide (anhydrous pellets) and methanol were from Carlo Erba reagents®. Hydrochloric acid (1M, volumetric solution) by Fisher chemical, Fisher Scientific®.

VirTis BenchTop Pro with Omnitronics by SP scientific was used for lyophilisation; LABOROTA 4000-efficient by Heidolph® was used to rotary evaporate F-MNPs and hydrolysed APTES; the centrifuge employed was the Sorvall ST 8 by ThermoFisher Scientific whereas the shaker was the Multi Reax by Heidolph®. Lastly, a neodymium fishing magnet (model: NJD90) by Wukong® was deployed for magnetic decantation.

All reagents and solvents were used as received without further purifications.

4.2.2. MNPs synthesis via chemical co-precipitation

The co-precipitation method for the synthesis of MNP is based on the reaction of iron salts in an alkaline aqueous solution. The reaction mechanism is the following [39], [62], [142]:



S.1. MNPs synthesis with ammonium hydroxide

Following the procedure described by Mahmad Rozi et al. [49], 1.057 g of FeCl₂·4H₂O and 2.523 g of FeCl₃·6H₂O were dissolved in 106.6 mL of deionized water, in a three-necked round bottom flask. The solution was stirred at 80° C and 500 rpm for 1 hour, under a nitrogen atmosphere. After this time, 13.3 mL of NH₄OH (25 % w/w) were rapidly added to the reaction mixture, which was stirred for another 1 hour, and then cooled at room temperature. In Table 6 details about the synthesis are summarised. MNPs were magnetically collected in the

bottom with an external magnet and washed three times with deionised water. Washings consisted of water addition and manual agitation.

Table 6: Synthesis of MNPs.

	Mass [g]	Mw [g/mol]	[mol]	Equivalents	Volume [mL]
FeCl₂·4H₂O	1.057	198.81	0.0053	1	-
FeCl₃·6H₂O	2.523	270.29	0.0093	1.75	-
H₂O					106.6
NH₄OH	3.003	35.04	0.0857	0.0162	13.3

S.2. MNPs synthesis with sodium hydroxide

In a three-necked round bottom flask, 1.057 g of FeCl₂·4H₂O and 2.523 g of FeCl₃·6H₂O were dissolved in 106.6 mL of deionized water. The solution was stirred at 100° C and 400 rpm for 1 hour under a nitrogen atmosphere. After this time, 8.59 mL of NaOH (9.98M) were rapidly added to the reaction mixture, which was stirred for another 1 hour. Then the mixture was cooled at room temperature. In Table 7 quantities and equivalents for the synthesis are presented. MNPs were magnetically collected in the bottom with an external magnet and washed three times with deionised water.

Table 7: Synthesis of MNPs.

	Mass [g]	Mw [g/mol]	[mol]	Equivalents	Volume [mL]
FeCl₂·4H₂O	1.057	198.81	0.0053	1	-
FeCl₃·6H₂O	2.523	270.29	0.0093	1.75	-
H₂O					106.6
NaOH	3.428	40	0.0857	0.0162	8.59

S.3. MNPs synthesis with excess of sodium hydroxide

In a three-necked round bottom flask, 1.057 g of FeCl₂·4H₂O and 2.523 g of FeCl₃·6H₂O were dissolved in 106.6 mL of deionized water. The solution was stirred at 100° C and 400 rpm for 1 hour, under a nitrogen atmosphere. After this time, 33.3 mL of NaOH (9.98M) were rapidly added to the reaction mixture, which was stirred for another 1 hour. Then the mixture was cooled at room temperature. In Table 8 quantities and equivalents for the synthesis are presented. MNPs were magnetically collected in the bottom with an external magnet and washed three times with deionised water.

Table 8: Synthesis of MNPs.

	Mass [g]	Mw [g/mol]	[mol]	Equivalents	Volume [mL]
FeCl₂·4H₂O	1.057	198.81	0.0053	1	-
FeCl₃·6H₂O	2.523	270.29	0.0093	1.75	-
H₂O					106.6
NaOH	13.292	40	0.3323	0.0626	33.3

4.2.3. APTES hydrolysis

According to the procedure described by Feng et al. [72], 10 mL of APTES (0.0427 mol) were added to 40 mL of 0.5 M HCl in a round bottom flask. The content was rotary evaporated in a 45°C bath for 20 minutes, until ethanol was removed. Then the solution was dried under vacuum, at 45°C for 5 minutes. Reagents and quantities used for the reaction are detailed in Table 9.

Table 9: APTES hydrolysis.

	Volume [mL]	Density [g/ml]	Mw [g/mol]	[mol]
APTES	10	0.946	221.37	0.0427
H₂O	20	1	18.01	
HCl	20	1.18	36.46	

When APTES is hydrolysed, a condensation reaction takes place to form a silane polymer. In the hydrolysis reaction, shown in Figure 14, hydroxyl groups (-OH) replace alkoxy groups (-OC₂H₅) to form reactive silanol groups, which condense with other silanol groups and produce siloxane bonds (Si-O-Si). During the reaction ethanol (C₂H₅OH) and water are produced as by-products [72].

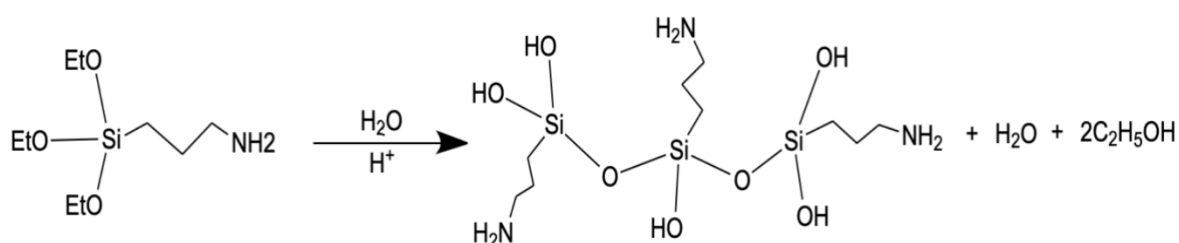


Figure 14: APTES hydrolysis and condensation reaction.

4.2.4. MNPs functionalization

For this work the functionalization was realised using (3-Aminopropyl)triethoxysilane, the choice was made in order to have a molecule able to bond the MNPs and also interact with VFAs.

F.1. MNPs functionalization with hydrolysed APTES, 1:9 molar ratio, 5-hours procedure

The reaction has been executed according to the procedure described by Mahmud Rozi et al. [49] and Feng et al [72]; it is shown in Figure 15.

In a three-necked round bottom flask, 0.555 g of MNPs have been dispersed in 50 mL of deionized water and 22.5 mL of hydrolysed APTES (0.918 M) were added. The mixture was stirred for 5 hours at 60° C under a nitrogen atmosphere. After cooling at room temperature, the product was washed once with deionised water and once with ethanol. Finally, it was rotary evaporated at 50° C for 5 minutes; details on quantities can be found in Table 10.

Table 10: MNPs functionalization with hydrolysed APTES.

	Mass [g]	Mw [g/mol]	[mol]	Equivalents	Volume [mL]
MNPs	0.555	231.54	0.0024	1	-
Hydrolysed APTES		-	0.0214	8.92	22.5
H₂O		18.01			50

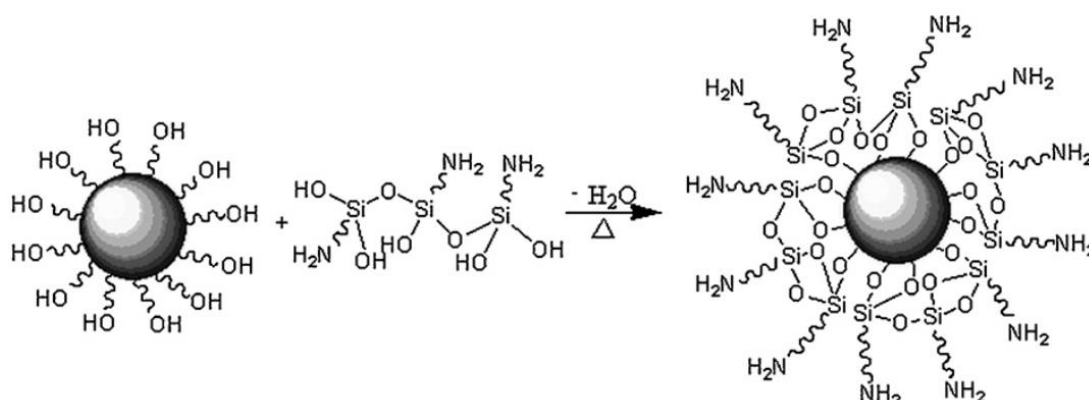


Figure 15: MNPs functionalization with hydrolysed APTES (image from [72])

F.2. MNPs functionalization with hydrolysed APTES, 1:18 molar ratio, 5-hours procedure

In a three-necked round bottom flask, 0.277 g of MNPs have been dispersed in 25 mL of deionized water and 24 mL of the hydrolysed APTES (0.918 M) were added. The mixture was stirred for 5 hours at 60° C under a nitrogen atmosphere. After cooling at room temperature, the product was washed once with deionised water and once with ethanol. Finally, it was rotary evaporated at 50 °C for 5 minutes; details on quantities and equivalents of the reagents can be found in Table 11, whereas Figure 15 shows the reaction.

Table 11: MNPs functionalization with hydrolysed APTES.

	Mass [g]	Mw [g/mol]	[mol]	Equivalents	Volume [mL]
MNPs	0.277	231.54	0.0012	1	-
Hydrolysed APTES		-	0.0214	17.83	24
H₂O		18.01			25

F.3. MNPs functionalization with hydrolysed APTES, 1:4 molar ratio, 5-hours procedure

In a three-necked round bottom flask, 0.555 g of MNPs have been dispersed in 50 mL of deionized water and 10.52 mL of the hydrolysed APTES (0.912 M) were added. The mixture was stirred for 5 hours at 60° C under a nitrogen atmosphere. After cooling at room temperature, the product was washed once with deionised water and once with ethanol. Finally, it was rotary evaporated at 50° C for 5 minutes; details on quantities and equivalents of the reagents can be found in Table 12, whereas Figure 15 shows the reaction.

Table 12: Functionalization with hydrolysed-APTES.

	Mass [g]	Mw [g/mol]	[mol]	Equivalents	Volume [mL]
MNPs	0.555	231.54	0.0024	1	-
Hydrolysed APTES		-	0.0096	4	10.52
H₂O		18.01			50

F.4. MNPs functionalization with hydrolysed APTES, 1:4 molar ratio, 1-hour procedure

In a three-necked round bottom flask, 0.370 g of MNPs have been dispersed in 150 mL ethanol/water solution (1:1 volume ratio) and 7 mL of the hydrolysed APTES (0.912 M) have been added. The mixture was stirred for 1 hour at 40° C under a nitrogen atmosphere. After cooling at room temperature, the product was washed once with deionised water and once with ethanol. Finally, it was rotary evaporated at 50° C for 5 minutes; details on quantities and equivalents of the reagents can be found in Table 13, whereas Figure 15 shows the reaction.

Table 13: Functionalization with hydrolysed-APTES.

	Mass [g]	Mw [g/mol]	[mol]	Equivalents	Volume [mL]
MNPs	0.370	231.54	0.0016	1	
Hydrolysed APTES		-	0.0064	4	7.0
H₂O		18.01			75
EtOH		46.07			75

F.5. MNPs functionalization with APTES, 1:4 molar ratio, 1-hour procedure

The reaction is the one proposed by Shen et al. [70] and Can et al. [71]. This time it is not necessary to hydrolyse APTES prior to use, as shown in Figure 16.

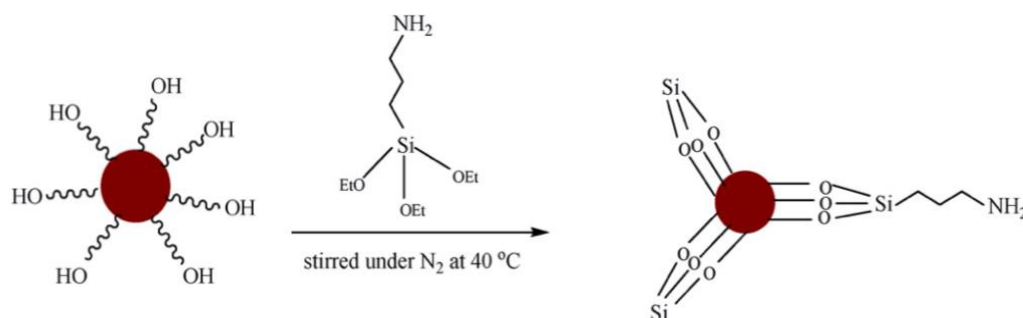


Figure 16: MNPs functionalized with APTES (picture from Can et al., [17])

For this reaction 0.370 g of MNPs have been dispersed in 150 mL ethanol/water solution (1:1 volume ratio), 1.41 g of APTES have been added and the solution has been stirred for 1 hour at 40° C under a nitrogen atmosphere. After cooling at room temperature, the F-MNPs have been washed with deionised water and then with ethanol. Finally, the product has been rotary evaporated at 50°C for 5 minutes; details on quantities and equivalents of the reagents can be found in Table 14.

Table 14: MNPs functionalization with APTES.

	Mass [g]	Mw [g/mol]	Density [g/ml]	[mol]	Equivalents	Volume [mL]
MNPs	0.370	231.54	-	0.00159	1	
APTES	1.41	221.37	0.946	0.0639	4	1.496
H₂O		18.01	1			75
EtOH		46.07				75

F.6. MNPs functionalization with APTES, 1:4 molar ratio, 5-hours procedure

For this reaction 0.555 g of MNPs have been dispersed in 50 mL of deionised water, 2.125 g of APTES have been added and the solution has been stirred for 5 hours at 60° C under a nitrogen atmosphere. After cooling at room temperature, the F-MNPs have been washed with deionised water and then with ethanol. Finally, the product has been rotary evaporated at 50°C for 5 minutes; details on quantities and equivalents of the reagents can be found in Table 15, whereas Figure 16 shows the reaction.

Table 15: MNPs functionalization with APTES.

	Mass [g]	Mw [g/mol]	Density [g/ml]	[mol]	Equivalents	Volume [mL]
MNPs	0.555	231.54	-	0.0024	1	
APTES	2.125	221.37	0.946	0.0096	4	2.25
H₂O		18.01	1			50

4.2.5. VFAs synthetic solution preparation

This work has been the first attempt at VFAs extraction using this method, so a synthetic VFAs solution was used. The aim was that of matching the VFAs composition at the end of the fermentation without including all the other residues, such as proteins, carbohydrates, organic soluble, and particulate residues. The VFAs' concentration was obtained by IRSA-CNR researchers at the end of the fermentation and is reported in Table 16.

Table 16: Ethanol and VFAs concentration [mg/L] via IRSA-CNR.

Ethanol	Acetate	Propionate	Isobutyrate	Butyrate	Isovalerate	Valerate	Caproate
2716	5330	974	208	2497	123	1236	5713

A total volume of 500 mL of the solution was prepared according to the following methodology. The first step was the weighing of all VFAs retrieved as salts, namely sodium acetate, sodium propionate, sodium butyrate and sodium hexanoate. Later, 400 mL of deionised water, ethanol and VFAs purchased as acids have been added. Details about the quantity of each VFA used are reported in Table 17. Subsequently, 7.83 mL of NaOH (1 M) corresponding to the same number of moles of acids (0.00783 mol), were added to have neutralization. Finally, HCl (1 M) and deionized water were used to obtain a total volume of 500 mL and a pH of 7. The resulting solution has been used for all the consequent absorption tests.

Table 17: Quantities used to prepare a synthetic solution of 500 mL.

Compound	Quantity
Sodium Acetate	2.665 g
Sodium Propionate	0.487 g
Sodium butyrate	1.2485 g
Sodium hexanoate	2.8565 g
Ethanol	1.72 mL
Isobutyric acid	0.109 mL
Valeric acid	0.658 mL
Isovaleric acid	0.066 mL

4.2.6. Adsorption experiments

For each experiment 10 mg of dry nanoparticles (MNPs obtained via S.3 or F-MNPs obtained via F.1) have been weighted and dispersed in 2 mL of VFAs solution. Tests were carried out under two different types of agitation: shaker and magnetic stirring. For the latter, a small stirring magnet has been added for the duration of the experiments and removed at the end.

The separation was performed through centrifugation, operating at 6000 rpm for 6 minutes. Finally, the supernatants were filtered and analysed. Both types of agitation experiments were conducted using four different times, namely 5 minutes, 30 minutes, 60 minutes, and 120 minutes. The tests have been performed both with MNPs and F-MNPs. Overall, 16 different tests were performed, as summarized in Table 18.

Table 18: Different times and agitation methods used for adsorption experiments.

	Nanoparticles	5 minutes	30 minutes	60 minutes	120 minutes
Magnetic stirring	MNPs	A.9	A.10	A.11	A.12
	F-MNPs	A.1	A.2	A.3	A.4
Shaker	MNPs	A.13	A.14	A.15	A.16
	F-MNPs	A.5	A.6	A.7	A.8

4.2.7. Desorption experiments

The two best performing adsorption tests (A.1 and A.8) were replicated two times and desorption experiments were conducted. Water and methanol were used as solvents for this step. Nanoparticles were collected from the adsorption experiments and dispersed in 4 mL of solvent. All desorption tests were performed using magnetic stirring with a fixed time of 30 minutes and the temperature was kept at 40° C. The separation was carried out through centrifugation, operating at 6000 rpm for 6 minutes. Then, the supernatants were filtered and analysed. The samples for which the desorption was performed in methanol undergone an additional step: 4 ml of deionised water were added, and the samples were rotary evaporated to remove as much as possible the CH₃OH present in the sample. All the desorption experiments are listed in Figure 18.

4.2.8. Second-cycle adsorption experiments

Nanoparticles collected from the desorption experiments were dispersed in 2 mL of VFAs solution, and then the same procedure of the first set of adsorption experiments, described in paragraph 0, was followed. The second-cycle adsorption experiments are listed in Figure 18.

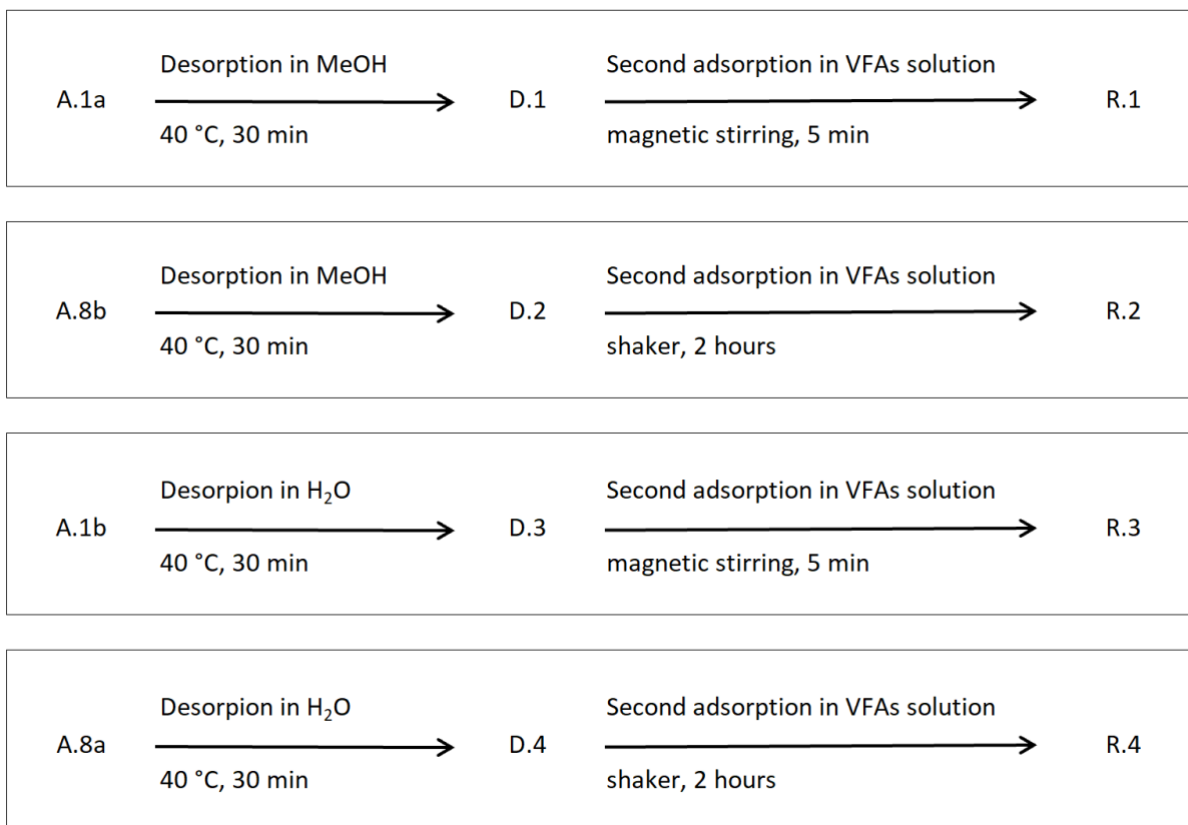


Figure 18: Summary of desorption and second-cycle adsorption tests.

Chapter 5: Results

5.1. MNPs synthesis by co-precipitation

Magnetite nanoparticles were synthesised by co-precipitation varying the reaction parameters to achieve fast magnetic decantation. The reaction was carried out using ammonium hydroxide, sodium hydroxide, and a large excess of sodium hydroxide, as well as different temperatures (80° C and 100° C) and stirring speeds (500 rpm and 400 rpm). After the reaction, the system was cooled down to room temperature and then the reaction liquid was separated from the solid product and the latter was washed three times with water. Magnetic decantation was used for solid-liquid separations. The clearing of the liquid indicated the proceeding of the decantation process; this was judged successfully completed when a black deposit was evident at the bottom of the three-necked round bottom flask topped by a transparent and colourless or slightly yellow supernatant, shown in Figure 19.

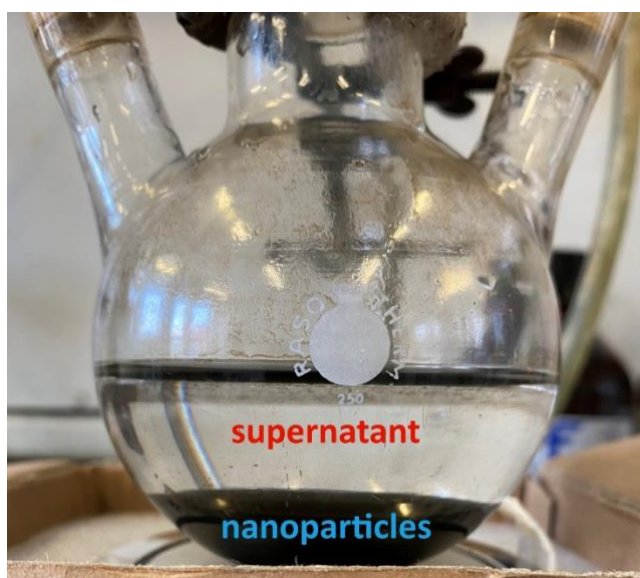


Figure 19: Magnetic decantation results in a dark nanoparticles' sediment at the bottom topped by a transparent and colourless supernatant

The co-precipitation (S.1) using ammonium hydroxide, a temperature of 80° C, and a stirring speed of 500 rpm performed poorly during magnetic decantation. Each solid-liquid separation required progressively more time. After 30 minutes of magnetic decantation, a layer of deposited particles was partially visible, but the supernatant was still noticeably turbid and dark brown. During this time the colour change associated with the nanoparticles' precipitation was slight but observable, after the 30 minutes mark changes were not noticeable anymore. This behaviour could be explained by a broad size distribution that comprises bigger particles that precipitate quickly and smaller particles that remain in suspension for longer. Corpuscles smaller than 20 nm, when dispersed to nano-size (sol), are subjected to Brownian forces several orders of magnitude larger than the attraction forces

exerted by the hand-held magnet [143]. Aggregated or larger particles will instead be subject to magnetic attraction forces greater than the Brownian forces that keep them in suspension, and therefore will be easily separable with a magnet.

In pursuance of faster magnetic decantation, S.1 was modified to slightly increase MNPs mean dimension. Thus magnetic stirring rpm were reduced, the reaction temperature was increased [38], [65], [144], and the pH was also increased [65], [66], [144]. A first experiment was conducted substituting ammonium hydroxide with the same moles of sodium hydroxide (S.2). The latter being a stronger alkali will dissociate completely increasing the solution's pH more. For the same purpose, another experiment was carried out using a large excess of sodium hydroxide (S.3).

Reaction S.2 was noticeably quicker. After the addition of NaOH, a rapid change of colour from rusty orange to black was observed indicating the formation of magnetite [145], [146]. During reaction cooling, the gravitational sedimentation of the MNPs was observed leading to an evident black deposit and a transparent and colourless supernatant after 50 minutes. The magnetic decantation steps after each washing performed significantly better requiring around 10 minutes over the magnet to obtain a transparent and colourless supernatant.

Reaction S.3, like the previous one, is observably faster than S.1. Already during the injection of the alkali, the reaction volume rapidly transitions from rusty orange to black. Gravitational sedimentation is observed during cooling and the supernatant is transparent and colourless after 30 minutes. The magnetic decantation after each washing was remarkably fast and the two phases were well separated after about 5 minutes, as shown in Figure 20.

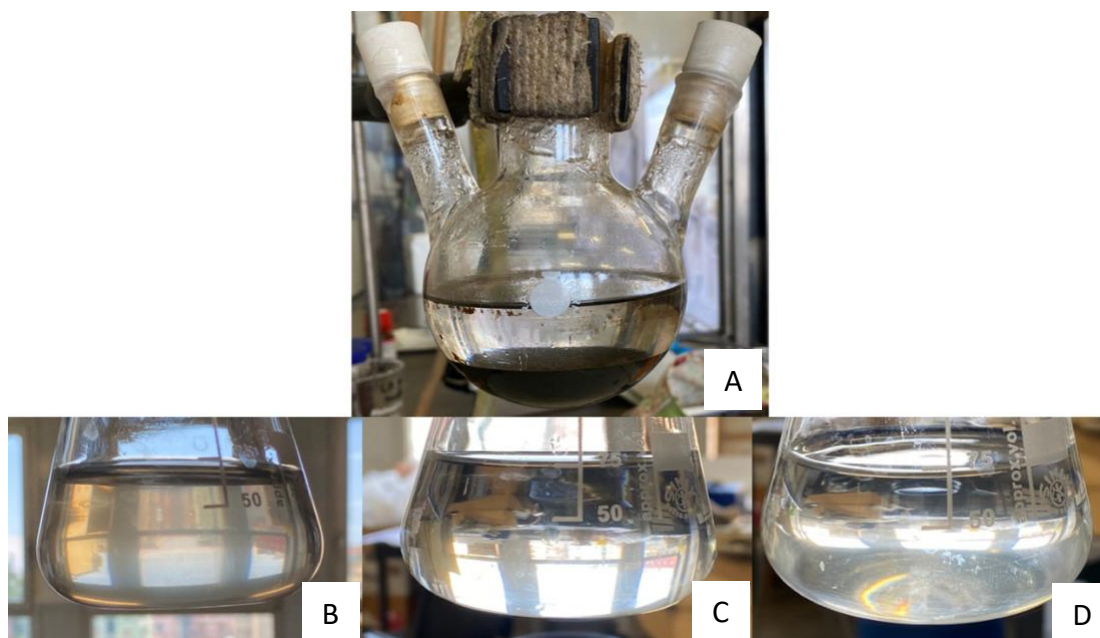


Figure 20: F.1 work-up. A) reaction liquid, B) first washing water, C) second washing water, D) third washing water.

In a second S.3 experiment run, half of the nanoparticles were washed with deionized water while the other half was washed with tap water. This was done to observe if the presence of dissolved salts, common in fermentation broths, could aid or hinder the magnetic decantation. No significant differences emerged.

Comparing the different separation times obtained, summarized in Table 19, the particles from the synthesis S.3 are the fastest both in gravitational sedimentation and magnetic decantation.

Table 19: Co-precipitation conditions of the three syntheses conducted (S.1, S.2, S.3) together with the resulting sedimentation and magnetic decantation; “n/a”, not available indicates that sedimentation was not observed during the 1 hour of cooling.

	Alkali type	Alkali amount [mol]	Stirring rate [rpm]	T [°C]	Sedimentation time [min]	Magnetic decantation time [min]	System description
S.1	NH ₄ OH	0.0857	500	80	n/a	~30	Turbid and brown supernatant
S.2	NaOH	0.0857	400	100	~50	~10	Clear and colourless supernatant
S.3	NaOH	0.3323	400	100	~30	~5	Clear and colourless supernatant

All MNPs synthesized were characterised using CHNS analysis. The different conditions resulted in slight differences in the mass percentage of carbon, hydrogen, and nitrogen presented in Table 20. Nitrogen was detected only in nanoparticles from synthesis S.1 and could be due to residues of ammonium hydroxide. Carbon presence is due to residues of carbonates from water; the mass percentage is higher for S.3 as washings with tap water were conducted. The hydrogen content is maximum for S.3, the synthesis with excess sodium hydroxide, this could indicate a larger number of -OH groups bonded to the surface of the magnetite nanoparticles.

Table 20: Percentages on a mass basis (% w/w) of nitrogen, carbon, and hydrogen obtained by CHNS elemental analysis of nanoparticles synthesised via S.1, S.2, and S.3.

	Nitrogen [% w/w]	Carbon [% w/w]	Hydrogen [% w/w]
S.1	0.17	-	0.83
S.2	0	0.25	0.68
S.3	0	1.15	0.93

In this preliminary phase, the presence of magnetic properties was assessed visually. The observed difference between separation times with or without the magnet is already an indication of its effect on the nanoparticles. By preparing two vials with MNPs dispersed in deionized water and placing only one on the magnet, the difference in precipitation rate,

indicated by the clearing of the solution, is evident to the naked eye. In addition, placing the magnet on the side of the vial or inserting a magnetic object, as shown in Figure 21, the nanoparticles move due to attraction. In further developments, the magnetic properties will be studied using Vibrating Sample Magnetometer (VSM) to detect if the increase in size favoured by larger temperature, lower rpm and high pH resulted in multi-domain and non-superparamagnetic nanoparticles.

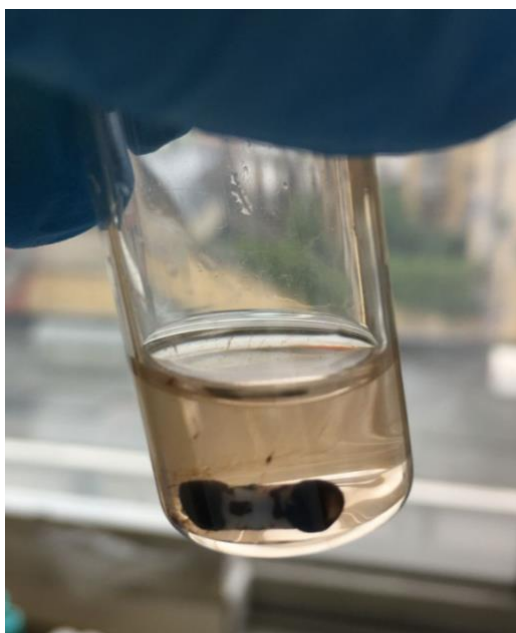


Figure 21: Nanoparticles attracted by a small magnetic bar introduced in the vial. After introduction the liquid rapidly clears and the nanoparticles are collected at the bar's extremities.

Based on magnetic decantation times the co-precipitation S.3 with an excess of sodium hydroxide was selected for further functionalization. The characterization reported below were all conducted on nanoparticles produced according to synthesis S.3, from now on indicated with the general term MNPs.

5.1.1. X-ray Powder Diffraction phase identification

XRD analysis of magnetic nanoparticles was carried out in order to identify the material and validate the efficacy of the modified co-precipitation synthesis procedure.

The diffractogram in Figure 22 is similar to what is reported in the literature [69], [72], [74], [147], [148]. It showed well-defined peaks indicating good sample crystallinity and patterns corresponding to Iron Oxide (Fe_3O_4), Calcium Carbonate (CaCO_3), and Iron Oxide Hydrate ($\text{Fe}_2\text{O}_3 \cdot \text{H}_2\text{O}$) (Figure 23).

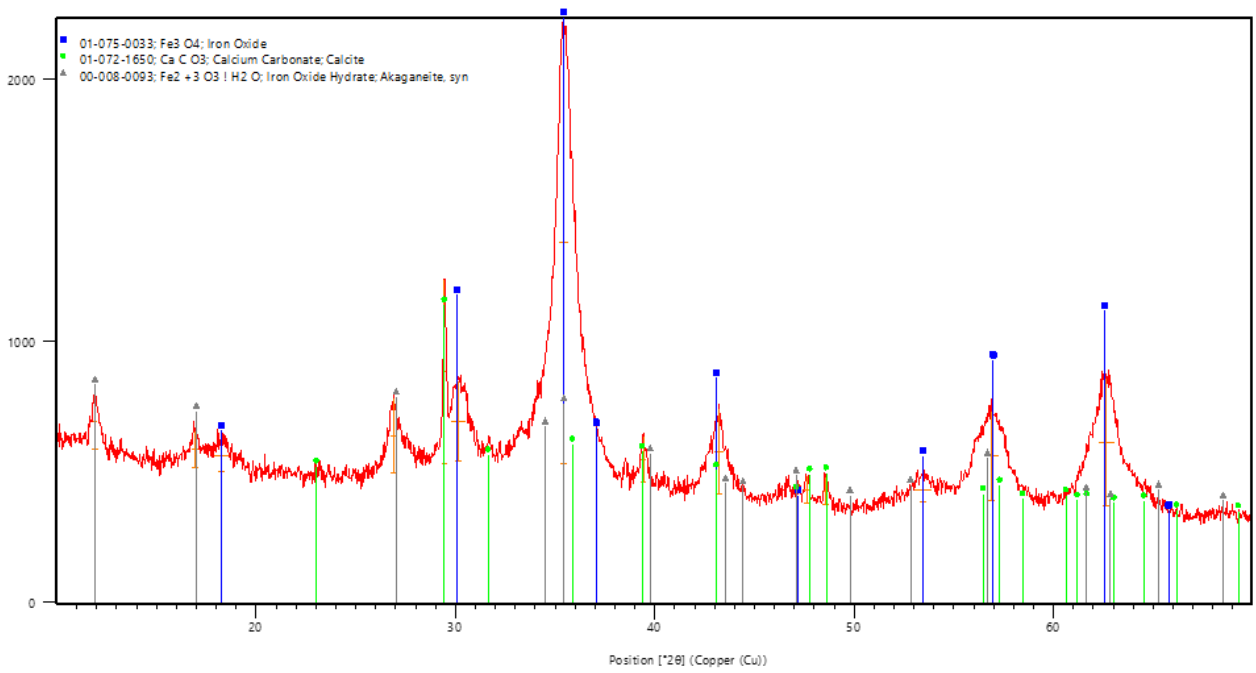


Figure 22: X-Ray diffractogram of MNPs from S.3; counts are indicated on the y-axis.

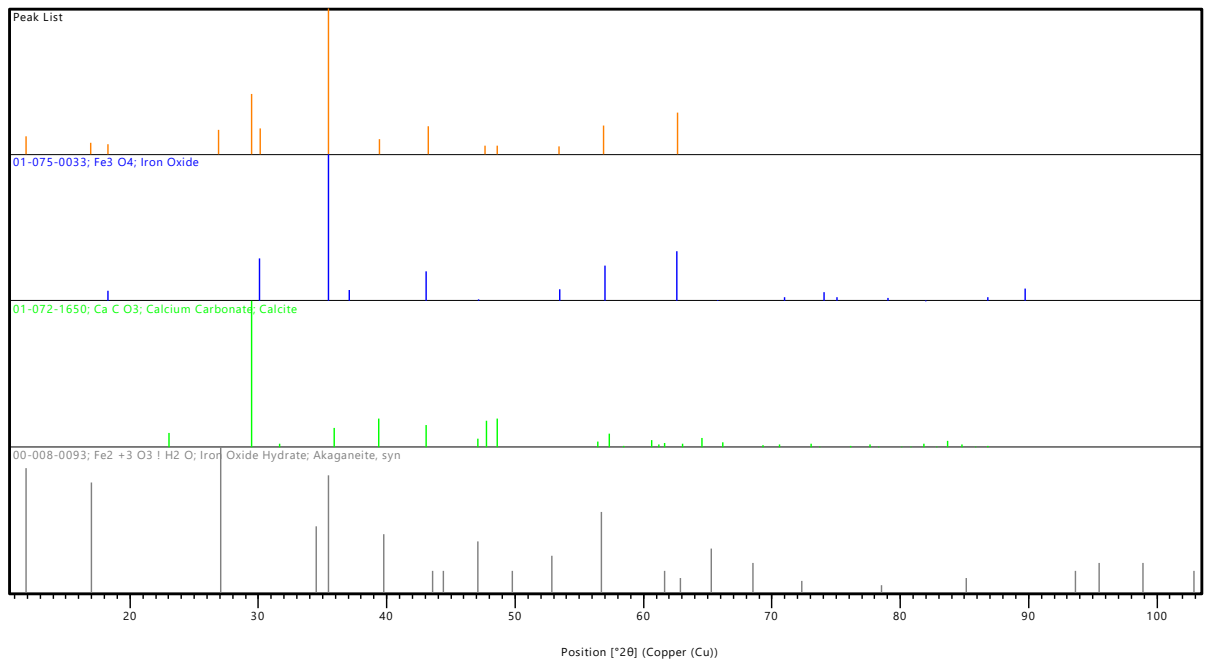


Figure 23: Peaks patterns of MNPs from S.3, iron oxide, calcium carbonate, and akaganeite.

The peak patterns corresponding to Iron Oxide (blue square) confirmed the presence of magnetite in the sample.

Calcium Carbonate identification occurred due to the use of non-deionized water during washings. This salt, commonly present in tap water, remained in the powder sample after lyophilization. Only deionized water was used in the syntheses carried out subsequently.

Presence of the intermediate akaganeite may indicate a partly incomplete reaction. Numerous phase changes occur during the synthesis of magnetite nanoparticles involving intermediates: goethite (α -FeOOH), akaganeite (β -FeOOH), and lepidocrocite (γ -FeOOH); akaganeite is the start of one of the two coexisting pathways that lead to magnetite [145], represented in Figure 24.

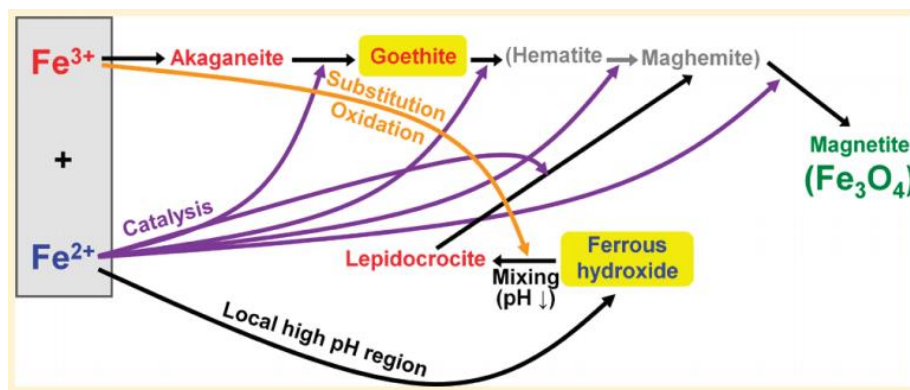


Figure 24: The two co-existing phase-change pathways during magnetite nanoparticles coprecipitation reaction individuated by Ahn et. al., 2012 [145]

Starting from XRD results an estimation of the average crystallite size can be performed exploiting the Scherrer equation applied to the reflection peak at $\theta=0.6186$ rad. A crystallite is a region of the solid with a regular crystalline structure, this formula (3) relates the crystallite dimension to the broadening of a peak in a diffraction pattern:

$$D = \frac{K \cdot \lambda}{\beta \cdot \cos\theta} = \frac{0.9 \cdot 0.15046 \text{ nm}}{1.090 \cdot \cos(0.6186)} = 7.65 \text{ nm} \quad (3)$$

Where D is the crystallite size in the direction perpendicular to the lattice planes, K is the crystallite-shape factor, λ is the wavelength of the X-rays, β is the full-width at half-maximum of the X-ray diffraction peak in radians and θ is the Bragg angles. The shape factor is a numerical value that depends on the crystallite shape but also on the definition of D used; with the definition given above, and missing information about the shape a good approximation is $K = 0.9$ [149].

The use of this method for estimating the crystallite dimension of magnetite nanoparticles is spread in the literature. Reported values range from 4 nm [146] to 80.5 nm [75] depending on the specific conditions used for the co-precipitation reaction.

For the synthesised MNPs a crystallite dimension of 7.65 nm was obtained, this is coherent with the values reported in literature under different reaction conditions [38], [146], [147], while bigger values were reported by [69], [75], [148]. This small crystallite dimension could be explained by the higher concentration of OH^- with respect to that of Fe^{2+} and Fe^{3+} , this oversaturation condition promotes smaller crystallites [64].

The estimate is of the crystallite dimension, so it can be considered as a lower bound for the particle dimension, that should be assessed with further analysis.

5.2. MNPs functionalization reaction with hydrolysed APTES

The surface of the magnetite nanoparticles is covered with hydroxyl groups, various molecules can be attached to them for tailoring the MNPs to their application. This process is referred to as coating or functionalization. The application of interest is the separation of short-chain volatile fatty acids. These compounds can be separated from dilute solutions using membrane-based processes, adsorption columns, or liquid-liquid extraction processes exploiting different chemical and physical properties. The idea behind the innovative use of nanoparticles is to exploit the functionalization of their surface to:

1. capture VFAs through chemical interactions;
2. separate magnetically the nanoparticle with the adsorbed VFAs;
3. release VFAs and restore the nanoparticles for re-using them;

The ability to both capture and release the VFAs will be achieved by designing a functionalization that interacts with carboxylic acids differently depending on the external conditions (e.g. pH, temperature, solvent). To do this the properties of short-chain carboxylic acids must be closely considered.

The short-chain carboxylic acids of interest are formed during the fermentation process developed by IRSA-CNR. These are acetic, propionic, isobutyric, butyric, isovaleric, valeric, and caproic acid. All have a single carboxylic group and a small alkyl moiety, which results in a hydrophilic behaviour. Moreover, these VFAs are weak acids characterized by relatively high pK_a values reported in Table 5. As a result, at neutral pH (representing VFAs in water) the acids are almost completely dissociated while at pH around 5 (representing VFAs in fermentation broth) the portion of acids that are dissociated drops to approximately 60 %.

The dissociated form is called carboxylate and is the conjugate base of the carboxylic acid; these anions are formed also by the dissolution of salts derived from carboxylic acid neutralization. To capture these anions the amine functional group was selected. This group gets protonated at neutral and acidic pH, resulting in a positive charge on the nitrogen atom that can effectively interact with the carboxylate. This interaction between the cation and the carboxylate anion can be exploited for the separation process.

The amine-bearing molecule selected is (3-Aminopropyl)triethoxysilane, a member of the organofunctional alkoxysilanes where the organic function is a primary amine while the alkoxy groups are represented by ethoxy groups ($-\text{OCH}_2\text{CH}_3$). The coating of a surface with this family of compounds is referred to as silanization, its application to magnetic nanoparticles is described in numerous papers [68], [70]–[72]. The adopted procedure is detailed in paragraph F.1, here results and observations will be presented.

Before functionalization, the bare MNPs were lyophilized to allow mass quantification. The freeze-drying process caused aggregation of the particles with the formation of irregular granules. These aggregates precipitated immediately when dispersed in water. Initially, sonication was tested to redisperse the nanoparticles in the functionalization reaction's liquid. This resulted in an evenly coloured dispersion difficult to separate by magnetic decantation. The time required for precipitation of the nanoparticles increased from 5 minutes to more than 30 minutes after sonication, leaving a turbid and light brown supernatant. A second redispersion test was conducted after finely grinding the aggregates with a ceramic pestle and mortar until a very fine and uniform black powder was obtained. This powder once redispersed in water behaved similarly to the nanoparticles immediately after synthesis, so this procedure was adopted to limit the aggregative effect of lyophilization.

During the execution of the functionalization reaction, the nanoparticles' dispersion changes colour from black to dark brown. Regarding the liquid-solid separations, no gravitational sedimentation was observed during reaction cooling, while magnetic decantation was observable but slower than that of non-functionalized particles. Removal of the reaction liquid and the first washing water was performed after 18 minutes on the magnet while the ethanol from the second washing was removed after 23 minutes. After these times had elapsed, the supernatants, showed in Figure 25, were still slightly cloudy and coloured but no visible changes had occurred in the previous 3 minutes.

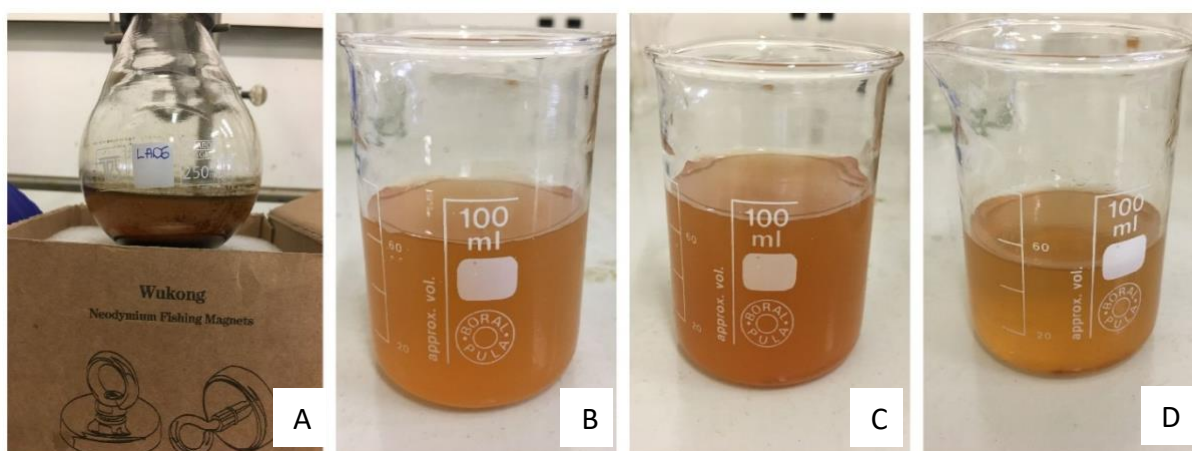


Figure 25: Magnetic decantation of functionalized magnetic nanoparticles. A) reaction flask during sedimentation, B) reaction liquid after 18 minutes, C) washing water after 18 minutes, D) washing ethanol after 23 minutes.

Since functionalization duration is 5 hours, we chose to shorten the magnetic decantation, avoiding reaching complete transparency of the supernatant, in order to finish the procedure within the day. The supernatants were kept under observation to verify the presence of nanoparticles. Sediments were observed on the bottom of the glass vial after 96 hours of gravitational sedimentation, and the supernatant looked transparent but slightly tinted of brown-orange.

In conclusion, silanization was selected to functionalise the surface of the synthesised MNPs with amine groups. The procedure resulted in longer magnetic decantation times that may be due to a higher F-MNPs' affinity with water or shielding of the magnetic core enacted by the coating of APTES. The final product after rotary evaporation is a fine dark-brown powder.

5.3. Characterization and comparison of MNPs and F-MNPs

Magnetic nanoparticles (S.3) and functionalized magnetic nanoparticles (F.1) characterization were carried on using analysis methodologies supported by the literature. Hereby the results are presented, discussed, and compared.

5.3.1. Infrared spectroscopy

Functionalization of magnetite nanoparticles was carried out using APTES and the presence of it bonded on the surface was verified qualitatively by Infrared Spectroscopy. The FT-IR spectra showed differences in the peak position and transmittance percentage as can be seen in Figure 26.

The sample of MNPs show a deep and evident peak at wave number 550-600 corresponding to the adsorption peak from Fe-O stretching vibrations; smaller and broader peaks present between 3200 and 3400 cm^{-1} and around 1600 cm^{-1} can be associated with the O-H stretching and deformed vibrations respectively [70], [73], [147].

The spectra for functionalized nanoparticles shows a similar peak from the Fe-O stretching vibration while the rounded peak between 3200 and 3400 cm^{-1} is more marked and the band at 1600 cm^{-1} is significantly stronger probably due to the overlapping of the O-H vibrations with the N-H stretching and bending vibrations respectively [70], [71]. In the F-MNPs spectra an evident adsorption band is revealed around 1400 cm^{-1} which can be assigned to the C-N stretching vibration [70]. Another difference is the appearance of a strong band around 1050 cm^{-1} associated with the Si-O stretching vibration [68], [72], [74], its presence confirms surface functionalization with (3-Aminopropyl)triethoxysilane.

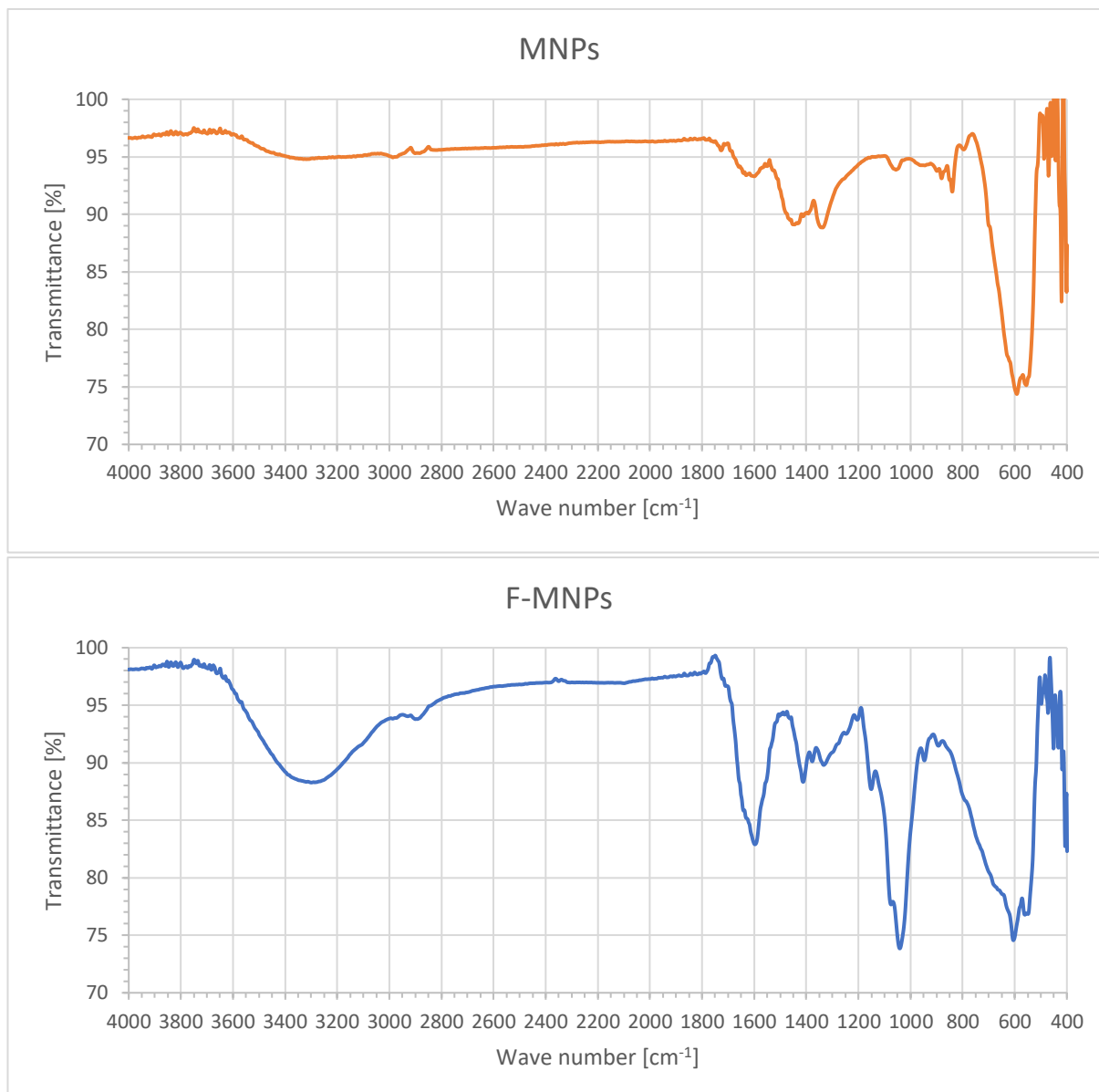


Figure 26: FT-IR spectra for MNPs (top) and F-MNPs (bottom).

5.3.2. Zeta potential

To further confirm functionalization and to observe the behaviour of surface groups [39] at different pH conditions, the zeta potential (indicated with ζ -potential) of both MNPs and F-MNPs was measured at pH values equal to 2, 4, 6, 7, 8, 10 and 12. The solutions were prepared using hydrochloric acid or sodium hydroxide. By performing measures over a pH range and plotting the data points the iso-electric point can be individuated, as illustrated in Figure 27.

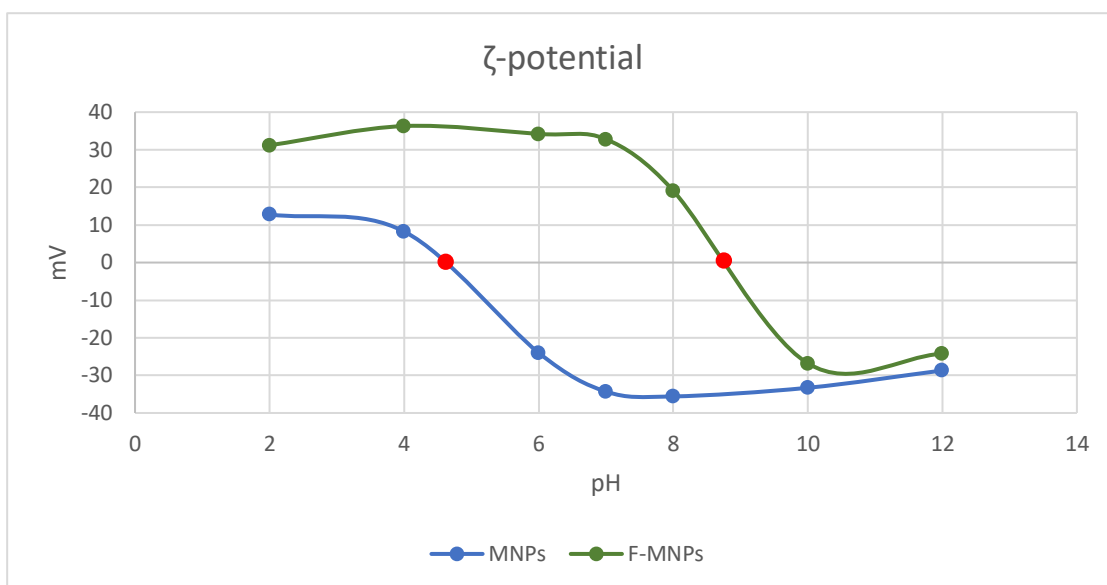


Figure 27: ζ -potential measured at pH values equal to 2, 4, 6, 7, 8, 10 and 12 for MNPs (left) and F-MNPs (right). The red dot indicates iso-electric points.

The iso-electric point of F-MNPs occurs near pH 9 while for the MNPs it occurs between 4 and 5. This means that the F-MNPs surface bears positive charges at pH values below 9, while the MNPs are positively charged only at pH below 4.5.

From this observation, it can be confirmed that the coating process results in a relevant change in the chemical behaviour of surface groups manifested at different pH values. This, together with the FT-IR results, confirm that the surface has been effectively functionalized resulting in attachment of APTES bearing amine functional groups.

5.3.3. CHNS elemental analysis

To have a quantitative measure of surface functionalization the CHNS elemental analysis on MNPs and F-MNPs was carried on. The resulting compositions, shown in Table 21, show an increase in carbon content from 1.15 % for MNPs to 3.49 % for nanoparticles functionalized using APTES, also the hydrogen percentage increased after functionalization, from 0.93 % to 1.13 %. The presence of nitrogen is only detected in the F-MNPs sample. These data are consistent with the presence of bonded APTES characterized by the chemical formula $C_9H_{23}NO_3Si$.

Table 21: CHNS elemental analysis results for MNPs and F-MNPs.

%	N	C	H
MNPs	0	1.15	0.93
F-MNPs	1	3.49	1.13

Ignoring contaminations introduced by reagents, the mass percentage of hydrogen present in MNPs derive from the hydroxyl groups on their surface; while the percentage of nitrogen in F-MNPs derives from the APTES's amine functions. From this information the number of hydroxyl groups and silane ligands on a nanoparticle can be found knowing the volume of the particle [150], as an accurate estimation of this data was not available the ratio of the number of hydroxyl and silane ligands, referred to as functionalization percentage, was computed (eq. (4), (5), (6)).

$$F [\%] = \frac{n_{NH_2}}{n_{OH}} \quad (4)$$

$$n_{NH_2} = \frac{\omega_N N_A \rho V}{MW_N}; \quad n_{OH} = \frac{\omega_H N_A \rho V}{MW_H} \quad (5)$$

$$F = \frac{\omega_N \cdot MW_H}{\omega_H \cdot MW_N} \cdot 100 = \frac{1 \cdot 1 [g/mol]}{0.93 \cdot 14 [g/mol]} \cdot 100 = 7.7 \% \quad (6)$$

Where n_{NH_2} is the number of amine functional groups bound to the functionalized particle (equal to the number of nitrogen atoms) and n_{OH} is the number of hydroxyl groups initially bound to the uncoated magnetite nanoparticle (equal to the number of hydrogen atoms); ω_N is the mass percentage of nitrogen of the F-MNPs sample and ω_H is the mass percentage of hydrogen of the MNPs sample, both obtained by CHNS elemental analysis; MW_N is the atomic weight of nitrogen and MW_H the one of hydrogen; N_A is the Avogadro's number while ρ and V are the density and the volume of the magnetite nanoparticle. The coating reaction resulted in a functionalization percentage of 7.7 %. Similar estimates were not encountered in the reviewed literature and thus no comparison can be made. Regardless, a low percentage is reasonable given the high steric hindrance of APTES molecules compared to hydroxyl groups on the surface. Further considerations regarding this figure will be better discussed in paragraph 5.7 following additional functionalization experiments.

5.3.4. DLS analysis

DLS was employed to estimate the particle size for MNPs and F-MNPs, three consecutive measurements were performed for each sample with a calibration time of 30 seconds and a total time between measures of approximately 3 minutes. As it can be observed from the results reported in Table 22, the mean size and the standard deviation increase in consecutive measurements both for MNPs and F-MNPs.

Table 22: DLS results of three consecutive measures (1st, 2nd and 3rd) on MNPs and F-MNPs. The intensity distribution was used, for multiple peaks the intensity percentages are reported in parenthesis.

measure n°	MNPs		F-MNPs	
	size [nm]	st. dev. [nm]	size [nm]	st. dev. [nm]
1st	175.8	12.9	185.8	32.54
2nd	680.8	47.37	240.1	57.64
3rd	1467	158.1	301.8 (84.2 % int.) 73.22 (12.2 % int.) 5365 (3.6 % int.)	112 17.02 331.2

This observation is explained by the formation of particle aggregates favoured by high surface energies and possibly magnetic forces [69]. The values obtained reveal greater aggregation for uncoated particles consistent with literature findings [69] [151]. The presence of three populations in the third measurement on the F-MNPs sample suggests the occurrence of aggregates with different sizes and potentially non-aggregated nanoparticles (population with a mean size of 73.22 nm). The fast aggregation observed suggest that also the first measure may describe clusters of nanoparticles rather than single ones. Moreover, the functionalized nanoparticle should be larger than the MNPs due to the coating layer; the measured dimension shows a slight increase from 175.8 nm for MNPs to 185.8 nm for F-MNPs but this difference is not significant and is most probably influenced by aggregation.

In conclusion, aggregation limits the accuracy of the dimension detected by DLS analysis. For estimating an accurate mean dimension transmission electron microscopy (TEM) imaging will be employed in further characterizations.

5.4. Adsorption of VFAs with MNPs and F-MNPs

Preliminary adsorption tests were conducted to assess the suitability of the developed nanoparticles for VFAs adsorption in aqueous solutions. The adhesion of these compounds to a surface can occur according to different interactions both of strong and weak nature depending on the properties of the surface and the feed conditions. In this project, the surface was designed to be studded with protonated amine groups capable of interacting with the negative charges of carboxylate ions. This interaction is made possible by the different behaviours of VFAs and amine groups when varying pH. Amine groups are in the protonated form up to about pH 8.5 (as seen from the zeta-potential analysis) while C2-C6 carboxylic acids are prevalently in their dissociated form at pH above 5 (as indicated by the pK_a values reported in Table 5). Consequently, selecting a pH between 5 and 8.5 will result in protonated amine groups on the surface of F-MNPs and carboxylates anions in solution.

An additional constraint on acceptable pH values comes from the degradation of magnetite in acidic environments. The H^+ ions interact with Fe_3O_4 to form $FeO(OH)$ along with a decrease of Fe^{3+} ions; this cause amorphization and partial destruction of the structure over time. The

lower the pH, the earlier this degradation phenomenon occurs; at pH 5 a reduction in crystallinity from 73 % to 65 % is observed in three days, and after seven days FeO(OH) is formed [42]. These observations are for uncoated nanoparticles left in solution continuously; in our case a protective layer of APTES is present and the F-MNPs remain in solution for less than one day. However, the intention is to use the particles as long as possible and for this, it is preferable to stay at neutral pH, at which no destruction of the Fe₃O₄ crystal should occur [42]. Following this, a pH of the VFAs solution of 7 was selected for testing. Using this pH value and primary amines, adsorption occurs through hydrogen bonds and hydrophobic interactions [80].

Adsorption tests were performed using F-MNPs according to the procedure described in paragraph 0. For each configuration, a control adsorption test using MNPs was conducted in parallel. The type of nanoparticle, the agitation method and the contact time used for each sample are reported in Table 23.

Table 23: Adsorption experiments conducted along with the type of nanoparticles, agitation method, and contact time used for each.

Sample name	Nanoparticles used	Stirring method	Contact time [min]
A.1	F-MNPs	magnetic stirring	5
A.2	F-MNPs	magnetic stirring	30
A.3	F-MNPs	magnetic stirring	60
A.4	F-MNPs	magnetic stirring	120
A.5	F-MNPs	shaker	5
A.6	F-MNPs	shaker	30
A.7	F-MNPs	shaker	60
A.8	F-MNPs	shaker	120
A.9	MNPs	magnetic stirring	5
A.10	MNPs	magnetic stirring	30
A.11	MNPs	magnetic stirring	60
A.12	MNPs	magnetic stirring	120
A.13	MNPs	shaker	5
A.14	MNPs	shaker	30
A.15	MNPs	shaker	60
A.16	MNPs	shaker	120

Performing magnetic decantation trials on the particles that have just been dispersed in the VFAs solution and on those that have completed the adsorption test (shaken for 5, 30, 60, or 120 minutes) revealed that the latter separates in much longer times. Immediately after dispersion, F-MNPs and MNPs precipitate under the magnet effect in less than one minute. Different is the behaviour of the samples after magnetic or shaker agitation; the vials after 5' of magnetic agitation show deposition of nanoparticles on the bottom after 7 hours of magnetic decantation, however, the supernatant appears transparent but dark brown in colour indicating residues of suspended nanoparticles. The samples after 5 minutes of

agitation with the shaker precipitate under the effect of the magnet in about 10 minutes, the supernatant appears transparent and pale-yellow. Increasing times both magnetically stirred and mechanically shaken samples take longer to decant.

To prevent the prolonged time required for magnetic decantation from affecting the adsorption results, the samples were centrifuged to separate the nanoparticles and the supernatant was immediately collected and filtered. Centrifugation always resulted in transparent and clear or light yellow supernatants.

Gas chromatography was conducted on the supernatants samples to estimate the concentration of VFAs remaining in the solution, results are reported in Table 24.

Table 24: Gas chromatography results in mg/L for the starting VFAs solution (first row) and adsorption tests.

	Ethanol [mg/L]	Acetate [mg/L]	Propionate [mg/L]	Isobutyrate [mg/L]	Butyrate [mg/L]	Isovalerate [mg/L]	Valerate [mg/L]	Caproate [mg/L]
VFAs solution	3309	4728	967	489	2368	191	1570	5805
A.1	2252	3356	661	338	1709	125	1147	4218
A.2	2531	4164	783	423	2092	149	1401	5224
A.3	2908	4095	818	423	2089	133	1392	5239
A.4	2614	4212	817	439	2104	145	1396	5319
A.5	2951	4274	840	446	2161	155	1436	5490
A.6	2498	3382	633	324	1816	123	1147	4333
A.7	2758	4166	816	414	2059	144	1369	5229
A.8	1994	3136	601	289	1592	137	1057	3950
A.9	2897	4249	792	414	2128	163	1408	5331
A.10	2497	3728	730	389	1840	128	1240	4746
A.11	2796	4472	863	454	2189	143	1475	5580
A.12	2597	3945	742	406	2034	168	1320	4934
A.13	2760	4504	847	460	2238	145	1467	5635
A.14	2538	4079	762	389	2037	129	1363	5060
A.15	2634	4038	746	428	1920	163	1330	5029
A.16	2635	3961	790	406	1953	158	1332	4979

The difference between the concentrations in the starting VFAs solution and in the supernatants is considered a good approximation of the quantity of acids adsorbed by the nanoparticles. Therefore the adsorption percentage can be computed for a generic analyte i as:

$$A\% = \frac{C_{i,0} - C_i}{C_{i,0}} \cdot 100 \quad (7)$$

Where $C_{i,0}$ is the concentration in the starting VFAs solution and C_i is the concentration in the supernatant after performing adsorption. The resulting adsorption percentages ranged from

3 % for caproic acid in sample A.13 (uncoated particles agitated for 5 minutes with the shaker) to 41 % for isobutyric acid in sample A.8 (functionalized particle agitated for 120 minutes with the shaker), the overall average adsorption percentage was 18 % and the standard deviation (σ) was 9 %.

The samples show differences in the percentages of adsorbed short-chain carboxylate anions. Among the samples using F-MNPs and magnetic stirring the lowest contact time of 5 minutes resulted in adsorption percentages higher than 25 % for all analytes, shown in Figure 28. Those in which the contact times were 30, 60 or 120 minutes show lower percentages of adsorption, around 10 %, except for isovalerate adsorption that exceeded 20 % in each sample. There are similarities between the results of samples A.2, A.3 and A.4, while the test A.1 resulted in different behaviour.

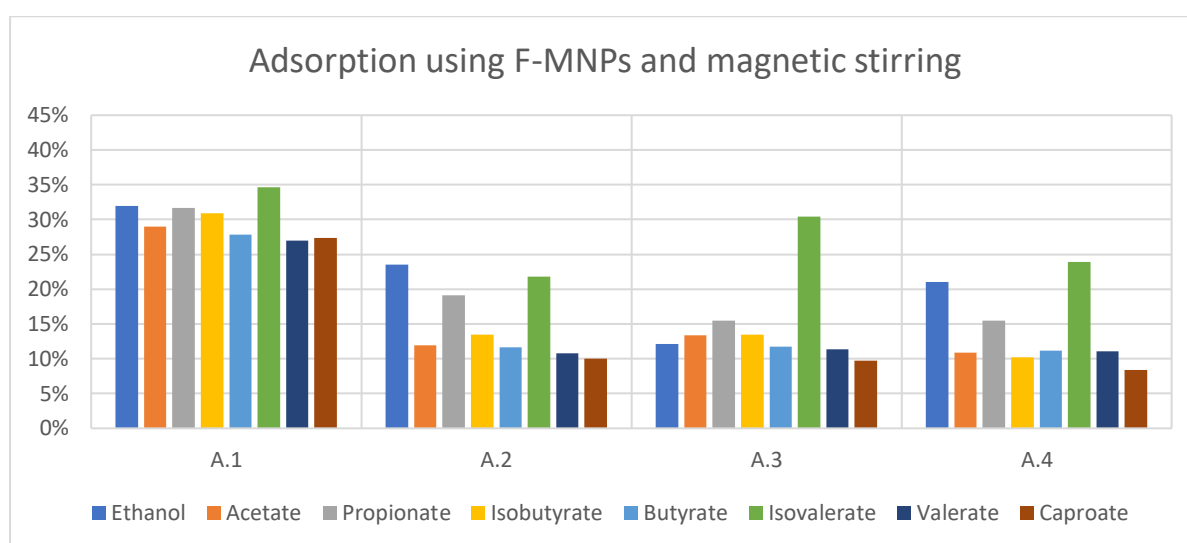


Figure 28: Percentages of adsorption of carboxylic acids using F-MNPs magnetically stirred for 5 (A.1), 30 (A.2), 60 (A.3), and 120 (A.4) minutes.

The GC results for adsorption samples produced using functionalized nanoparticles and the shaker for agitation are represented in Figure 29. The highest adsorption percentages were shown by the sample with longer contact time (A.8), in which each data is over 25 %, with ethanol, propionate and isobutyrate reaching the highest percentages, respectively 40 %, 38 % and 41 %. Slightly lower figures are obtained for sample A.6, particularly for ethanol (25 %) and butyrate (23 %) while other analytes all result in over 25 % adsorption. Among samples A.5 and A.7, which showed overall lower adsorption percentages, the first has the lowest observed values among all F-MNPs samples. In this only ethanol, propionate and isovalerate exceed 10 %, and caproate adsorption is particularly lacking with only 5 % being adsorbed.

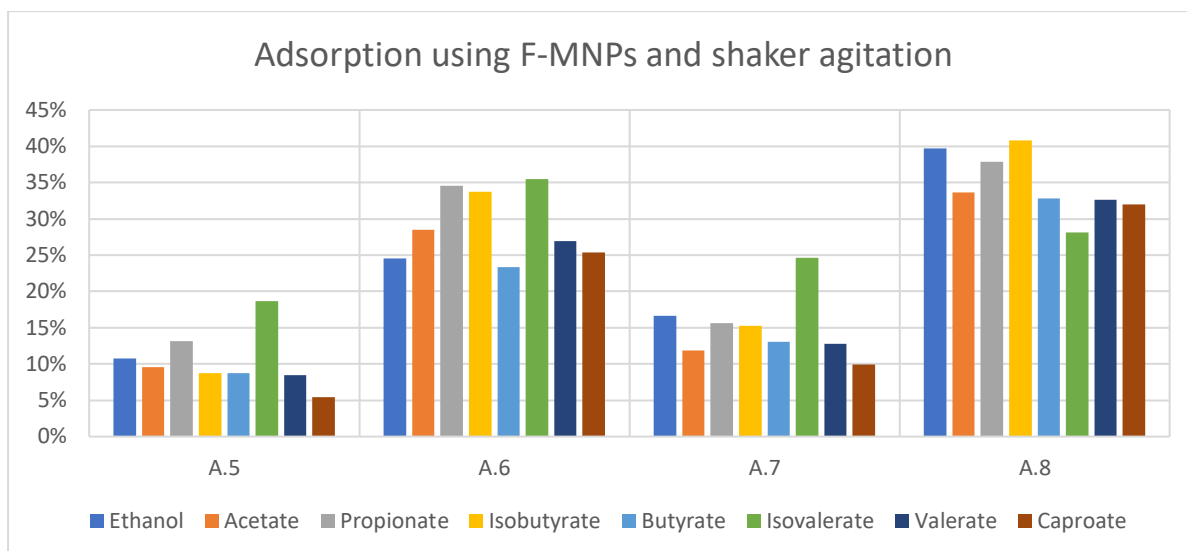


Figure 29: Percentages of adsorption of carboxylic acids using F-MNPs agitated with a shaker for 5 (A.5), 30 (A.6), 60 (A.7), and 120 (A.8) minutes.

Figure 30 show the percentages of adsorption achieved using uncoated magnetic nanoparticles and magnetic stirring. In sample A.10 the MNPs have adsorbed around 20 % of all carboxylates with a maximum adsorption value of 33 % for isovalerate, these values are comprised in the range observed for functionalized nanoparticles. A.12 is the closest to this with most values around 15 % and ethanol and propionate at 22 % and 23 % respectively, while the average adsorption is 12 % for sample A.9 and 10 % for sample A.11. This last show marked differences in the adsorbed amount of the analytes, only 4 % for caproate and 5 % for acetate against 16 % for ethanol and 25 % for isovalerate; indicating that some volatile fatty carboxylates were absorbed more than three times as much as others.

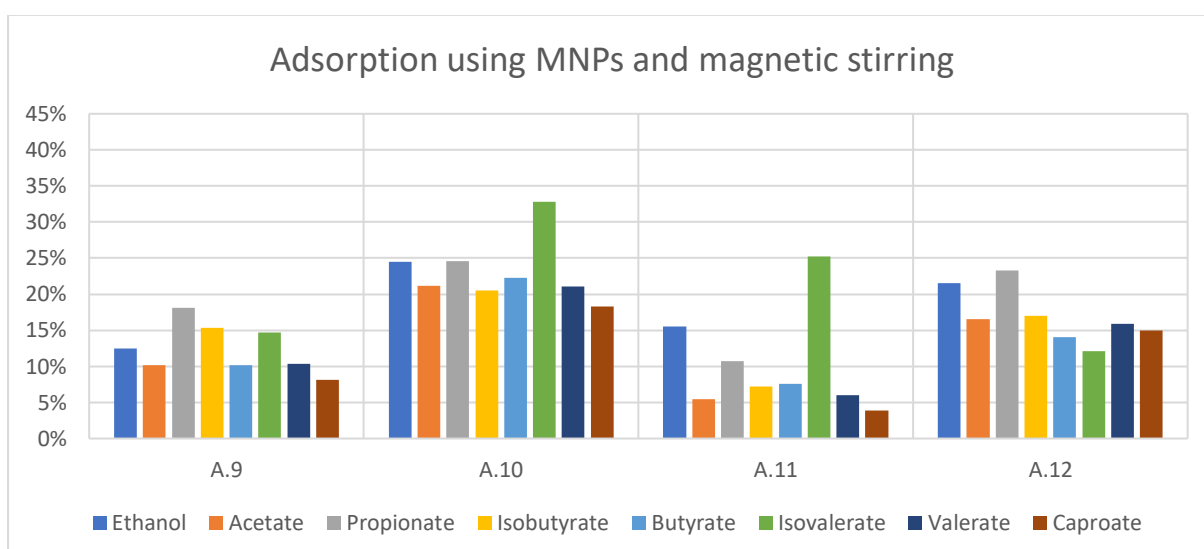


Figure 30: Percentages of adsorption of carboxylic acids using MNPs magnetically stirred for 5 (A.9), 30 (A.10), 60 (A.11), and 120 (A.12) minutes

Finally, the gas chromatography results for samples A.13, A.14, A.15 and A.16 are reported in Figure 31. These tests used uncoated magnetic nanoparticles and were agitated using a shaker for 5, 30, 60 or 120 minutes. Sample A.13 shows adsorption percentages for acetate, isobutyrate, butyrate, valerate and caproate which are half or less of what was obtained in the other experiments of this cluster; these results in adsorption of around 15 % for each carboxylate. In addition to this, sample A.13 shows inhomogeneity in the values similar to what was observed in sample A.11 (Figure 30) with ethanol, propionate and isovalerate being the most adsorbed.

A particularly high adsorption percentage of 32 % for isovalerate was observed in sample A.14 similarly to what was observed in sample A.10.

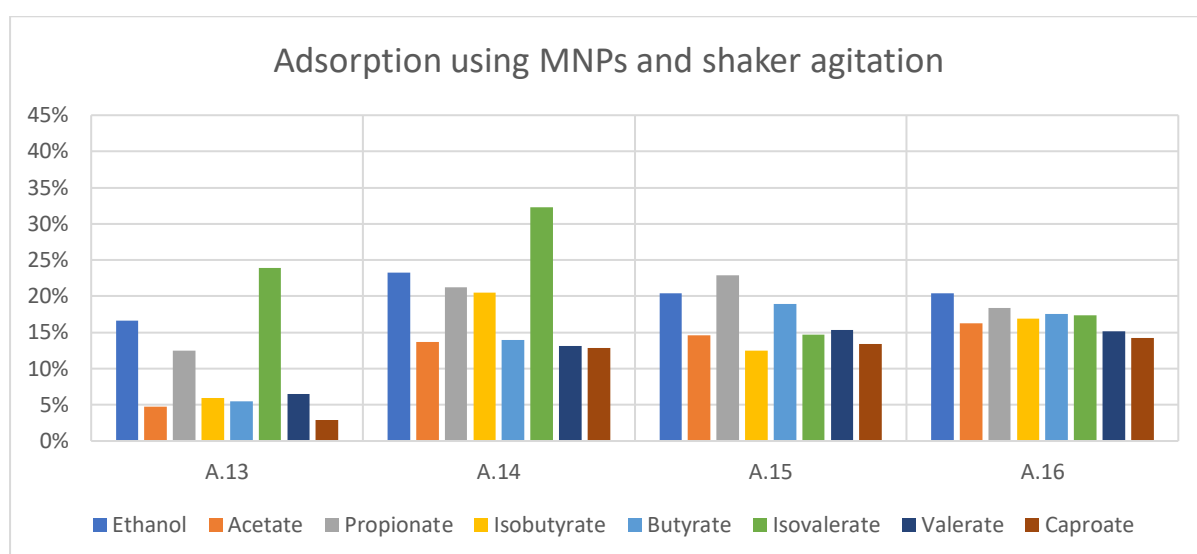


Figure 31: Percentages of adsorption of carboxylic acids using MNPs agitated with a shaker for 5 (A.13), 30 (A.14), 60 (A.15), and 120 (A.16) minutes

The experiments showing uniformly high uptakes for all analytes are:

- A.1 functionalized magnetic nanoparticles magnetically stirred for 5 minutes;
- A.8 functionalized magnetic nanoparticles agitated with a shaker for 120 minutes.

These were replicated two times each following the same procedure to assess replicability. The gas chromatography results of original samples and replicates are reported in Table 25 for A.1, and in Table 26 for A.8. In these also the mean values and the standard deviations for each analyte is presented.

Table 25: Carboxylate concentration after adsorption using F-MNPs magnetically stirred for 5 minutes, three replicates A.1, A.1a, A.1b.

	Ethanol [mg/L]	Acetate [mg/L]	Propionate [mg/L]	Isobutyrate [mg/L]	Butyrate [mg/L]	Isovalerate [mg/L]	Valerate [mg/L]	Caproate [mg/L]
A.1	2252	3356	661	338	1709	125	1147	4218
A.1a	3080	4402	870	447	2313	172	1474	5571
A.1b	3403	4497	817	440	2039	131	1449	5609
mean	2912	4085	783	408	2020	143	1356	5133
st. dev.	594	633	109	61	303	26	182	793

Table 26: Carboxylate concentration after adsorption using F-MNPs agitated with a shaker for 120 minutes, three replicates A.8, A.8a, A.8b.

	Ethanol [mg/L]	Acetate [mg/L]	Propionate [mg/L]	Isobutyrate [mg/L]	Butyrate [mg/L]	Isovalerate [mg/L]	Valerate [mg/L]	Caproate [mg/L]
A.8	1994	3136	601	289	1592	137	1057	3950
A.8a	3010	4344	871	425	2158	141	1434	5480
A.8b	2903	4147	838	427	2114	148	1447	5525
mean	2635	3876	770	380	1954	142	1313	4985
st. dev	558	648	147	79	315	6	222	897

For each concentration value, the adsorption percentages were computed using Equation (7). Replicates of adsorption test A.1, namely A.1a and A.1b, show significantly lower adsorption percentages, reported in Table 25. Sample A.1a has the lowest figures, all percentages are smaller or equal to 10 % with a minimum of 2 % for butyrate and a maximum of 10 % for propionate and isovalerate. Sample A.1b shows inhomogeneous absorption values: some are once again below the threshold of 10 % (acetate, isobutyrate, valerate, and caproate) however other values are close to 15 % (propionate and butyrate), the absorption of isovalerate is equal to 31 % and the percentage of ethanol absorption is -3 %. The negative value results from a concentration of ethanol after adsorption 95 ppm higher than the starting concentration. The difference is small and can be attributed to inaccuracies intrinsic to the measurement or the calibration performed.

The variability observed between these replicates is confirmed by standard deviations in the same order of magnitude as the mean values for each analyte (Figure 32).

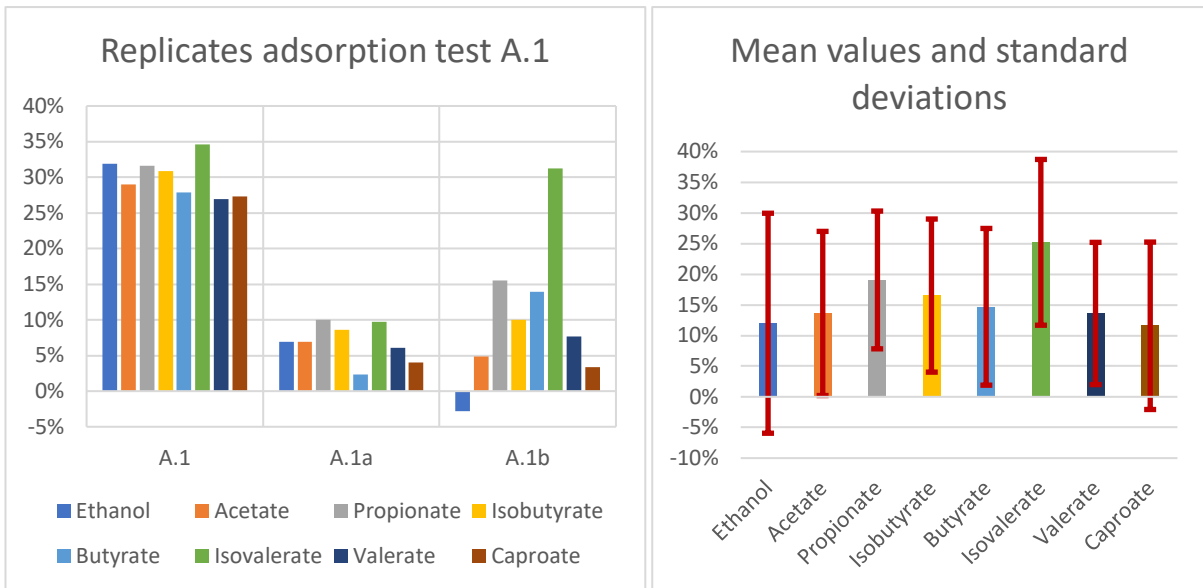


Figure 32: Adsorption percentages for test A.1, A.1a, A.1b together with the mean values and standard deviations (red bars) for each analyte.

The adsorption percentages for replicates of test A.8, indicated as A.8a and A.8b, are represented in Figure 33. The high figures obtained in the first run are not met by the replicates, one exception is isovalerate adsorption corresponding to 28 % in A.8, 26 % in A.8a, and 22 % in A.8b resulting in a standard deviation as low as 3 %. The remaining short chain carboxylates had values close to 10 % in both replicas, the least adsorbed is caproate with values similar to those observed in A.1a and A.1b. Except for isovalerate, the standard deviations and the mean values are in the same order of magnitude confirming the high variability observed between the replicates for test A.8.

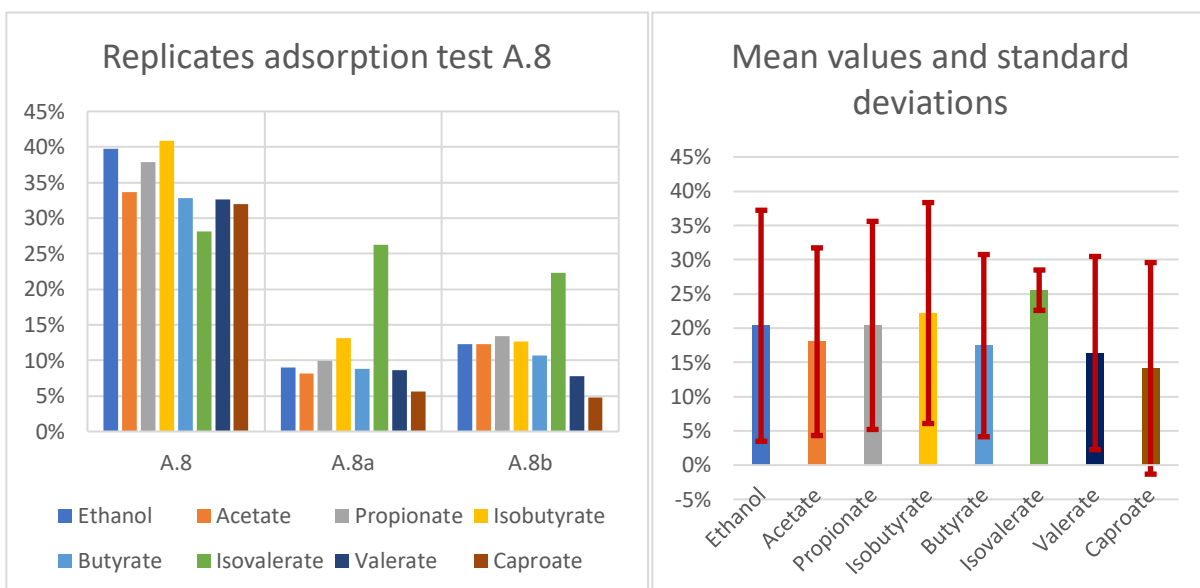


Figure 33: Adsorption percentages for test A.8, A.8a, A.8b together with the mean values and standard deviations (red bars) for each analyte.

Summarising the observations detailed above: functionalized nanoparticles in samples A.1 and A.8 show uniformly high uptakes for all analytes (above 25 %) while nanoparticles in samples A.5, A.11, and A.13 adsorbed very low amounts of acetate, isobutyrate, butyrate, valerate and caproate (between 3 % and 10 %), other samples showed adsorption in between these two extremes with some exceptions for the isovalerate percentage.

Samples with the highest adsorption percentages were replicated and the new results did not meet such high values indicating mean adsorption percentages closer to 10-15 % and significant variability.

The results obtained confirm that the quantity of short-chain carboxylates in solution decrease after short or prolonged contact with the functionalized and unfunctionalized nanoparticles under agitation. All carboxylates tested can be adsorbed on the surface of the nanoparticles and there is no evidence of strong selectivity in the capture process.

From the presented data, it is not possible to confidently conclude whether it is optimal to use MNPs or F-MNPs, a specific stirring methodology, and a precise time as only one replicate per experiment was performed. Nevertheless, when it comes to application reusability and stability are of great importance, and so F-MNPs should be preferred over MNPs since the latter are less stable [43]. Degradation studies under different conditions should be conducted to confirm this.

Additionally replicates for the two best performing samples suggested a high variability in results that could be due to differences in the conditions, for example, different ambient temperatures in the days of testing (22°C to 28°C). The adsorption in the executed procedure should be caused by the formation of hydrogen bonds [80], these interactions can continuously form and break so the instantaneous quantity of VFAs captured can vary; still, the observed variability is quite high to be explained only by this dynamic phenomena. An additional possible explanation is the presence of broad size distribution with aggregates that are not completely broken using a mortar and pestle; this disparity in the extent of agglomeration in different adsorption samples may reduce the surface available for the capture of the VFAs. In further studies, the procedure should be standardized in order to reduce external influences and verify the cause of the variability observed in this work.

5.5. Desorption of VFAs from F-MNPs

Desorption tests were conducted to verify the feasibility of the VFAs release after capture and to have insight into the strength and persistence of the interactions between nanoparticles and short-chain carboxylates.

Replicates using the same adsorption conditions were selected; after centrifugation and subsequent total removal of the supernatants the solid sediments were treated with methanol or water at 40°C, under magnetic stirring at 500 rpm for 30 minutes.

Subsequently, the desorption samples were centrifuged, the supernatants were collected, filtered, and finally analysed by gas chromatography.

The methanol supernatant could not be analysed as is by gas chromatography with the developed analytical method. For further studies, new calibrations lines for gas chromatography of VFAs in methanol or a tailored HPLC procedure are needed. In this work, 4 mL of deionized water were added to the methanol supernatant and the liquid was rotary evaporated to reduce the concentration of methanol as much as possible, verifying that the final volume was 4 mL. This gave less reliable concentration measurements which were considered acceptable for these preliminary tests.

The sample name, starting adsorption sample, the solvent used, and GC results are presented in Table 27 for each test conducted. Some measurements are not reported because they were considered inaccurate by the analytical laboratory due to the presence of unidentified peaks in the chromatogram or the presence of methanol residues that disturb the estimate of underlying peaks' areas.

Table 27: Gas chromatography results expressed as mg/L for desorption sample D.1, D.2, D.3, and D.4, together with starting adsorption sample and solvent used.

	Ethanol [mg/L]	Acetate [mg/L]	Propionate [mg/L]	Isobutyrate [mg/L]	Butyrate [mg/L]	Isovalerate [mg/L]	Valerate [mg/L]	Caproate [mg/L]
D.1	-	22.9	3.9	-	13.1	-	7.9	31.3
D.2	-	43.4	9.2	3.5	24.8	-	15.8	62.7
D.3	14.9	29.3	4.7	-	11.2	-	8.4	37.4
D.4	78.2	25.5	4.3	-	12.6	-	7.9	35.6

An interesting result is the presence of ethanol in D.3. Even if the quantity is small its presence indicates that a part of this analyte was indeed adsorbed on the surface of the nanoparticles in sample A.1b and that the negative adsorption percentage found previously (-3 %) is the result of a measurement error.

The desorption percentage for each analyte i , in each sample, was defined as the ratio between the milligrams of i in the supernatant after desorption ($mg_{i,des}$) and the milligrams of i adsorbed on the nanoparticles ($mg_{i,ads}$), estimated as:

$$D_i\% = \frac{mg_{i,des}}{mg_{i,ads}} \cdot 100 = \frac{C_{i,des} \cdot 4 \cdot 10^{-3}}{(C_{i,0} - C_i) \cdot 2 \cdot 10^{-3}} \cdot 100 \quad (8)$$

Where $C_{i,0}$ is the concentration of i in the starting VFAs solution, and C_i is the concentration of i in the adsorption supernatant expressed in [mg/L] (Table 25, Table 26); $C_{i,des}$ is the concentration in the desorption supernatant expressed in [mg/L] (Table 27); $4 \cdot 10^{-3}$ is the desorption solvent's volume in [L] and $2 \cdot 10^{-3}$ is the liquid volume for adsorption in [L]. The estimation was not possible for analytes with missing data values, the following considerations only refer to available estimations.

The highest desorption percentage was obtained for ethanol in sample D.4 (52 %) and the lowest was that of propionate in sample D.3 (6 %), as illustrated in Figure 34. The overall average is 21 % and the standard deviation is 14 %, indicating a highly varied sample of measurements.

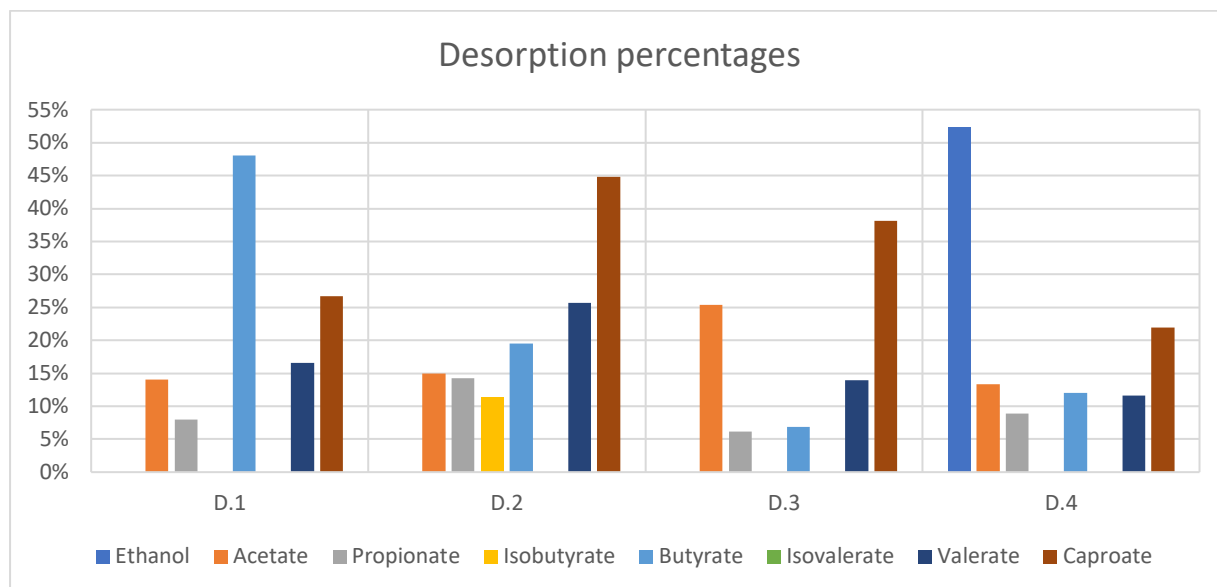


Figure 34: Percentage of desorbed carboxylic acids compared to those adhering to the surface after absorption for sample D.1 (A.1a in methanol), D.2 (A.8b in methanol), D.3 (A.1b in water), D.4 (A.8a in water).

The results obtained confirm that short-chain carboxylates are present in the supernatants after the desorption step. Despite this was not verified for every analyte in every sample, due to difficulties in the analysis, the reversible nature of the capture process is confirmed. Further experiments are needed to optimize this step given the low numerosity of the current sample, which does not allow detection of whether one solvent is more effective or whether carboxylates behave in significantly different ways.

The relatively low figures (most below 20 %) indicate a resilient interaction between carboxylate and the F-MNPs' surface which facilitates the capture in diluted environments but may require specific conditions during desorption. For further dedicated studies, the nature of the interaction in place should be investigated and solvents with different pH should be tested. Alkali presence could result in the release of carboxylates, as amine groups change their electrical charges, but will cause neutralization of the carboxylate requiring an additional subsequent salt-breaking step. To avoid this step volatile alkalis can be used so that the alkali-carboxylic acid complex can be thermally decomposed to obtain the carboxylic acid [96]. The desorption could also be facilitated by acidic environments, where the carboxylates are protonated to obtain carboxylic acids, but in these conditions, magnetic nanoparticles are prone to amorphization and breakdown [42].

Furthermore, the solvents' volumes used for desorption should be minimized to avoid excessive dilution that would increase separation and purification costs. Dilution is evidently counterproductive when the desorption solvent is water, the use of large volumes for

desorption after adsorption from dilute solutions is clearly illogical. Therefore the reasonable alternatives are the use of very low volumes of water or organic solvents. Nanoparticles dispersed in high-boiling organic solvents may be treated directly in a distillation column to separate VFAs.

The possibilities introduced above require the determination of the maximum temperature, maximum pH, and minimum pH that can be sustained by the magnetite core and the APTES coating.

In conclusion, the developed nanoparticles can capture and release VFAs, yet the need for detailed and dedicated studies on the optimization of these steps and the kinetics at play is evident.

5.6. Second-cycle adsorption of VFAs with F-MNPs

The developed nanoparticles are aimed to be employed multiple times for VFAs extraction. Their reusability is a decisive property for the development of a process that treats wastes while limiting the generation of new ones.

The experiments to valid this possibility were conducted by performing a second adsorption test on nanoparticles separated after desorption. The procedure for this second adsorption was kept the same as that of the first adsorption; if for example the first one was conducted by stirring magnetically for 5 minutes, also this one will be stirred in the same way and for the same time to limit the variables at play.

The two phases were separated by centrifugation which proved effective leaving transparent and colourless or pale-yellow supernatants, as observed for the first adsorption step. After filtration of the liquid, gas chromatography analysis was conducted. All concentrations of carboxylates in solution have decreased after adsorption except ethanol in samples R.1 and R.2, as shown in Table 28.

Table 28: Gas chromatography results expressed as mg/L for second adsorption samples R.1, R.2, R.3, and R.4, together with stirring methods and contact times used; values in red are higher than the concentration in the starting VFAs solution.

	Ethanol [mg/L]	Acetate [mg/L]	Propionate [mg/L]	Isobutyrate [mg/L]	Butyrate [mg/L]	Isovalerate [mg/L]	Valerate [mg/L]	Caproate [mg/L]
R.1	5657	4417	860	450	2173	141	1484	5668
R.2	3909	3570	710	382	1761	125	1270	4741
R.3	2666	3963	774	412	1918	130	1365	5200
R.4	2515	3851	725	379	2296	134	1271	4853

In sample R.2 the ethanol concentration is 18 % (600 mg/L) higher than the starting concentration in the VFAs solution; In sample R.1 an even higher concentration is detected, being 71 % (2350 mg/L) greater than the concentration in the starting solution. Both are

second adsorption tests following desorption in methanol. This alcohol interacts with the chromatographic column in a similar manner to ethanol, so the two compounds produce two very close and possibly overlapped peaks in the chromatogram. This phenomenon causes integration to obtain the peak area, and therefore the associated concentration of ethanol, to be unreliable. Therefore, residues of methanol from desorption may explain the overestimated values for ethanol.

For all other data, the absorption percentages calculated using Equation (7) range between 2 % for caproate in R.1. and 35 % for isovalerate in R.2, as shown in Figure 35.

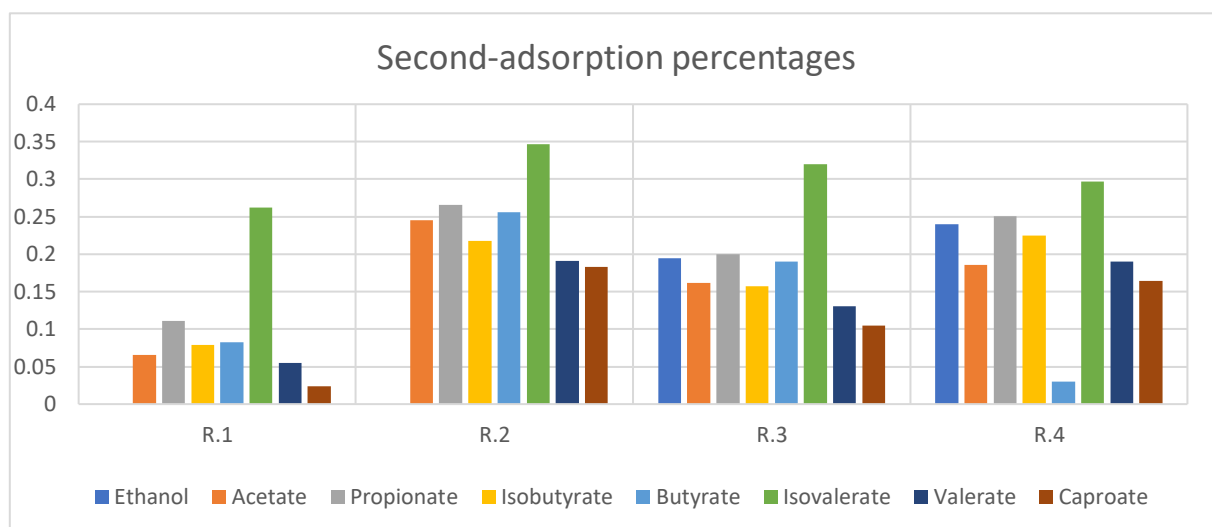


Figure 35: Percentages of adsorption of carboxylic acids after second adsorption for sample R.1 (magnetically stirred for 5'), R.2 (agitated with shaker for 120'), R.3 (magnetically stirred for 5'), and R.4 (agitated with shaker for 120').

During these second adsorption tests, nanoparticles captured on average 18 % of the carboxylates, with a standard deviation of 8 %. The lowest percentages are from sample R.1 where only isovalerate and propionate exceed the 10 % threshold. Sample R.2, also obtained with nanoparticles previously treated with methanol, shows much higher percentages, all values are either close to or above 20 %. Sample R.4 is close to these values except for the drastically lower figure associated with butyrate (3 %). As for experiment R.3, the absorption values all remain between 20 and 10 %, except for the isovalerate figure which reaches 32 %.

The quantity of carboxylates adsorbed on the surface of the functionalized nanoparticles during this second adsorption step is relatively high considering that the previous desorption was not complete, and so part of the interaction sites on F-MNPs' surface was already occupied. These non-desorbed VFAs reduce the number of amines groups available for interaction, add steric hindrance but may also interact with carboxylates in solution due to their high affinity.

An additional effect that can explain high adsorption despite the presence of non-desorbed VFAs is the dispersion of the particles. These had undergone adsorption, desorption, and adsorption again, so have been stirred for longer times and at higher temperatures (40° C

during desorption) than the nanoparticles of the first adsorption. Longer stirring may result in better dispersion and hence more surface available for adsorption. The temperature maintained during agitation may also have influenced the dispersion, the effect of this parameter on adsorption should be better examined.

As for the previous steps, it is not possible to identify a better second-adsorption method but only to assess the effectiveness of the developed nanoparticles under different conditions.

The results obtained confirm the reduction of carboxylates in solution by contact with nanoparticles that had already undergone one adsorption and one desorption step, i.e. a complete capture cycle. This confirms the possibility of reusing the nanoparticles for a second adsorption step, however further tests to confirm that also second-desorption is feasible and assess the total number of cycles tolerated by the nanoparticles are necessary.

5.7. Functionalization reaction optimization

The coating, or functionalization, is vital to limit MNPs agglomeration and oxidation, and also to have the desired chemical functional groups on MNPs surface. Considering the importance of functionalization, and the lack of studies investigating the effects of parameters involved, part of the thesis work was devoted to optimising the functionalization reaction. The optimization aims at maximizing the number of amine groups on the surface of nanoparticles, as measured by the functionalization percentage.

Starting from two different literature procedures, described in paragraph F.1 and F.5, the influence of reaction time, coating agent type (APTES or hydrolysed-APTES), and quantity of coating agent have been studied.

For the sake of a clear presentation, the procedure characterised by 5 hours duration, 60°C, and water as reaction liquid [49] will be referred to as the 5-hours procedure, while the one characterised by 1 hour duration, 40°C and a solution of ethanol/water (1:1 volume ratio) as reaction liquid [70] will be referred to as the 1-hour procedure.

To assess the percentage of functionalization achieved with each reaction the equation (6) was employed, using CHNS elemental analysis results.

The first reaction tested (F.1), the one employed for adsorption and desorption tests, is characterised by a preliminary APTES hydrolysis step and was performed following the 5-hours procedure with a 1:9 molar ratio [49]. The resulting F-MNPs have a mean functionalization percentage of 7.7 %.

The first experimental condition investigated was the molar ratio: the *5-hours reaction* was carried out with 1:18 (F.2) and 1:4 (F.3). Both exhibited different behaviours during the work-up with respect to F.1.

F.2 resulted in slower decantation and darker supernatants (Figure 36), the reaction liquid was dark brown and slightly turbid after a 30 minutes magnetic decantation. Since reaction liquid separation performed poorly, for the washing with water the system was left decanting

overnight, but still, an orange supernatant was obtained. Finally, the second wash with ethanol gave a clearer supernatant, but the magnetic decantation took more than one hour. Progressively clearer supernatants, going from reaction liquid to last washing, might indicate the presence of undesired compounds being washed away from the nanoparticles. In further tests, the supernatants should be analysed to see if the colour is due to a very fine suspension of particles or unwanted compounds deriving from the functionalization reaction.

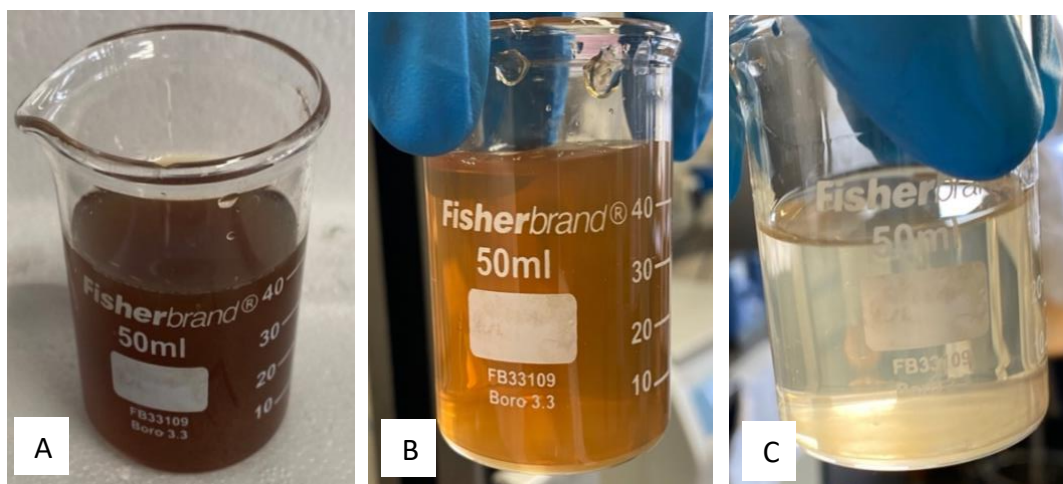


Figure 36: F.2 work-up supernatants. A) reaction liquid, B) washing water, C) washing ethanol.

On the contrary, the separation of the reaction liquid for F.3 took about an hour and resulted in a clear but slightly turbid supernatant (Figure 37), and for the washing water and the ethanol about 10 minutes were enough to observe a good separation.

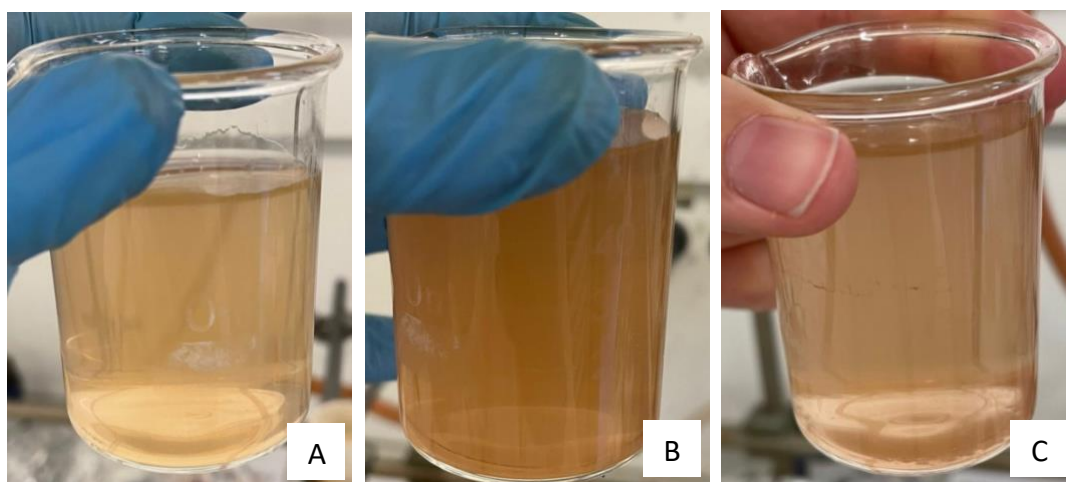


Figure 37: F.3 work-up supernatants. A) reaction liquid, B) washing water, C) washing ethanol

Based on the behaviour of F-MNPs during the work-up, F.3 seemed to be the best functionalization reaction in terms of speed and magnetic decantation efficiency.

In Table 29 functionalization percentage results are displayed, the optimal ratio is 1:4. This is in line with what X. C. Shen et al. (2004) [70] reported but they determine the optimal surface modification based on improved colloidal stability, and not based on a direct measure of functionalization percentage, as in this work.

Table 29: Functionalization percentages of reactions with different MNPs to APTES molar ratio; for all the reactions hydrolysed-APTES was employed and the reaction time was of 5 hours.

	F.1	F.2	F.3
MNPs/APTES molar ratio	1:9	1:18	1:4
Functionalization %	7.7 %	5.9 %	10.7 %

The smaller functionalization percentage achieved by F.2 could be explained by the tendency of APTES to polymerise when present in excess, this can cause the formation of heterogeneous multilayers on the surface [152] or might increase the steric hindrance of the ligand, therefore reducing the obtained functionalization.

The best performing molar ratio of MNPs/APTES, equal to 1:4, was kept constant in the subsequent experiments, to observe the influence of the other parameters.

F.4 was performed with hydrolysed-APTES as the coating agent but using the 1-hour procedure. The magnetic decantation of the reaction liquid took more than 1 hour and resulted in a light brown turbid supernatant; water and ethanol washing had similarly coloured supernatant but took less time, respectively 18 and 10 minutes (Figure 38).

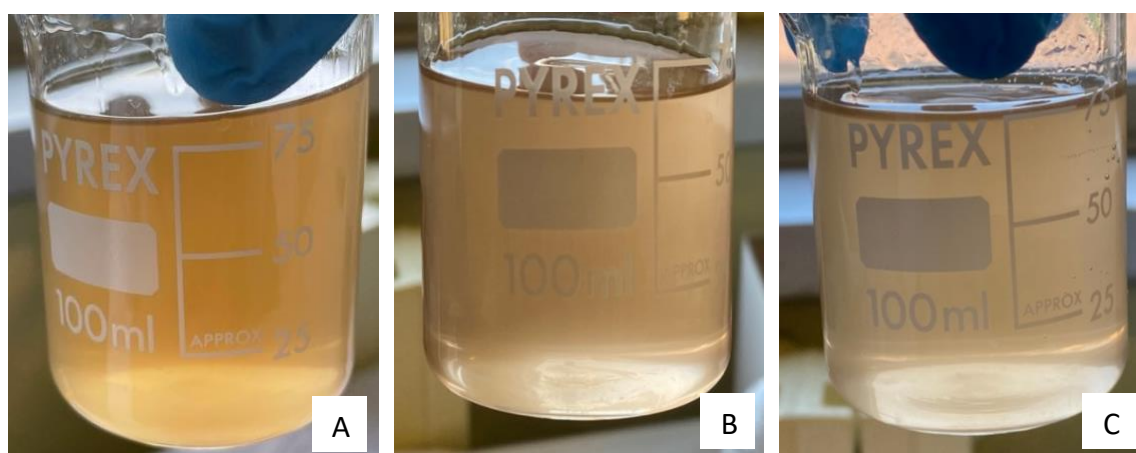


Figure 38: F.4 work-up supernatants. A) reaction liquid, B) washing water, C) washing ethanol

F.5 was performed with APTES as the coating agent and experimental conditions of the 1-hour procedure. Similarly, the reaction liquid took more than one hour while water and ethanol washing around 15 and 20 minutes, all of them resulted in clear supernatants (Figure 39).

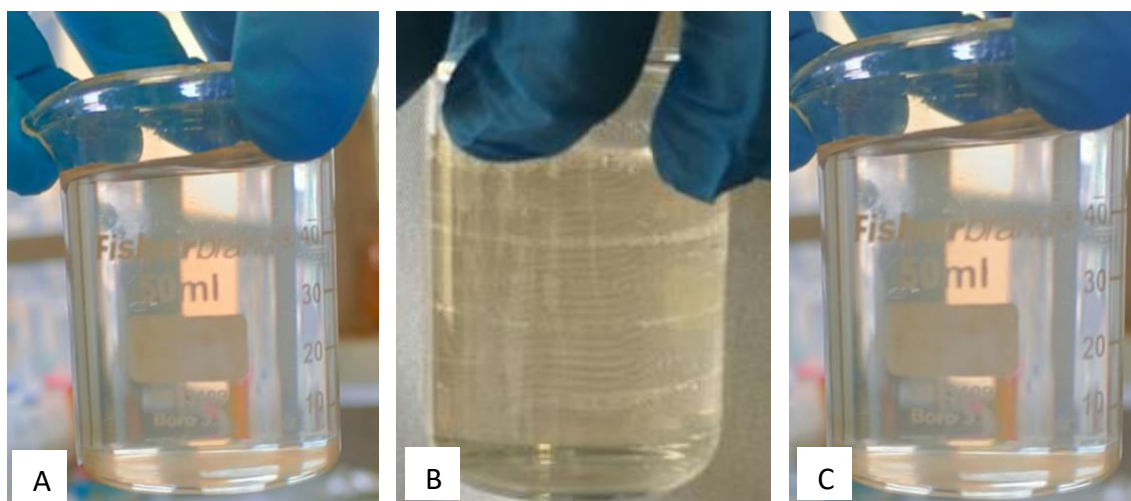


Figure 39: F.5 work-up supernatants. A) reaction liquid, B) washing water, C) washing ethanol

Lastly, F.6 was carried out with APTES as the coating agent and the 5-hours procedure. For this experiment centrifugation was exploited. For the reaction liquid and the washing water, 6 minutes at 8000 rpm were enough to obtain a clear supernatant, while for the washing with ethanol 9 minutes at 8000 rpm were needed.

Functionalization percentages were calculated for each reaction using equation (6) and the results are summarised in Table 30.

Table 30: Functionalization reaction with different experimental conditions

	F.3	F.4	F.5	F.6
Coating type	Hydrolysed-APTES	Hydrolysed-APTES	APTES	APTES
Reaction	5 hours	1 hour	1 hour	5 hours
Functionalization %	10.7 %	8.4 %	2.6 %	8 %

Looking at tests using hydrolysed-APTES (F.3 and F.4) and APTES (F.5 and F.6) in both pairs the 1-hour procedure resulted in a lower functionalization percentage. The use of hydrolysed-APTES has produced F-MNPs with higher functionalization percentages following both procedures. Despite this, the tests F.4 (8.4 %) and F.6 (8 %) performed similarly.

In further studies the optimal functionalization should be selected after having investigated: the influence of functionalization percentage on the quantity of VFAs adsorbed and desorbed; if there is an influence of the use of non-hydrolysed APTES on the adsorption and desorption; the cost-benefit analysis of the configurations. Regarding the latter, the question is whether it is economically convenient to make an additional reaction, namely APTES hydrolysis, and a 5 hours functionalization to gain only about 3 % more in functionalization percentage. Considering that by avoiding the hydrolysis and keeping the 5-hours procedure it is possible to get 8 % and that by keeping the hydrolysis step and using the 1-hour procedure a value of 8.4 % can be reached. These research questions are of great interest but are out of the scope of this preliminary analysis.

Additional characterizations are useful to have further insights into the nature of the magnetic core and the coating layer (monolayer or complex multilayer). Specifically, SEM and TEM analyses, to evaluate particles shape and average particle size, and VSM analysis, to assess MNPs and F-MNPs magnetic behaviour should be performed. Three samples were chosen to be analysed: the sample of MNPs, the sample of F-MNPs with the highest functionalization percentage among those with APTES, and the sample of F-MNPs with the highest functionalization percentage among those with hydrolysed-APTES. In the following sub-paragraph, SEM results are presented, while VSM and TEM results are not available yet.

5.7.1. Scanning Electron Microscopy results

SEM micrographs were obtained for uncoated MNPs (S3), F-MNPs with hydrolysed-APTES (F.3), and F-MNPs with APTES (F.6). Non-uniform aggregates with irregular shapes are observed for all three samples, this is in line with what Indrayana (2019)[144] finds after producing MNPs with the co-precipitation method, the micrographs are shown side by side in Figure 40.

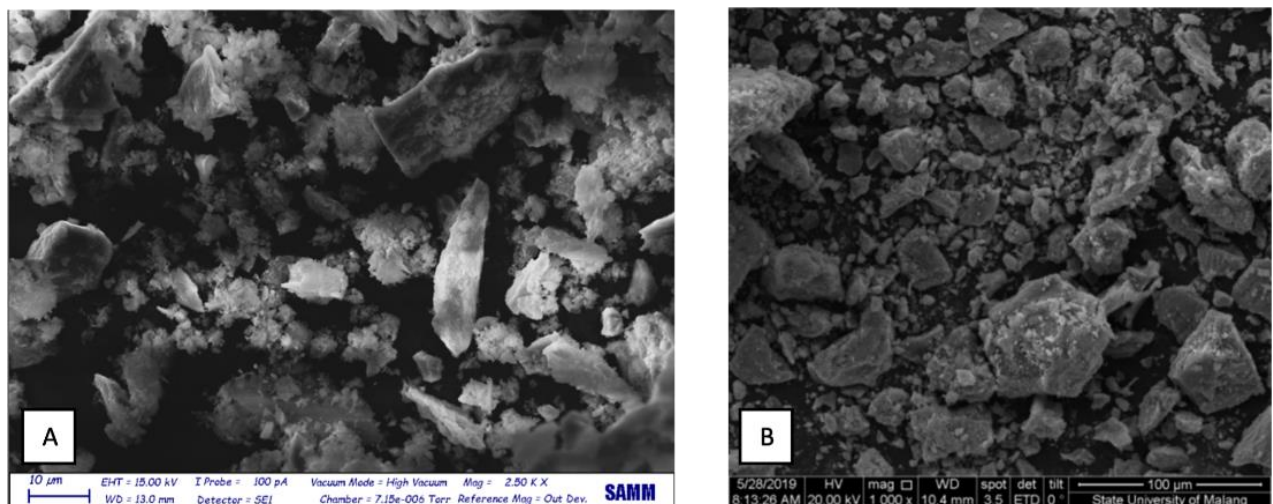


Figure 40: SEM micrograph of sample S3 (A) compare with literature image (B) from Indrayana (2019)

The broad size distribution observed can be justified by the imperfect nucleation process, but it is more probably due to the agglomeration of the particles, as observed also by Y. F. Shen et al., (2009) [77]. The fast agglomeration has already been verified by DLS, was visibly evident after lyophilization and is also supported by the SEM micrograph of sample S.3 in Figure 41, in which smaller grouped bodies are visible.

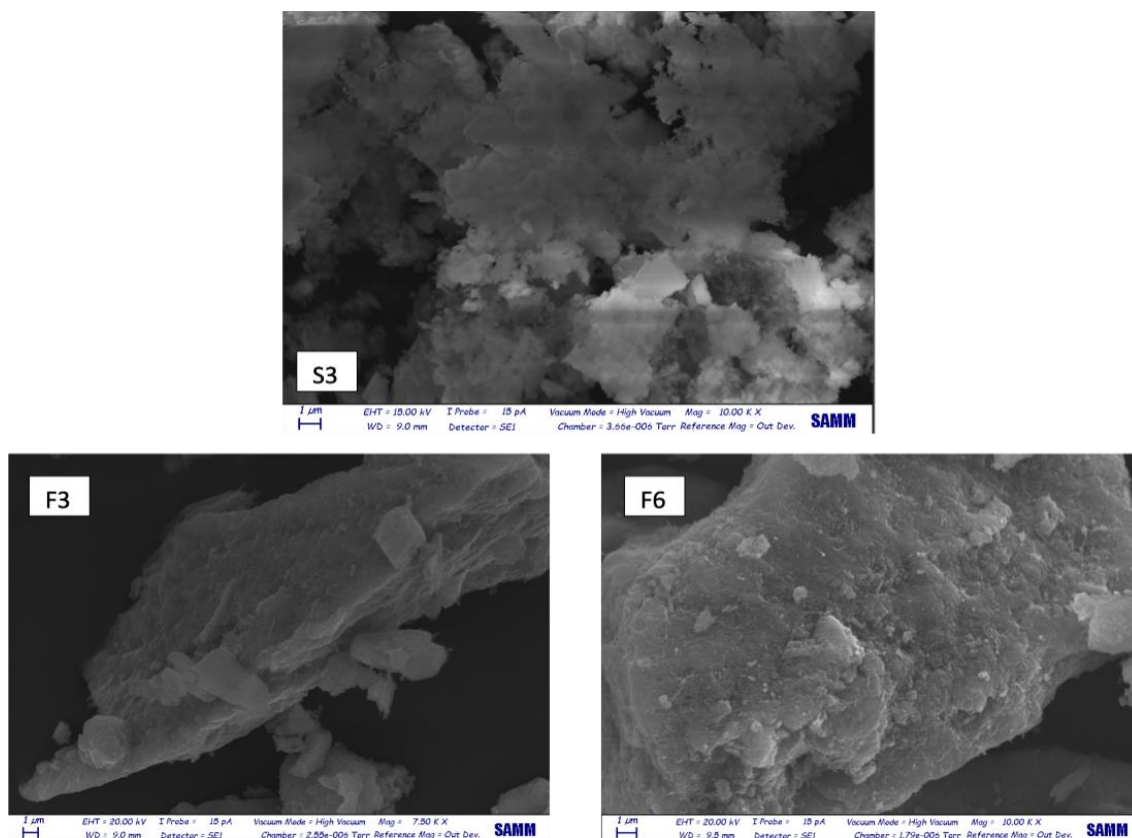


Figure 41: SEM micrograph of samples S3, F3 and F6

MNPs were grounded in a mortar and pestle prior to the analysis to destroy the aggregates formed during lyophilization. Despite that, SEM analysis suggests that the sample still has aggregates with varied grain sizes. The lyophilization was used to have quantitative data for optimizing functionalization but will not be used in industrial practice.

Conclusively, the SEM analysis resulted to be unsatisfactory and unsuitable to measure the size of the nanoparticles and to detect differences between MNPs and F-MNPs. Therefore, TEM analysis is being conducted to have a proper estimation of the particles' dimension and morphology.

Chapter 6: Conclusions

Production of valuable products starting from organic food waste is a prolific field of research in this decade, it's an opportunity to exploit wastes that represent a burden and that otherwise would be disposed of. This thesis work is framed in this context and has proposed an innovative way to recover VFAs from diluted aqueous solutions through the use of specific functionalized magnetic nanoparticles.

The first step achieved was the synthesis, via chemical co-precipitation, of the iron oxides magnetic nanoparticles (MNPs). The characterization obtained using XRD showed that magnetite nanoparticles were successfully produced, while DLS and SEM analysis confirmed MNPs' tendency to aggregate into clusters.

Successively, APTES was selected as the ligand for the coating due to its amine functions, these are able to interact with dissociated carboxylic acids in solution. The functionalization reaction was performed and the resulting nanoparticles' characterization using FT-IR, Z-potential, and CHNS analyses confirmed successful bonding of APTES to the surface. Regarding the magnetic behaviour, both MNPs and F-MNPs will be studied using VSM in the near future.

Once the F-MNPs were ready, also the synthetic solution of VFAs was prepared and adsorption tests started. MNPs and F-MNPs were tested with two different agitation methods, four different contact times and a fixed mass of nanoparticles-to-volume of VFAs solution ratio. The adsorption occurred in all the conditions and nanoparticles didn't show strong selectivity for one analyte over the others.

The two tests showing uniformly high uptakes for all analytes were replicated, but showed lower uptake values of VFAs, indicating a high experimental variability. Among the possible causes for variability, the inhomogeneity in the aggregation extent in different adsorption samples was considered the most plausible.

These replicates were used to perform desorption tests in deionised water and methanol. The desorption was verified with both solvents even though residues of methanol reduced the number of accurate data available. For further analysis, the development of a new analytical method or new calibration lines is suggested. The desorption was not complete indicating a resilient interaction between carboxylates and amine groups, that may require peculiar conditions for desorption. The possibilities of using volatile alkali, acidic environments or high boiling organic solvents for desorption should be investigated in the future.

A second adsorption test was conducted after desorption and resulted in similar capture values with respect to the first cycle despite the desorption was not complete. A possible explanation is the disaggregation of the nanoparticles after repeated agitation steps with respect to nanoparticles after only one adsorption; an additional phenomenon at play could be the affinity between adsorbed VFAs and VFAs in solution.

The tests conducted verified the feasibility of each process step. From these experiments, it is not possible to conclude whether it is optimal to use MNPs or F-MNPs for adsorption, nor to identify which are the best conditions for each step (e.g. agitation methodology, contact

time, temperature, pH) as only one replicate per experiment was performed. Optimization of each step to improve performance should be the object of further studies.

Finally, considering the vital role of the coating for the use of MNPs, the functionalization reaction was optimized by maximising the number of amine groups on the nanoparticles' surface. The highest functionalization percentage achieved is 10.7 %, using the 5-hours procedure with hydrolysed-APTES and MNPs/APTES molar ratio equal to 1:4.

This first experimental study of this novel methodology paves the way for future studies on many different aspects. A more in depth-characterization of the nanoparticles should be performed to better understand their behaviours in terms of aggregation, degradation under different conditions, magnetic response, type of interaction with carboxylates, and size distribution both before and after functionalization. The interaction of nanoparticles with fermentation culture could also be compelling to enable the in-situ extraction.

Adsorption and desorption steps should be investigated to reduce the variability observed, identify the governing equations and select the optimal conditions to maximize capture and release of VFAs; some parameters were considered in the preliminary tests, but many others could be potentially interesting (e.g. mass of nanoparticle-to-volume of solution ratio, pH, temperatures and agitation rates, solvents, number of capture-cycles). These future phases of development should use real fermentation broth to observe if capture is hindered by poisoning of the nanoparticles' surface with other compounds in solution. For example, if the proposed functionalization is maintained the occupation of interaction sites by anions commonly present in fermentation broths, like H_2PO_4^- , HPO_4^{2-} , Cl^- , and SO_4^{2-} [88], should be considered.

Finally, a detailed cost analysis should be conducted to support technological decisions in order to achieve a concretely feasible process.

Bibliography

- [1] UN Department of Economic and Social Affairs, "Goal 12." <https://sdgs.un.org/goals/goal12> (accessed Aug. 06, 2021).
- [2] S. Gaiani, S. Caldeira, V. Adorno, A. Segrè, and M. Vittuari, "Food wasters: Profiling consumers' attitude to waste food in Italy," *Waste Manag.*, vol. 72, pp. 17–24, 2018, doi: 10.1016/j.wasman.2017.11.012.
- [3] J. Jörissen, C. Priefer, and K. R. Bräutigam, "Food waste generation at household level: Results of a survey among employees of two European research centers in Italy and Germany," *Sustain.*, vol. 7, no. 3, pp. 2695–2715, 2015, doi: 10.3390/su7032695.
- [4] United Nations Environment Programme, H. (WRAP) Forbes, T. (WRAP) Quested, and C. (UNEP) O'Connor, *Food Waste Index Report 2021*. 2021.
- [5] - Food and Agriculture Organization of the United Nations FAO, *Food wastage footprint*. 2013.
- [6] "The Sustainable Development Goals Report 2020," pp. 4–5, 2020, doi: 10.18356/2282dd98-en.
- [7] European Parliament and Council of the European Union, *Directive 2008/98/EC of the European Parliament and of the Council*. 2008, pp. 3–30.
- [8] E. Papargyropoulou, R. Lozano, J. K. Steinberger, N. Wright, and Z. Bin Ujang, "The food waste hierarchy as a framework for the management of food surplus and food waste," *J. Clean. Prod.*, vol. 76, pp. 106–115, 2014, doi: 10.1016/j.jclepro.2014.04.020.
- [9] D. A. Teigiserova, L. Hamelin, and M. Thomsen, "Towards transparent valorization of food surplus, waste and loss: Clarifying definitions, food waste hierarchy, and role in the circular economy," *Sci. Total Environ.*, vol. 706, no. January 2020, p. 136033, 2020, doi: 10.1016/j.scitotenv.2019.136033.
- [10] J. Gustavsson, C. Cederberg, and U. Sonesson, "Global food losses and food waste - Extent, causes and prevention," 2011.
- [11] C. Caldeira, V. De Laurentiis, S. Corrado, F. van Holsteijn, and S. Sala, "Quantification of food waste per product group along the food supply chain in the European Union: a mass flow analysis," *Resour. Conserv. Recycl.*, vol. 149, no. August 2018, pp. 479–488, 2019, doi: 10.1016/j.resconrec.2019.06.011.
- [12] B. Buchner *et al.*, "Food waste: causes, impacts and proposals," Elsevier, 2012. doi: 10.3390/su10023381.
- [13] ISPRA, *Rapporto Rifiuti Urbani, Edizione 2020*, vol. 44, no. 8. 2020.
- [14] Republic of Italy, "Decreto Legislativo 3 aprile 2006, n. 152 'Norme in materia ambientale', Gazzetta Ufficiale n. 88 del 14 aprile 2006 - Supplemento Ordinario n. 96," *Gazz. Uff. Ital.*, p. 172, 2006.
- [15] C. Giordano, F. Alboni, and L. Falasconi, "Quantities, determinants, and awareness of households' food waste in Italy: A comparison between diary and questionnaires quantities," *Sustain.*, vol. 11, no. 12, 2019, doi: 10.3390/su10023381.
- [16] M. Cerciello, M. Agovino, and A. Garofalo, "Estimating food waste under the FUSIONS definition: What are the driving factors of food waste in the Italian provinces?," *Environ. Dev. Sustain.*, vol. 21, no. 3, pp. 1139–1152, 2019, doi: 10.1007/s10668-017-0080-0.
- [17] S. Heaven, Y. Zhang, R. Arnold, T. Paavola, F. Vaz, and C. Cavinato, "Compositional analysis of food waste from study sites in geographically distinct regions of Europe," 2010.
- [18] M. Grosso and L. Falasconi, "Addressing food wastage in the framework of the UN Sustainable Development Goals," *Waste Manag. Res.*, vol. 36, no. 2, pp. 97–98, 2018, doi: 10.1177/0734242X17751968.
- [19] G. Capson-Tojo, M. Rouez, M. Crest, J. P. Steyer, J. P. Delgenès, and R. Escudié, "Food waste valorization via anaerobic processes: a review," *Rev. Environ. Sci. Biotechnol.*, vol. 15, no. 3, pp. 499–547, 2016, doi: 10.1007/s11157-016-9405-y.

- [20] C. M. Braguglia, A. Gallipoli, A. Gianico, and P. Pagliaccia, "Anaerobic bioconversion of food waste into energy: A critical review," *Bioresour. Technol.*, vol. 248, pp. 37–56, 2018, doi: 10.1016/j.biortech.2017.06.145.
- [21] H. Fisgativa, A. Tremier, and P. Dabert, "Characterizing the variability of food waste quality: A need for efficient valorisation through anaerobic digestion," *Waste Manag.*, vol. 50, pp. 264–274, Apr. 2016, doi: 10.1016/J.WASMAN.2016.01.041.
- [22] G. Strazzera, F. Battista, N. H. Garcia, N. Frison, and D. Bolzonella, "Volatile fatty acids production from food wastes for biorefinery platforms: A review," *J. Environ. Manage.*, vol. 226, no. May, pp. 278–288, 2018, doi: 10.1016/j.jenvman.2018.08.039.
- [23] R. Zhang *et al.*, "Characterization of food waste as feedstock for anaerobic digestion," *Bioresour. Technol.*, vol. 98, no. 4, pp. 929–935, Mar. 2007, doi: 10.1016/J.BIORTECH.2006.02.039.
- [24] R. M. Fanelli, "Using causal maps to analyse the major root causes of household food waste: Results of a survey among people from central and southern Italy," *Sustain.*, vol. 11, no. 4, 2019, doi: 10.3390/su11041183.
- [25] Waste Watcher Observatory on Food and Sustainability, "Osservatorio sugli SPRECHI ALIMENTARI DOMESTICI delle FAMIGLIE ITALIANE Waste Watcher 2019," 2020.
- [26] A. Gianico, A. Gallipoli, G. Gazzola, C. Pastore, B. Tonanzi, and C. M. Braguglia, "A novel cascade biorefinery approach to transform food waste into valuable chemicals and biogas through thermal pretreatment integration," *Bioresour. Technol.*, vol. 338, no. July, p. 125517, 2021, doi: 10.1016/j.biortech.2021.125517.
- [27] J. Gustavsson, C. Cederberg, U. Sonesson, and A. Emanuelsson, "The methodology of the FAO study: 'Global Food Losses and Food Waste-extent, causes and prevention'-FAO, 2011," 2013.
- [28] ESTà, "Economia circolare del cibo a Milano," Milano, 2020.
- [29] "Land Application - an overview | ScienceDirect Topics." <https://www.sciencedirect.com/topics/agricultural-and-biological-sciences/land-application> (accessed Aug. 09, 2021).
- [30] W. M. Randall Seeker, "Waste combustion," *Symp. Combust.*, vol. 23, no. 1, pp. 867–885, Jan. 1991, doi: 10.1016/S0082-0784(06)80341-3.
- [31] "Trattamenti Biologici - Centro Studi MatER." <https://www.mater.polimi.it/wikimater/trattamenti-biologici/> (accessed Jul. 18, 2021).
- [32] H. H. Khoo, T. Z. Lim, and R. B. H. Tan, "Food waste conversion options in Singapore: Environmental impacts based on an LCA perspective," *Sci. Total Environ.*, vol. 408, no. 6, pp. 1367–1373, Feb. 2010, doi: 10.1016/J.SCITOTENV.2009.10.072.
- [33] C. Xu, W. Shi, J. Hong, F. Zhang, and W. Chen, "Life cycle assessment of food waste-based biogas generation," *Renew. Sustain. Energy Rev.*, vol. 49, pp. 169–177, Sep. 2015, doi: 10.1016/J.RSER.2015.04.164.
- [34] "REVENUE project." <https://www.revenueproject.eu/>.
- [35] M. Ramos-Suarez, Y. Zhang, and V. Outram, *Current perspectives on acidogenic fermentation to produce volatile fatty acids from waste*, vol. 20, no. 2. Springer Netherlands, 2021.
- [36] M. P. Zacharof and R. W. Lovitt, "Complex effluent streams as a potential source of volatile fatty acids," *Waste and Biomass Valorization*, vol. 4, no. 3, pp. 557–581, 2013, doi: 10.1007/s12649-013-9202-6.
- [37] P. A. Hernandez *et al.*, "Selective Extraction of Medium-Chain Carboxylic Acids by Electrodialysis and Phase Separation," *ACS Omega*, vol. 6, no. 11, pp. 7841–7850, 2021, doi: 10.1021/acsomega.1c00397.
- [38] C. C. Hua *et al.*, "Size-controlled synthesis and characterization of Fe₃O₄ nanoparticles by chemical coprecipitation method," *Sains Malaysiana*, vol. 37, no. 4, pp. 389–394, 2008.
- [39] A. Ali *et al.*, "Synthesis, characterization, applications, and challenges of Iron Oxide Nanoparticles," *Powder Technol.*, vol. 7, no. 6, pp. 49–67, 2016.
- [40] A. V. Samrot, C. S. Sahithya, J. Selvarani A, S. K. Purayil, and P. Ponnaiah, "A review on

- synthesis, characterization and potential biological applications of superparamagnetic iron oxide nanoparticles," *Curr. Res. Green Sustain. Chem.*, vol. 4, no. September 2020, p. 100042, 2021, doi: 10.1016/j.crgsc.2020.100042.
- [41] K. N. Koo, A. F. Ismail, M. H. D. Othman, N. Bidin, and M. A. Rahman, "Preparation and characterization of superparamagnetic magnetite (Fe₃O₄) nanoparticles: A short review," *Malaysian J. Fundam. Appl. Sci.*, vol. 15, no. 1, pp. 23–31, 2019, doi: 10.11113/mjfas.v15n2019.1224.
- [42] A. Kozlovskiy, D. Tuleubayeva, and K. K. Kadyrzhanov, "Study of Fe₃O₄ nanoparticles degradation process," *Eurasian J. Phys. Funct. Mater.*, 2018.
- [43] W. Wu, Q. He, and C. Jiang, "Magnetic iron oxide nanoparticles: Synthesis and surface functionalization strategies," *Nanoscale Res. Lett.*, vol. 3, no. 11, pp. 397–415, 2008, doi: 10.1007/s11671-008-9174-9.
- [44] M. R. Ghazanfari, M. Kashefi, S. F. Shams, and M. R. Jaafari, "Perspective of Fe₃O₄ Nanoparticles Role in Biomedical Applications," *Biochem. Res. Int.*, vol. 2016, no. February 2017, 2016, doi: 10.1155/2016/7840161.
- [45] U. Jeong, X. Teng, Y. Wang, H. Yang, and Y. Xia, "Superparamagnetic colloids: Controlled synthesis and niche applications," *Adv. Mater.*, vol. 19, no. 1, pp. 33–60, 2007, doi: 10.1002/adma.200600674.
- [46] M. Faraji, Y. Yamini, and M. Rezaee, "Magnetic nanoparticles : synthesis , stabilization , functionalization , characterization , and applications," *J. Iran. Chem. Soc.*, vol. 7, no. 1, pp. 1–37, 2010.
- [47] F. E. Kruis, H. Fissan, and A. Peled, "Synthesis of nanoparticles in the gas phase for electronic, optical and magnetic applications - A review," *Journal of Aerosol Science*, vol. 29, no. 5–6. pp. 511–535, 1998, doi: 10.1016/S0021-8502(97)10032-5.
- [48] A. V. Samrot, C. S. Sahithya, J. Selvarani A, S. K. Purayil, and P. Ponnaiah, "A review on synthesis, characterization and potential biological applications of superparamagnetic iron oxide nanoparticles," *Curr. Res. Green Sustain. Chem.*, vol. 4, no. September 2020, p. 100042, 2021, doi: 10.1016/j.crgsc.2020.100042.
- [49] S. K. Mahmad Rozi, S. Bakhshaei, N. S. Abdul Manan, and S. Mohamad, "Superhydrophobic magnetic nanoparticle-free fatty acid regenerated from waste cooking oil for the enrichment of carcinogenic polycyclic aromatic hydrocarbons in sewage sludges and landfill leachates," *RSC Adv.*, vol. 6, no. 90, pp. 87719–87729, 2016, doi: 10.1039/c6ra15319d.
- [50] G. Kandasamy and D. Maity, "Recent advances in superparamagnetic iron oxide nanoparticles (SPIONs) for in vitro and in vivo cancer nanotheranostics," *Int. J. Pharm.*, vol. 496, no. 2, pp. 191–218, 2015, doi: 10.1016/j.ijpharm.2015.10.058.
- [51] K. B. Narayanan and N. Sakthivel, "Biological synthesis of metal nanoparticles by microbes," *Adv. Colloid Interface Sci.*, vol. 156, no. 1–2, pp. 1–13, 2010, doi: 10.1016/j.cis.2010.02.001.
- [52] P. Ravindra, "Protein-mediated synthesis of gold nanoparticles," *Mater. Sci. Eng. B Solid-State Mater. Adv. Technol.*, vol. 163, no. 2, pp. 93–98, 2009, doi: 10.1016/j.mseb.2009.05.013.
- [53] S. Ashraf *et al.*, "Protein-mediated synthesis, pH-induced reversible agglomeration, toxicity and cellular interaction of silver nanoparticles," *Colloids Surfaces B Biointerfaces*, vol. 102, pp. 511–518, 2013, doi: 10.1016/j.colsurfb.2012.09.032.
- [54] M. Okuda, J. C. Eloi, S. E. Ward Jones, A. Sarua, R. M. Richardson, and W. Schwarzacher, "Fe₃O₄ nanoparticles: Protein-mediated crystalline magnetic superstructures," *Nanotechnology*, vol. 23, no. 41, 2012, doi: 10.1088/0957-4484/23/41/415601.
- [55] P. Dauthal and M. Mukhopadhyay, "Noble Metal Nanoparticles: Plant-Mediated Synthesis, Mechanistic Aspects of Synthesis, and Applications," *Ind. Eng. Chem. Res.*, vol. 55, no. 36, pp. 9557–9577, 2016, doi: 10.1021/acs.iecr.6b00861.
- [56] A. Nentwich, "Production of nanoparticles and nanomaterials," *Planet-Austria.At*, vol. 6, no. November, pp. 1–4, 2011, [Online]. Available: http://planet-austria.at/0xc1aa500d_0x002544e3.pdf.

- [57] D. M. Mattox, "Ion plating - past, present and future," *Surf. Coatings Technol.*, vol. 133–134, pp. 517–521, 2000, doi: 10.1016/S0257-8972(00)00922-1.
- [58] D. Ling and T. Hyeon, "Chemical design of biocompatible iron oxide nanoparticles for medical applications," *Small*, vol. 9, no. 9–10, pp. 1450–1466, 2013, doi: 10.1002/smll.201202111.
- [59] V. R. Manfrinato *et al.*, "Resolution limits of electron-beam lithography toward the atomic scale," *Nano Lett.*, vol. 13, no. 4, pp. 1555–1558, 2013, doi: 10.1021/nl304715p.
- [60] T. Sugimoto and E. Matijević, "Formation of uniform spherical magnetite particles by crystallization from ferrous hydroxide gels," *J. Colloid Interface Sci.*, vol. 74, no. 1, pp. 227–243, Mar. 1980, doi: 10.1016/0021-9797(80)90187-3.
- [61] D. Zins, V. Cabuil, and R. Massart, "New aqueous magnetic fluids," *J. Mol. Liq.*, vol. 83, no. 1–3, pp. 217–232, Dec. 1999, doi: 10.1016/S0167-7322(99)00087-2.
- [62] J. L. Li, D. C. Li, S. L. Zhang, H. C. Cui, and C. Wang, "Analysis of the factors affecting the magnetic characteristics of nano-Fe₃O₄ particles," *Chinese Sci. Bull.*, vol. 56, no. 8, pp. 803–810, 2011, doi: 10.1007/s11434-010-4126-z.
- [63] Z. Lei, B. Chen, Y. M. Koo, and D. R. Macfarlane, "Introduction: Ionic Liquids," *Chem. Rev.*, vol. 117, no. 10, pp. 6633–6635, 2017, doi: 10.1021/acs.chemrev.7b00246.
- [64] M. C. Mascolo, Y. Pei, and T. A. Ring, "Room Temperature Co-Precipitation Synthesis of Magnetite Nanoparticles in a Large pH Window with Different Bases," *Materials (Basel)*, vol. 6, no. 12, pp. 5549–5567, 2013, doi: 10.3390/ma6125549.
- [65] M. Mahdavi *et al.*, "Synthesis, surface modification and characterisation of biocompatible magnetic iron oxide nanoparticles for biomedical applications," *Molecules*, vol. 18, no. 7, pp. 7533–7548, 2013, doi: 10.3390/molecules18077533.
- [66] J. Sun *et al.*, "Synthesis and characterization of biocompatible Fe₃O₄ nanoparticles," *J. Biomed. Mater. Res. Part A*, vol. 80A, no. 2, pp. 333–341, Feb. 2007, doi: 10.1002/JBM.A.30909.
- [67] L. Mohammed, H. G. Gomma, D. Ragab, and J. Zhu, "Magnetic nanoparticles for environmental and biomedical applications: A review," *Particuology*, vol. 30, pp. 1–14, 2017, doi: 10.1016/j.partic.2016.06.001.
- [68] S. Villa, P. Riani, F. Locardi, and F. Canepa, "Functionalization of Fe₃O₄ NPs by silanization: Use of amine (APTES) and thiol (MPTMS) silanes and their physical characterization," *Materials (Basel)*, vol. 9, no. 10, 2016, doi: 10.3390/ma9100826.
- [69] Y. Wei, B. Han, X. Hu, Y. Lin, X. Wang, and X. Deng, "Synthesis of Fe₃O₄ nanoparticles and their magnetic properties," *Procedia Eng.*, vol. 27, no. 2011, pp. 632–637, 2012, doi: 10.1016/j.proeng.2011.12.498.
- [70] X. C. Shen, X. Z. Fang, Y. H. Zhou, and H. Liang, "Synthesis and characterization of 3-aminopropyltriethoxysilane-modified superparamagnetic magnetite nanoparticles," *Chem. Lett.*, vol. 33, no. 11, pp. 1468–1469, 2004, doi: 10.1246/cl.2004.1468.
- [71] K. Can, M. Ozmen, and M. Ersoz, "Immobilization of albumin on aminosilane modified superparamagnetic magnetite nanoparticles and its characterization," *Colloids Surfaces B Biointerfaces*, vol. 71, no. 1, pp. 154–159, 2009, doi: 10.1016/j.colsurfb.2009.01.021.
- [72] B. Feng *et al.*, "Synthesis of Fe₃O₄/APTES/PEG diacid functionalized magnetic nanoparticles for MR imaging," *Colloids Surfaces A Physicochem. Eng. Asp.*, vol. 328, no. 1–3, pp. 52–59, 2008, doi: 10.1016/j.colsurfa.2008.06.024.
- [73] S. K. Mahmud Rozi, S. Bakhshaei, N. S. Abdul Manan, and S. Mohamad, "Superhydrophobic magnetic nanoparticle-free fatty acid regenerated from waste cooking oil for the enrichment of carcinogenic polycyclic aromatic hydrocarbons in sewage sludges and landfill leachates," *RSC Adv.*, vol. 6, no. 90, pp. 87719–87729, 2016, doi: 10.1039/c6ra15319d.
- [74] V. C. Karade *et al.*, "APTES monolayer coverage on self-assembled magnetic nanospheres for controlled release of anticancer drug Nintedanib," *Sci. Rep.*, vol. 11, no. 1, pp. 1–12, 2021, doi: 10.1038/s41598-021-84770-0.
- [75] D. Wan, W. Li, G. Wang, and X. Wei, "Size-controllable synthesis of Fe₃O₄ nanoparticles

- through oxidation-precipitation method as heterogeneous Fenton catalyst," *J. Mater. Res.*, vol. 31, no. 17, pp. 2608–2616, 2016, doi: 10.1557/jmr.2016.285.
- [76] X.-Q. Zhang, S.-W. Gong, Y. Zhang, T. Yang, C.-Y. Wangband, and N. Gu, "Prussian blue modified iron oxide magnetic nanoparticles and their highperoxidase-like activity.pdf." 2010.
- [77] Y. F. Shen, J. Tang, Z. H. Nie, Y. D. Wang, Y. Ren, and L. Zuo, "Preparation and application of magnetic Fe₃O₄ nanoparticles for wastewater purification," *Sep. Purif. Technol.*, vol. 68, no. 3, pp. 312–319, 2009, doi: 10.1016/j.seppur.2009.05.020.
- [78] W. F. Elmobarak and F. Almomani, "Application of magnetic nanoparticles for the removal of oil from oil-in-water emulsion: Regeneration/reuse of spent particles," *J. Pet. Sci. Eng.*, vol. 203, no. February, p. 108591, 2021, doi: 10.1016/j.petro.2021.108591.
- [79] J. F. Liu, Z. S. Zhao, and G. Bin Jiang, "Coating Fe₃O₄ magnetic nanoparticles with humic acid for high efficient removal of heavy metals in water," *Environ. Sci. Technol.*, vol. 42, no. 18, pp. 6949–6954, 2008, doi: 10.1021/es800924c.
- [80] C. S. López-Garzón and A. J. J. Straathof, "Recovery of carboxylic acids produced by fermentation," *Biotechnol. Adv.*, vol. 32, no. 5, pp. 873–904, 2014, doi: 10.1016/j.biotechadv.2014.04.002.
- [81] L. Reyes, C. Nikitine, L. Vilcoq, and P. Fongarland, "Green is the new black-A review of technologies for carboxylic acid recovery from black liquor," *Green Chem.*, vol. 22, no. 23, pp. 8097–8115, 2020, doi: 10.1039/d0gc02627a.
- [82] E. Alkaya, S. Kaptan, L. Ozkan, S. Uludag-Demirer, and G. N. Demirer, "Recovery of acids from anaerobic acidification broth by liquid-liquid extraction," *Chemosphere*, vol. 77, no. 8, pp. 1137–1142, 2009, doi: 10.1016/j.chemosphere.2009.08.027.
- [83] A. van den Bruinhorst, S. Raes, S. A. Maesara, M. C. Kroon, A. C. C. Esteves, and J. Meuldijk, "Hydrophobic eutectic mixtures as volatile fatty acid extractants," *Sep. Purif. Technol.*, vol. 216, no. September 2018, pp. 147–157, 2019, doi: 10.1016/j.seppur.2018.12.087.
- [84] A. Banel and B. Zygmunt, "Application of gas chromatography-mass spectrometry preceded by solvent extraction to determine volatile fatty acids in wastewater of municipal, animal farm and landfill origin," *Water Sci. Technol.*, vol. 63, no. 4, pp. 590–597, 2011, doi: 10.2166/wst.2011.204.
- [85] H. Yesil, H. Taner, F. Ugur Nigiz, N. Hilmioglu, and A. E. Tugtas, "Pervaporative Separation of Mixed Volatile Fatty Acids: A Study Towards Integrated VFA Production and Separation," *Waste and Biomass Valorization*, vol. 11, no. 5, pp. 1737–1753, 2020, doi: 10.1007/s12649-018-0504-6.
- [86] M. Atasoy, I. Owusu-Agyeman, E. Plaza, and Z. Cetecioglu, "Bio-based volatile fatty acid production and recovery from waste streams: Current status and future challenges," *Bioresour. Technol.*, vol. 268, no. May, pp. 773–786, 2018, doi: 10.1016/j.biortech.2018.07.042.
- [87] W. de A. Cavalcante, R. C. Leitão, T. A. Gehring, L. T. Angenent, and S. T. Santaella, "Anaerobic fermentation for n-caproic acid production: A review," *Process Biochem.*, vol. 54, pp. 106–119, 2017, doi: 10.1016/j.procbio.2016.12.024.
- [88] E. V. Fufachev, B. M. Weckhuysen, and P. C. A. Bruijninx, "Toward Catalytic Ketonization of Volatile Fatty Acids Extracted from Fermented Wastewater by Adsorption," *ACS Sustain. Chem. Eng.*, vol. 8, no. 30, pp. 11292–11298, 2020, doi: 10.1021/acssuschemeng.0c03220.
- [89] S. J. Andersen *et al.*, "Electrolytic extraction drives volatile fatty acid chain elongation through lactic acid and replaces chemical pH control in thin stillage fermentation," *Biotechnol. Biofuels*, vol. 8, no. 1, pp. 1–14, 2015, doi: 10.1186/s13068-015-0396-7.
- [90] H. Yesil, B. Calli, and A. E. Tugtas, "A hybrid dry-fermentation and membrane contactor system: Enhanced volatile fatty acid (VFA) production and recovery from organic solid wastes," *Water Res.*, vol. 192, p. 116831, 2021, doi: 10.1016/j.watres.2021.116831.
- [91] Y. Du, B. Schuur, C. Samorì, E. Tagliavini, and D. W. F. Brilman, "Secondary amines as switchable solvents for lipid extraction from non-broken microalgae," *Bioresour. Technol.*,

- vol. 149, pp. 253–260, Dec. 2013, doi: 10.1016/J.BIORTECH.2013.09.039.
- [92] L. Garcia Alba *et al.*, “Hydrothermal treatment (HTT) of microalgae: Evaluation of the process as conversion method in an algae biorefinery concept,” *Energy and Fuels*, vol. 26, no. 1, pp. 642–657, 2012, doi: 10.1021/ef201415s.
- [93] L. Luque *et al.*, “Pyrolysis based bio-refinery for the production of bioethanol from demineralized ligno-cellulosic biomass,” *Bioresour. Technol.*, vol. 161, pp. 20–28, 2014, doi: 10.1016/j.biortech.2014.03.009.
- [94] R. J. Van Putten, J. C. Van Der Waal, E. De Jong, C. B. Rasrendra, H. J. Heeres, and J. G. De Vries, “Hydroxymethylfurfural, a versatile platform chemical made from renewable resources,” *Chem. Rev.*, vol. 113, no. 3, pp. 1499–1597, 2013, doi: 10.1021/cr300182k.
- [95] J. Zakzeski, P. C. A. Bruijninx, A. L. Jongerius, and B. M. Weckhuysen, “The catalytic valorization of lignin for the production of renewable chemicals,” *Chem. Rev.*, vol. 110, no. 6, pp. 3552–3599, 2010, doi: 10.1021/cr900354u.
- [96] E. Reyhanitash, T. Brouwer, S. R. A. Kersten, A. G. J. van der Ham, and B. Schuur, “Liquid–liquid extraction-based process concepts for recovery of carboxylic acids from aqueous streams evaluated for dilute streams,” *Chem. Eng. Res. Des.*, vol. 137, pp. 510–533, 2018, doi: 10.1016/j.cherd.2018.07.038.
- [97] Z. Xu, Z. Shi, and L. Jiang, “Acetic and Propionic Acids,” *Compr. Biotechnol. Second Ed.*, vol. 3, pp. 189–199, 2011, doi: 10.1016/B978-0-08-088504-9.00162-8.
- [98] L. Liu *et al.*, “Microbial production of propionic acid from propionibacteria: Current state, challenges and perspectives,” *Crit. Rev. Biotechnol.*, vol. 32, no. 4, pp. 374–381, 2012, doi: 10.3109/07388551.2011.651428.
- [99] M. Dwidar, J. Y. Park, R. J. Mitchell, and B. I. Sang, “The future of butyric acid in industry,” *Sci. World J.*, vol. 2012, 2012, doi: 10.1100/2012/471417.
- [100] A. M. Petersen, T. Franco, and J. F. Görgens, “Comparison of recovery of volatile fatty acids and mixed ketones as alternative downstream processes for acetogenesis fermentation,” *Biofuels, Bioprod. Biorefining*, vol. 12, no. 5, pp. 882–898, 2018, doi: 10.1002/bbb.1901.
- [101] P. O. Saboe *et al.*, “In situ recovery of bio-based carboxylic acids,” *Green Chem.*, vol. 20, no. 8, pp. 1791–1804, 2018, doi: 10.1039/c7gc03747c.
- [102] T. Kurzrock and D. Weuster-Botz, “New reactive extraction systems for separation of bio-succinic acid,” *Bioprocess Biosyst. Eng.*, vol. 34, no. 7, pp. 779–787, 2011, doi: 10.1007/s00449-011-0526-y.
- [103] B. Urbas, “4405717 Recovery of acetic acid from a fermentation broth,” *Biotechnol. Adv.*, vol. 1, no. 2, p. 371, 1983, doi: 10.1016/0734-9750(83)90845-5.
- [104] P. G. Jessop, S. M. Mercer, and D. J. Heldebrant, “CO₂-triggered switchable solvents, surfactants, and other materials,” *Energy Environ. Sci.*, vol. 5, no. 6, pp. 7240–7253, 2012, doi: 10.1039/c2ee02912j.
- [105] P. Pollet, E. A. Davey, E. E. Ureña-Benavides, C. A. Eckert, and C. L. Liotta, “Solvents for sustainable chemical processes,” *Green Chem.*, vol. 16, no. 3, pp. 1034–1055, 2014, doi: 10.1039/c3gc42302f.
- [106] L. Liu, Q. Wei, Y. Zhou, and X. Ren, “Using dialkyl amide: Via forming hydrophobic deep eutectic solvents to separate citric acid from fermentation broth,” *Green Chem.*, vol. 22, no. 8, pp. 2526–2533, 2020, doi: 10.1039/c9gc04401a.
- [107] B. B. Hansen *et al.*, “Deep Eutectic Solvents: A Review of Fundamentals and Applications,” *Chem. Rev.*, vol. 121, no. 3, pp. 1232–1285, 2021, doi: 10.1021/acs.chemrev.0c00385.
- [108] D. Rodríguez-Llorente *et al.*, “Sustainable Recovery of Volatile Fatty Acids from Aqueous Solutions Using Terpenoids and Eutectic Solvents,” *ACS Sustain. Chem. Eng.*, vol. 7, no. 19, pp. 16786–16794, 2019, doi: 10.1021/acssuschemeng.9b04290.
- [109] O. Kunio Koga and S. Ryoichi Kishimoto, “METHOD OF RECOVERY OF ACETIC ACID United States Patent (19),” no. 19, 1982.
- [110] A. Keshav, K. L. Wasewar, S. Chand, and H. Uslu, “Effect of binary extractants and modifier-

- diluents systems on equilibria of propionic acid extraction," *Fluid Phase Equilib.*, vol. 275, no. 1, pp. 21–26, 2009, doi: 10.1016/j.fluid.2008.09.012.
- [111] S. Kumar, D. Datta, and B. V. Babu, "Experimental data and theoretical (chemodel using the differential evolution approach and linear solvation energy relationship mModel) predictions on reactive extraction of monocarboxylic acids using tri-n-octylamine," *J. Chem. Eng. Data*, vol. 55, no. 10, pp. 4290–4300, 2010, doi: 10.1021/je100449c.
- [112] V. Inyang and D. Lokhat, "Reactive Extraction of Malic Acid using Trioctylamine in 1–Decanol: Equilibrium Studies by Response Surface Methodology Using Box Behnken Optimization Technique," *Sci. Rep.*, vol. 10, no. 1, pp. 1–10, 2020, doi: 10.1038/s41598-020-59273-z.
- [113] A. Gaeta-Bernardi and V. Parente, "Organic municipal solid waste (MSW) as feedstock for biodiesel production: A financial feasibility analysis," *Renew. Energy*, vol. 86, pp. 1422–1432, 2016, doi: 10.1016/j.renene.2015.08.025.
- [114] N. A. Mostafa, "Production and recovery of volatile fatty acids from fermentation broth," *Energy Convers. Manag.*, vol. 40, no. 14, pp. 1543–1553, 1999, doi: 10.1016/S0196-8904(99)00043-6.
- [115] A. Yousuf, F. Bonk, J. R. Bastidas-Oyanedel, and J. E. Schmidt, "Recovery of carboxylic acids produced during dark fermentation of food waste by adsorption on Amberlite IRA-67 and activated carbon," *Bioresour. Technol.*, vol. 217, pp. 137–140, 2016, doi: 10.1016/j.biortech.2016.02.035.
- [116] S. Rebecchi, D. Pinelli, L. Bertin, F. Zama, F. Fava, and D. Frascari, "Volatile fatty acids recovery from the effluent of an acidogenic digestion process fed with grape pomace by adsorption on ion exchange resins," *Chem. Eng. J.*, vol. 306, pp. 629–639, 2016, doi: 10.1016/j.cej.2016.07.101.
- [117] S. D. Alexandratos, "Ion-Exchange resins: A retrospective from industrial and engineering chemistry research," *Ind. Eng. Chem. Res.*, vol. 48, no. 1, pp. 388–398, 2009, doi: 10.1021/ie801242v.
- [118] S. M. Husson and C. J. King, "Regeneration of lactic and succinic acid-laden basic sorbents by leaching with a volatile base in an organic solvent," *Ind. Eng. Chem. Res.*, vol. 37, no. 8, pp. 2996–3005, 1998, doi: 10.1021/ie970775p.
- [119] E. Reyhanitash, S. R. A. Kersten, and B. Schuur, "Recovery of Volatile Fatty Acids from Fermented Wastewater by Adsorption," *ACS Sustain. Chem. Eng.*, vol. 5, no. 10, pp. 9176–9184, 2017, doi: 10.1021/acssuschemeng.7b02095.
- [120] C. I. Cabrera-Rodríguez, M. Moreno-González, F. A. de Weerd, V. Viswanathan, L. A. M. van der Wielen, and A. J. J. Straathof, "Esters production via carboxylates from anaerobic paper mill wastewater treatment," *Bioresour. Technol.*, vol. 237, pp. 186–192, 2017, doi: 10.1016/j.biortech.2017.02.030.
- [121] M. P. Zacharof and R. W. Lovitt, "Recovery of volatile fatty acids (VFA) from complex waste effluents using membranes," *Water Sci. Technol.*, vol. 69, no. 3, pp. 495–503, 2014, doi: 10.2166/wst.2013.717.
- [122] Á. Bóna, P. Bakonyi, I. Galambos, K. Bélafi-Bakó, and N. Nemestóthy, "Separation of volatile fatty acids from model anaerobic effluents using various membrane technologies," *Membranes (Basel)*, vol. 10, no. 10, pp. 1–15, 2020, doi: 10.3390/membranes10100252.
- [123] R. van Reis and A. Zydney, "Bioprocess membrane technology," *J. Memb. Sci.*, vol. 297, no. 1–2, pp. 16–50, 2007, doi: 10.1016/j.memsci.2007.02.045.
- [124] M. Parchami, S. Wainaina, A. Mahboubi, D. l'Ons, and M. J. Taherzadeh, "MBR-Assisted VFAs production from excess sewage sludge and food waste slurry for sustainable wastewater treatment," *Appl. Sci.*, vol. 10, no. 8, pp. 1–20, 2020, doi: 10.3390/APP10082921.
- [125] S. Wainaina, M. Parchami, A. Mahboubi, I. S. Horváth, and M. J. Taherzadeh, "Food waste-derived volatile fatty acids platform using an immersed membrane bioreactor," *Bioresour. Technol.*, vol. 274, no. November 2018, pp. 329–334, 2019, doi: 10.1016/j.biortech.2018.11.104.

- [126] S. Aydin, H. Yesil, and A. E. Tugtas, "Recovery of mixed volatile fatty acids from anaerobically fermented organic wastes by vapor permeation membrane contactors," *Bioresour. Technol.*, vol. 250, no. November 2017, pp. 548–555, 2018, doi: 10.1016/j.biortech.2017.11.061.
- [127] H. Yesil, A. E. Tugtas, A. Bayrakdar, and B. Calli, "Anaerobic fermentation of organic solid wastes: Volatile fatty acid production and separation," *Water Sci. Technol.*, vol. 69, no. 10, pp. 2132–2138, 2014, doi: 10.2166/wst.2014.132.
- [128] J. G. Wijmans and R. W. Baker, "The solution-diffusion model: a review," *Membr. Sci.*, vol. 96, no. C, pp. 16–46, 1995, doi: 10.1016/S0166-4115(08)60038-2.
- [129] J. Huang and M. M. Meagher, "Pervaporative recovery of n-butanol from aqueous solutions and ABE fermentation broth using thin-film silicalite-filled silicone composite membranes," *J. Memb. Sci.*, vol. 192, no. 1–2, pp. 231–242, 2001, doi: 10.1016/S0376-7388(01)00507-5.
- [130] S. Keleşer, Y. Salt, A. Hasanoğlu, S. Özkan, and S. Dinçer, "Desorption of ethylacetate-water mixture by using crosslinked polydimethylsiloxane membrane," *Desalination*, vol. 200, no. 1–3, pp. 44–45, 2006, doi: 10.1016/j.desal.2006.03.236.
- [131] Y. Zhang and I. Angelidaki, "Bioelectrochemical recovery of waste-derived volatile fatty acids and production of hydrogen and alkali," *Water Res.*, vol. 81, pp. 188–195, 2015, doi: 10.1016/j.watres.2015.05.058.
- [132] A. Vertova, G. Aricci, S. Rondinini, R. Miglio, L. Carnelli, and P. D'Olimpio, "Electrodialytic recovery of light carboxylic acids from industrial aqueous wastes," *J. Appl. Electrochem.*, vol. 39, no. 11, pp. 2051–2059, 2009, doi: 10.1007/s10800-009-9871-9.
- [133] C. Huang, T. Xu, Y. Zhang, Y. Xue, and G. Chen, "Application of electrodialysis to the production of organic acids: State-of-the-art and recent developments," *J. Memb. Sci.*, vol. 288, no. 1–2, pp. 1–12, 2007, doi: 10.1016/j.memsci.2006.11.026.
- [134] "Dynamic Light Scattering DLS | Malvern Panalytical." <https://www.malvernpanalytical.com/en/products/technology/light-scattering/dynamic-light-scattering> (accessed Jul. 30, 2021).
- [135] "Electrophoretic Light Scattering ELS | Measure Electrophoretic Mobility | Malvern Panalytical." <https://www.malvernpanalytical.com/en/products/technology/light-scattering/electrophoretic-light-scattering> (accessed Jul. 30, 2021).
- [136] "X-ray Analysis | XRF & XRD Analysis | Malvern Panalytical." <https://www.malvernpanalytical.com/en/products/technology/xray-analysis> (accessed Aug. 01, 2021).
- [137] "X-ray Diffraction | Protocol." <https://www.jove.com/v/10446/x-ray-diffraction> (accessed Aug. 01, 2021).
- [138] "SEM Principles | Principles of Scanning Electron Microscopy | Thermo Fisher Scientific - IT." <https://www.thermofisher.com/it/en/home/materials-science/learning-center/applications/scanning-electron-microscope-sem-electron-column.html> (accessed Aug. 01, 2021).
- [139] "Guide to FT-IR Spectroscopy | Bruker." <https://www.bruker.com/en/products-and-solutions/infrared-and-raman/ft-ir-routine-spectrometer/what-is-ft-ir-spectroscopy.html> (accessed Aug. 01, 2021).
- [140] V. P. Fadeeva, V. D. Tikhova, and O. N. Nikulicheva, "Elemental analysis of organic compounds with the use of automated CHNS analyzers," *J. Anal. Chem.*, vol. 63, no. 11, pp. 1094–1106, 2008, doi: 10.1134/S1061934808110142.
- [141] "Introduction to Gas Chromatography—Principles, Characteristics, and Process – Creative Proteomics Blog." <https://www.creative-proteomics.com/blog/index.php/introduction-to-gas-chromatography-principles-characteristics-and-process/> (accessed Aug. 02, 2021).
- [142] K. Tao, H. Dou, and K. Sun, "Interfacial coprecipitation to prepare magnetite nanoparticles: Concentration and temperature dependence," *Colloids Surfaces A Physicochem. Eng. Asp.*, vol. 320, no. 1–3, pp. 115–122, 2008, doi: 10.1016/j.colsurfa.2008.01.051.
- [143] K. Mandel and F. Hutter, "The magnetic nanoparticle separation problem," *Nano Today*, vol.

- 7, no. 6, pp. 485–487, 2012, doi: 10.1016/j.nantod.2012.05.001.
- [144] I. P. T. Indrayana, “A COMPREHENSIVE STUDY ON THE MICROSTRUCTURE AND OPTICAL PROPERTIES OF Fe₃O₄ NANOPARTICLES BY VARIATION OF TEMPERATURE AND NaOH CONCENTRATION,” *J. Online Phys.*, vol. 5, no. 1, pp. 6–17, 2019, doi: 10.22437/jop.v5i1.8166.
- [145] T. Ahn, J. H. Kim, H. M. Yang, J. W. Lee, and J. D. Kim, “Formation pathways of magnetite nanoparticles by coprecipitation method,” *J. Phys. Chem. C*, vol. 116, no. 10, pp. 6069–6076, 2012, doi: 10.1021/jp211843g.
- [146] Â. L. Andrade, M. A. Valente, J. M. F. Ferreira, and J. D. Fabris, “Preparation of size-controlled nanoparticles of magnetite,” *J. Magn. Magn. Mater.*, vol. 324, no. 10, pp. 1753–1757, 2012, doi: 10.1016/j.jmmm.2011.12.033.
- [147] H. El Ghandour, H. M. Zidan, M. M. H. Khalil, and M. I. M. Ismail, “Synthesis and some physical properties of magnetite (Fe₃O₄) nanoparticles,” *Int. J. Electrochem. Sci.*, vol. 7, no. 6, pp. 5734–5745, 2012.
- [148] C. Xu, X. Lu, and H. Dai, “The Synthesis of Size-Adjustable Superparamagnetism Fe₃O₄ Hollow Microspheres,” *Nanoscale Res. Lett.*, vol. 12, no. 1, pp. 4–13, 2017, doi: 10.1186/s11671-017-1986-z.
- [149] U. Holzwarth and N. Gibson, “The Scherrer equation versus the ‘Debye-Scherrer equation,’” *Nat. Nanotechnol.*, vol. 6, no. 9, p. 534, 2011, doi: 10.1038/nnano.2011.145.
- [150] C. I. Olariu *et al.*, “Multifunctional Fe₃O₄ nanoparticles for targeted bi-modal imaging of pancreatic cancer,” *J. Mater. Chem.*, vol. 21, no. 34, pp. 12650–12659, 2011, doi: 10.1039/c1jm11370d.
- [151] D. Maity and D. C. Agrawal, “Synthesis of iron oxide nanoparticles under oxidizing environment and their stabilization in aqueous and non-aqueous media,” *J. Magn. Magn. Mater.*, vol. 308, no. 1, pp. 46–55, 2007, doi: 10.1016/j.jmmm.2006.05.001.
- [152] Y. Sun *et al.*, “Quantification of amine functional groups on silica nanoparticles: A multi-method approach,” *Nanoscale Adv.*, vol. 1, no. 4, pp. 1598–1607, 2019, doi: 10.1039/c9na00016j.